# Structural remodeling of L-type calcium channel subunits in human and murine atherosclerosis

Dissertation

zur

Erlangung des Doktorgrades (Dr. rer. nat.)

der

Mathematisch-Naturwissenschaftlichen Fakultät

der

Rheinischen Friedrich-Wilhelms-Universität Bonn

vorgelegt von

Ann Kristin Böhnke

aus

Witten

Bonn 2012

Angefertigt mit Genehmigung der Mathematisch-Naturwissenschaftlichen Fakultät
der Rheinischen Friedrich-Wilhelms-Universität Bonn

1. Gutachter: Prof. Dr. Stefan Herzig

2. Gutachter: Prof. Dr. Klaus Mohr

Tag der Promotion: 22.11.2012

Erscheinungsjahr: 2012

Für meine Familie

&

Frank

# Table of contents

# Abbreviations

| | |
|---|---|
| # | number |
| % (w/v) | mass concentration (weight/volume) |
| A. | arteria |
| ABP | α binding pocket |
| AC | alternating current |
| AHA | American Heart Association |
| AID | α interaction domain |
| ApoE -/- | apolipoprotein E knockout |
| bp | basepairs |
| C | carboxy |
| CaM | calmodulin |
| CaMK II | calcium calmodulin dependent protein kinase II |
| $Ca_V1.2$ | pore-forming subunit of L-type calcium channel |
| $Ca_V1.2_{ex21}$ | exon 21-containing $Ca_V1.2$ |
| $Ca_V1.2_{ex22}$ | exon 22-containing $Ca_V1.2$ |
| CDF | calcium-dependent facilitation |
| CDI | calcium-dependent inactivation |
| cDNA | complementary deoxyribonucleic acid |
| CRP | C-reactive protein |
| Ct | threshold cycle |
| CVI | cerebralvascular insufficiency |
| DHP | dihydropyridine |
| dNTP | deoxynucleoside triphosphate |
| dT | deoxy-thymine |
| E | efficiency |
| E.coli | Escherichia coli |
| eGFP | enhanced green fluorescent protein |
| ER | endoplasmic reticulum |
| f | female |

| | |
|---|---|
| F | forward primer |
| GABA | γ-aminobutyric acid |
| gDNA | genomic deoxyribonucleic acid |
| h | hours |
| HA | hemagglutinin |
| HDL | high density lipoprotein |
| HE | hemalum |
| HEK | human embryonic kidney |
| I | current |
| I/V | current-voltage relationships |
| kDa | kilo dalton |
| LB | lysogeny broth |
| LCM | laser-capture microdissection |
| LDL | low density lipoprotein |
| LTCC | L-type calcium channel |
| m | male |
| min | minutes |
| mRNA | messenger ribonucleic acid |
| N | amino |
| NK | nucleotide kinase |
| no. | number |
| $OD_{600}$ | optical density at wavelength 600 nm |
| PBS | phosphate buffered saline |
| PCR | polymerase chain reaction |
| qRT-PCR | quantitative real-time PCR |
| R | reverse primer |
| RIN | RNA integrity number |
| RNA | ribonucleic acid |
| rpm | revolutions per minute |
| RT-PCR | reverse transcription polymerase chain reaction |
| S | slope |

| | |
|---|---|
| SEM | standard error of the mean |
| SH3 | Src homology 3 |
| SM | smooth muscle |
| SMA | smooth muscle actin |
| SMC | smooth muscle cell |
| SM-MHC | smooth muscle myosin heavy chain |
| Src | sarcoma |
| VDCC | voltage-dependent calcium channel |
| VDI | voltage-dependent inactivation |
| VSMC | vascular smooth muscle cell |
| wt | wildtype |
| WTS | whole-tissue sample |

# 1. Introduction

## 1.1. Atherosclerosis

Atherosclerosis is a progressive and chronic disease of the arterial blood vessels [1, 2]. An initial change in endothelial cells and subsequent inflammatory processes lead to formation of atheromatous plaques and arterial remodelling [1, 3-6]. The main consequences of atherosclerosis are myocardial infarction, stroke, peripheral artery disease and aortic aneurysm [2, 7]. It constitutes the major cause of death in western world [8, 9].

Atherosclerotic lesions pass through different stages of development and can be classified with the help of the American Heart Association (AHA) classification scheme.

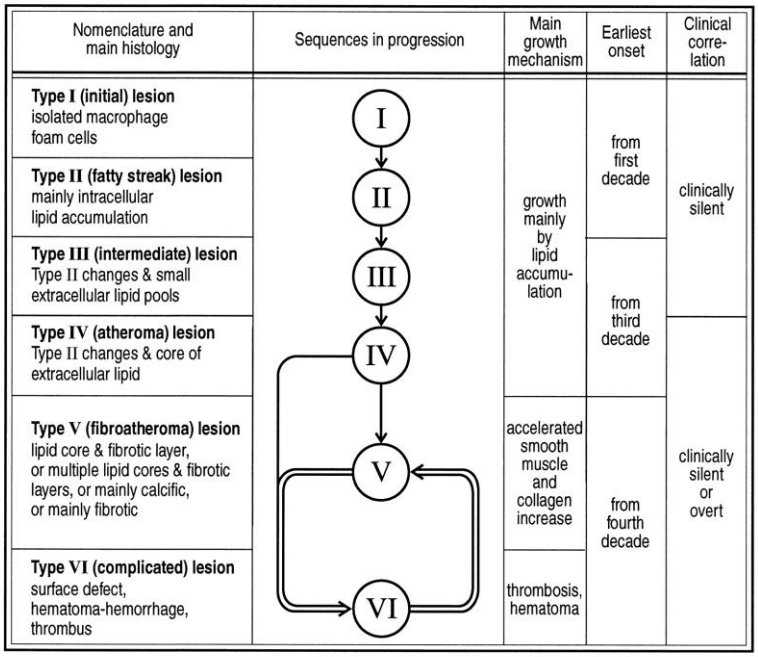


**Figure 1.1:1 AHA Classification: Terms used for atherosclerotic lesions in histological classifications (taken from [10]). Flow diagram in center column indicates pathways in evolution and progression of human atherosclerotic lesions indicated in roman numerals. The left flow diagram defines the different stages of atherosclerosis. Arrows indicate the possible direction of changes in between the stages.**

Risk factors for the development of atherosclerotic vascular disease include modifiable and non-modifiable factors [2]. Modifiable risk factors like dyslipidemia, cigarette smoking, hypertension and diabetes are well known [11, 12]. Several studies display smoking and

diabetes as the strongest among these "traditional" risk factors [13-15]. Recent studies also describe hypertension as a important risk factor leading to increased arterial wall tension, altered endothelial function by angiotensin II and disturbed repair process [1]. Regarding dyslipidemia, elevated triglyceride, decreased high density lipoprotein (HDL) or increased low density lipoprotein (LDL) level is associated with a high risk of atherosclerosis [1, 16-18].

The current therapy regimes are based on these risk factors, including lifestyle changes and risk factor modification. The latter is mainly achieved by the pharmacotherapy of hypertension and dyslipidemia [19]. Lipid lowering agents and in particular statins have proven beneficial in several large studies [20-23]. The Heart Protection Study, for example, showed a reduction of risk of adverse cardiovascular events and death in patients with coronary and non-coronary atherosclerosis by about 25 % [20]. Besides lowering LDL and C-reactive protein (CRP) level, statin therapy also seems to exert an anti-inflammatory [24, 25] and plaque stabilization effect [26, 27]. The therapy of hypertension also reduces the risk of adverse cardiovascular outcomes [28]. So far, there is no proof of positive effects on inflammation and arterial remodeling, but following the CAMELOT study, antihypertensive therapy with either amlodipine of enalapril significantly lowered progression of coronary atherosclerosis [29]. The use of antiplatelet drugs within the therapy reduces the risk of cardiovascular events in patients with atherosclerosis [19].

Non-modifiable risk factors for atherosclerosis include age, male gender and family history [11]. Showing a strong heritable component, various epidemiological studies dealt with the identification of the genetic background and found genetic polymorphisms in at least 100 genes related to the pathogenesis of atherosclerosis. Further research is needed to understand the exact linkage and to identify new targets for therapeutic intervention among these [12, 30].

Looking closer into molecular mechanisms of atherogenesis, a qualitative change in the endothelial cells is observed initially. Endothelial cells express adhesion molecules that bind leukocytes to their surfaces (Figure 1.1:2 and Figure 1.1:3 B) when triggered through irritative stimuli [1, 4-6, 12]. These stimuli can include dyslipidemia, hypertension or pro-inflammatory mediators. In the arterial wall, the assimilated monocytes differentiate into macrophages that by inclosing lipoprotein particles turn into foam cells (Figure 1.1:2 and

Figure 1.1:3 B). Entry of cholesterol-containing low-density lipoprotein (LDL) in the artery wall is facilitated by the changes in the endothelial permeability [1, 4, 5]. The endothelial dysfunction seems to be integral to the development and progression of the disease [12]. Modified lipid particles undergo endocytosis by monocyte-derived macrophages and this leads to intracellular cholesterol accumulation. Hence, dyslipidemia and inflammation are both major factors in the development of atheromatous plaques and intersect each other throughout all stages of atherosclerosis [1, 4-6].

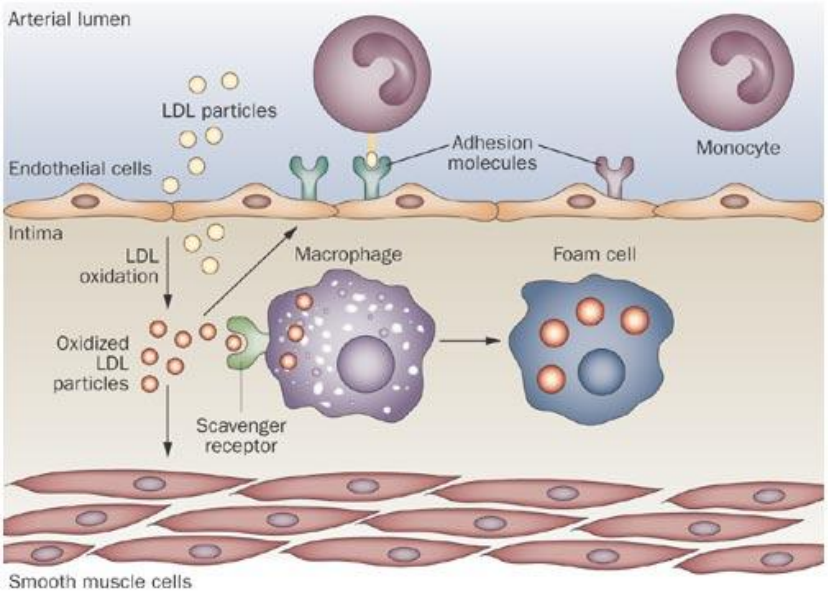


**Figure 1.1:2 Role of LDL particles in the development of atherosclerotic lesions (adapted from [5]). LDL particles penetrate and accumulate in the intima of the arterial wall. Modified LDL particles can induce expression of adhesion molecules and endothelial cell activation. Macrophages internalize LDL particles with the help of scavenger receptors and turn into foam cells. Oxidized lipids may also modulate SMC function, like increasing of the adhesion to macrophages and foam cells in plaques.**

Atheroma formation also includes the migration of smooth muscle cells (SMC) from the tunica media into the tunica intima of the arterial wall (Figure 1.1:3 C). Unlike in most animal, the human intima already features resident SMCs [1]. The SMCs of the media undergo a phenotypic change into a migratory and secretory cell that migrate into the tunica intima and proliferates due to mediators such as growth factors and cytokines [1, 12]. The SMCs in the intima form a fibrous cap covering the plaque overlaying a collection of foam cells. The inefficient clearance of dead cells lead to accumulation of cellular debris and extracellular lipids, forming a so-called necrotic core (Figure 1.1:3 D) [31]. These plaques

lead to clinical manifestations by producing flow-limitations and hence to tissue ischemia or by forming thrombi that can roam into distal arteries [1].

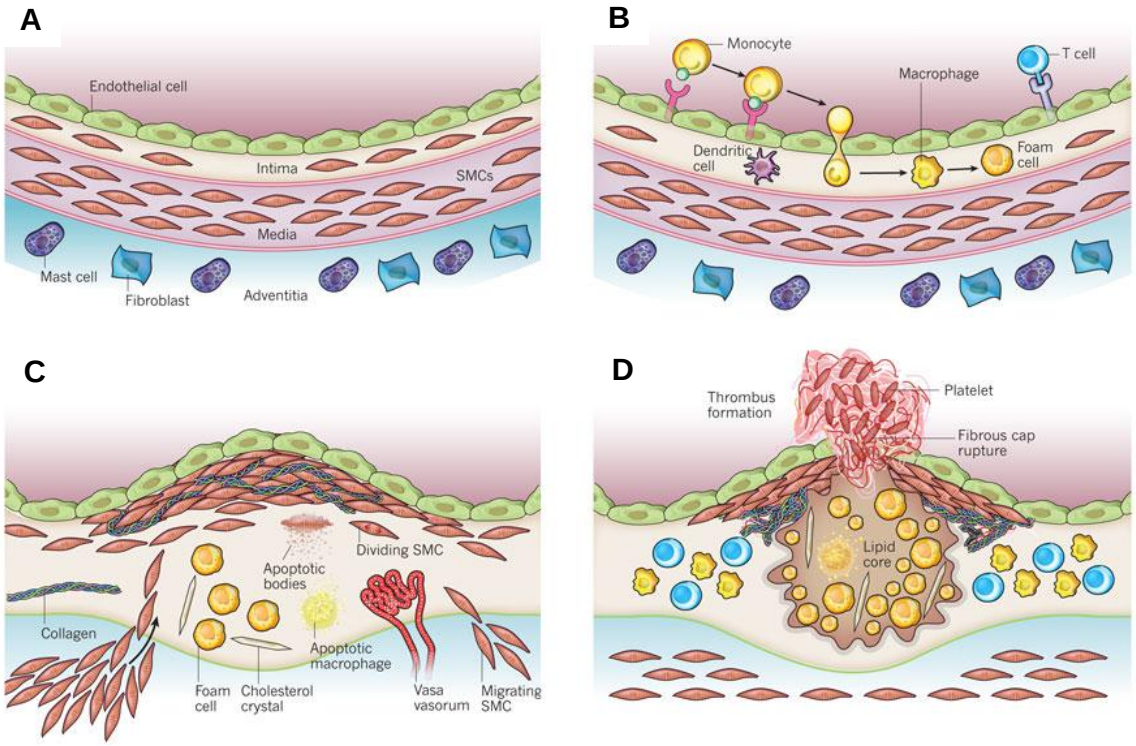


**Figure 1.1:3 Development of atherosclerotic lesions (adapted from [1]). (A) Normal artery consisting of 3 layers. The intima is covered with a monolayer of endothelial cells and in contrast to a lot of animal models, the human intima contains resident SMCs. The media is a SMC layer embedded in extracellular matrix. The adventia constitute the outer layer of arteries and contains mast cells, nerve ends and microvessels. (B) Initial steps of atherosclerosis including binding of leukocytes, migration of these into the intima, maturation of monocytes into macrophages and the resulting foam cells. (C) Later stage of lesion development showing the migration of SMC into the intima and their proliferation. SMC produce extracellular matrix molecules like collagen and elastin. Accumulated dead cells and extracellular lipid form a so-called lipid or necrotic core. (D) Formation of a thrombus as a result of disruption of atherosclerotic plaque. The fracture of the fibrous cap enables blood coagulation that extends into vessel lumen and disturbs blood flow.**

Throughout this process of migration and proliferation, vascular SMCs (VSMCs) exhibit a diverse range of phenotypes. Literature often refers to contractile and synthetic phenotypes [32, 33], but this 2-stage model does not describe all variations of VSMCs at the different stages of atherosclerosis. Morphological, biochemical, physiological and molecular properties are also changing within different lesion types and in between different location of the SMCs [34]. SMCs in the intima have shown increased expression of proliferative markers and decreased expression of proteins characteristic for differentiated VSMC like smooth muscle α actin (SM α actin) or smooth muscle myosin heavy chain (SM MHC) [35-37]. A switch in actin expression from α actin to the β form is detected within the

transformation of SMC from a contractile into a synthetic type. The β actin protein is usually expressed in fibroblastes and therefore the dedifferentiated cells are also called 'myofibroblasts', combining features of SMCs and fibroblasts [32].

For proliferation of VSMC, an increase of cytosolic intracellular calcium ($Ca^{2+}$) is needed [38]. Enhanced $Ca^{2+}$ is needed for cell cycle progression at $G_1$/S phase and cell division in M phase [39]. The intracellular $Ca^{2+}$ is actuated by the balance between $Ca^{2+}$ influx from extracellular through voltage-dependent calcium channels, $Ca^{2+}$ release from stores in the sarcoplasmic reticulum and $Ca^{2+}$-lowering regulators such as $Ca^{2+}$-transport ATPases [40]. Furthermore, $Ca^{2+}$ is important for the regulation of the tonus of vasculature - the contraction of VSMC is triggered by $Ca^{2+}$ current through the voltage-gated calcium channels [40, 41]. During the development of atherosclerosis, alterations in calcium handling in VSMC are found [42, 43]. The dedifferentiation of VSMC during atherogenesis is associated with reduced expression [44] and function [45] of L-type calcium channels (LTCCs). So LTCCs seem to play a role in the development of atherosclerosis and may trigger loss of contractility and proliferation in VSMCs. The exact mechanism behind this is still not fully clarified and further examination is needed.

## 1.2. Voltage-dependent calcium channels

As described above in the context of VSMCs, the $Ca^{2+}$ ion is important for various biological processes. $Ca^{2+}$ entry into the cell in response to membrane depolarization through voltage-dependent calcium channels (VDCC) initiates muscle contraction, endocrine secretion, neurotransmission and gene transcription [41, 46-48]. There are different types of VDCCs which are distinguished by their diverse physiological and pharmacological properties. This distinction led to an alphabetical nomenclature for the different classes of calcium currents (see Table 1.2:1) [49].

**Table 1.2:1 Extract of the classification of voltage-gated $Ca^{2+}$ channels by their physiological function and pharmacology (adapted from [49]). Not shown is the Cav2 subfamily with P/Q, N and R currents.**

| Channel | Current | Localization | Specific Antagonists | Cellular Functions |
|---|---|---|---|---|
| Cav1.1 | L | Skeletal muscle transverse tubules | Dihydropyridines, phenylalkylamines, benzothiazepines | Excitation-contraction coupling |
| Cav1.2 | L | Cardiac myocytes, endocrine cells, neuronal cell bodies and proximal dendrites | Dihydropyridines, phenylalkylamines, benzothiazepines | Excitation-contraction coupling, hormone release, regulation of transcription, synaptic integration |
| Cav1.3 | L | Endocrine cells, neuronal cell bodies and dendrites | Dihydropyridines, phenylalkylamines, benzothiazepines | Hormone release, regulation of transcription, synaptic integration |
| Cav1.4 | L | Retina | Not established | Neurotransmitter release from rods and bipolar cells |
| Cav3.1 & Cav3.2 | T | Neuronal cell bodies and dendrites, cardiac myocytes | None | Pacemaking, repetitive firing |
| CaV3.3 | T | Neuronal cell bodies and dendrites | None | Pacemaking, repetitive firing |

In VSMCs two types of VDCC are found: L-type and T-type calcium channels [40].

T-type calcium channels induce a transient current characterized by rapid inactivation and slow deactivation. They activate at highly negative membrane potentials and therefore also called low-voltage-activated $Ca^{2+}$ currents [40, 41]. T-type calcium channels are involved in action potential and repetitive firing in a variety of cells [49].

L-type calcium currents are mediated by the Cav1 subfamily. These currents are characterized by high voltage threshold for activation, slow voltage-dependent inactivation and long-lasting currents (for barium ions as charge carriers). Therefore they are also called high-voltage-activated $Ca^{2+}$ currents. The L-type calcium channels account for the major calcium currents recorded in cardiac, smooth and skeletal muscle and endocrine cells and trigger contraction and secretion. In neurons, L-type calcium currents regulate gene expression and are important for integrating synaptic inputs [41, 49]. The Cav1 subfamily includes four different isoforms (Cav1.1 to Cav 1.4, Table 1.2:1) with different biophysical

properties, expression patterns and affinity towards calcium channel blockers. Highly specific calcium channel antagonists targeting the LTCC comprise three principal classes: 1,4-dihydropyridines (DHPs) such as nifedipine, benzothiazepines like diltiazem and phenylalkylamines typified by verapamil [50]. The $Ca^{2+}$ channel block with DHPs is isoform-specific and is achieved by selective binding to the inactivated state of LTCCs. This implicates a greater blockade of channels in cells with a depolarized resting membrane potential (like VSMC) and for channel isoforms showing more rapid inactivation [51]. Therefore DHPs are reducing vascular resistance rather than having an effect on cardiac contractility. In contrast, the $Ca^{2+}$ channel blocker verapamil is less voltage-dependent and relatively selective for myocardial $Ca^{2+}$ channels [50].

Genetic defects in the pore-forming subunit of the LTCCs can lead to loss-of-function or gain-of-function mutations, so-called channelopathies [52]. Representatives are the Timothy syndrome ($Ca_V1.2$, characterized by severe arrhythmia and multiorgan disfunction), sinoatrial node dysfunction and deafness syndrome (SANDD, $Ca_V1.3$) and night blindness ($Ca_V1.4$). Interestingly, the mutation found in the Timothy syndrome also alters DHP sensitivity and lead to a fourfold increase in $IC_{50}$ for nisoldipine [53].

Cardiovascular voltage-gated L-type calcium channels are heteromeric protein complexes consisting of a pore-forming $Ca_V1.2$ subunit (also referred to as $\alpha_{1c}$ subunit after prior nomenclature [54]), an intracellular $\beta$ subunit and a $\alpha_2\delta$ subunit complex.

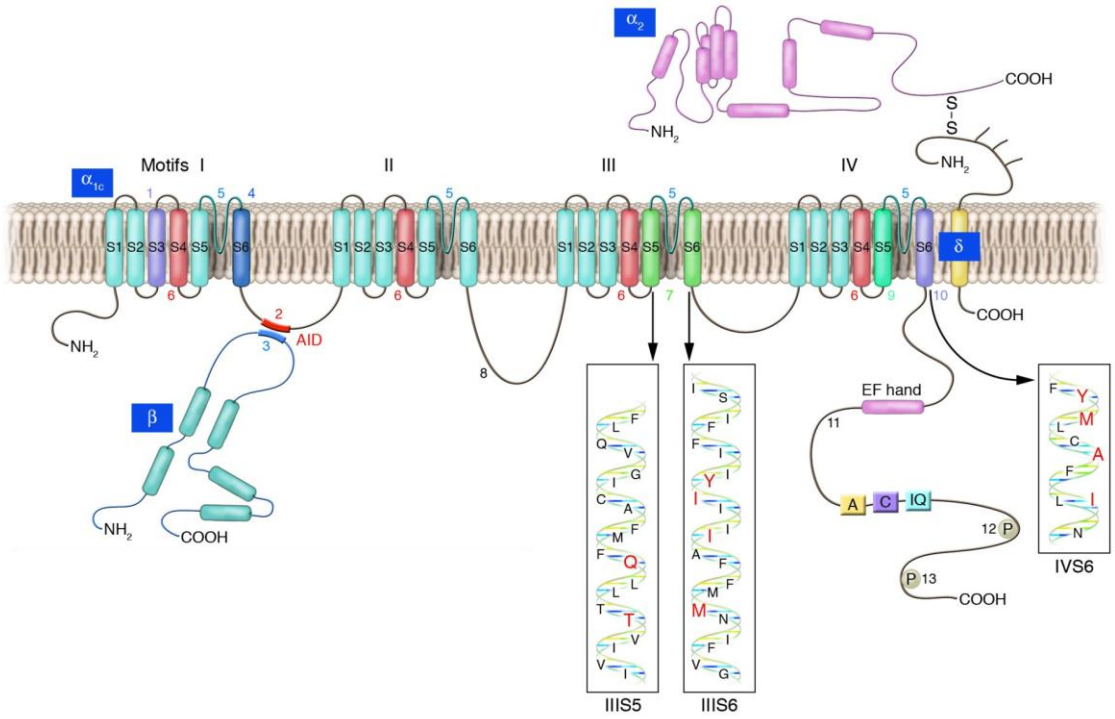


**Figure 1.2:1 The cardiovascular L-type calcium channel complex adapted from [55]. Subunit interaction sides are indicated. The numbers mark important areas for specific channel functions. The EF hand, A, C, and IQ motifs represent specific peptide sequences involved in calmodulin (CaM) binding. Red letters in IIIS5, IIIS6 and IVS6 mark key amino acids required for DHP binding.**

## 1.2.1. The pore-forming Cav1.2 subunit

The Cav1.2 pore-forming subunit is the largest subunit with a size of around 190-250 kDa and comprises the conduction pore, the voltage sensor, gating apparatus and binding sides for channel regulation by second messengers and $Ca^{2+}$ antagonists. Therefore it determines most of the channel's properties [56]. The Cav1.2 subunit is composed of 4 homologous transmembrane domains (I-IV), each consist of 6 segments (S1-S6). The carboxyl- (C) and the amino- (N) terminus are located intracellular (Figure 1.2:1).

The LTCCs are able to respond to activity by self-regulatory mechanisms including voltage-dependent inactivation (VDI), calcium-dependent inactivation (CDI) and calcium-dependent facilitations (CDF). These mechanisms arise mainly from the interaction of Cav1.2 with β subunits or the calcium sensor calmodulin [57]. The calcium-binding protein calmodulin (CaM) is binding to the IQ motif at the C-terminus of the pore and mediates the CDI and CDF of the channel [58]. The CDF in smooth muscle and cardiac cells thought to be caused by a combination of phosphorylation by $Ca^{2+}$ /calmodulin-regulated protein kinase II (CaMKII) and the described binding of $Ca^{2+}$/CaM [41]. The CaMKII also interacts with the

C-terminus in a region close to the IQ motif leading to phosphorylation of two C-terminal sites in the channel and subsequent increase of $Ca^{2+}$ influx [59].

The gene of the pore-forming subunit Cav1.2 is subject to extensive alternative splicing. The resulting splice variants lead to distinct physiological [53, 60, 61] and pharmacological [62-65] properties of the LTCC. Cell-specific expression of alternatively spliced exons increases the functional variations for specific cellular activities in response to changing physiological signals [66].

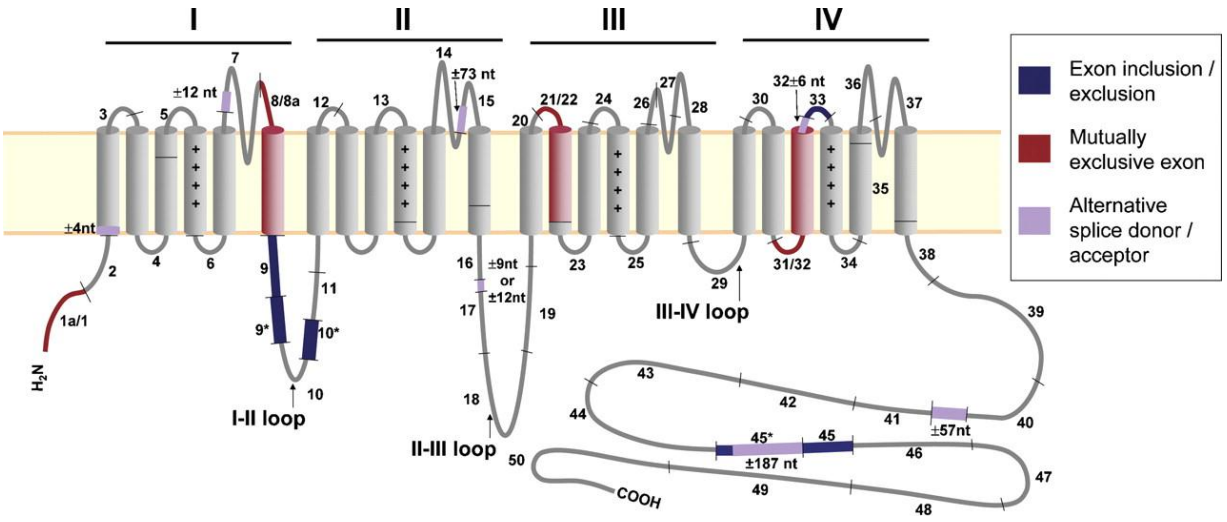


**Figure 1.2:2 Schematic transmembrane topology of the pore forming Cav1.2 and protein segments encoded by numbered exons (adapted from [66]). Spliced exons are marked in different color codes.**

An example for different tissue distribution of alternatively spliced exons is the proposed genotypic structure of a "smooth muscle" and "cardiac muscle" isoform of Cav1.2. The splice variant for cardiac muscle is supposed to consist of the splice combination 1a/8a/ exclusion of 9*/31 while the proposed smooth muscle splice combination is 1/8/9*/32. These differential splice pattern (in particular exon 9*) of Cav1.2 also contributes to the more hyperpolarized activation properties of the smooth muscle LTCC compared to the analogous $Ca^{2+}$ channels found in heart [60, 66]. Furthermore, a recent study discovered the role of exon 9 as a binding side for Galectin-1, a protein reported to regulate VSMC function. Galectin-1 only binds to the I-II loop in the absence of exon 9* and lead to a decreased surface expression of LTCCs [67].

The mutually exclusive exons 8/8a encoding for the IS6 segment have been shown to modulate sensitivity to DHPs - the inclusion of 8 instead of 8a conferred a higher sensitivity

to DHPs and therefore contribute to the tissue selectivity of DHPs [64, 65]. In contrast, the exons encoding for the other DHP binding sites, i.e. IIIS5, IIIS6, and IVS6, are constitutive exons not subject to alternative splicing. The sensitivity to DHPs can also change with differently spliced exons of Cav1.2 not involved in DHP binding. For example, the splice shift of mutually exclusive exons 21/22 leads to a reduced sensitivity to DHPs with exon 21 [62, 63].

Recently, several studies examine the association of altered splicing of Cav1.2 with various diseases. One example is the alternative splicing of exon 31 and 32. In fetal heart, exon 32 is predominant whereas the main isoform of Cav1.2 in adult heart contains exon 31. In human heart failure, level of expression switch and the fetal isoform containing exon 32 reemerges [68].

Thus alternative splicing of the pore forming Cav1.2 subunit can provide a level of fine-tuning of channel activity to adapt to specific cellular conditions or in response to various signals. As splicing can modulate biophysiological properties as well as pharmacological properties of the LTCC channel, it is of importance to find out more about the role of different splice variants of Cav1.2 in development and progression of disease.

### 1.2.2. The β subunit

The auxiliary β subunit interacts with a highly conserved motif in the I –II loop of the Cav1.2 subunit, the so-called α interaction side (AID), and is a major determent of LTCC function and expression.

The primary sequence encoded 5 domains with V1, V2 and V3 as variable domains and C1 and C2 as conserved domains (Figure 1.2:3). Structural studies discovered a SH3 domain (Src homology 3 domain) and a nucleotide kinase (NK) domain formed by the C1 and C2 domains, respectively [57]. The two regions are connected by a HOOK domain (V2), the N- and C-termini are formed by the V1 and V3 region. A high-resolution crystal structure of the β-AID complex revealed an α binding pocket (ABP) in the deep groove at the distal end of the β NK domain that interacts with the AID motif of the pore forming Cav1.2 [69].

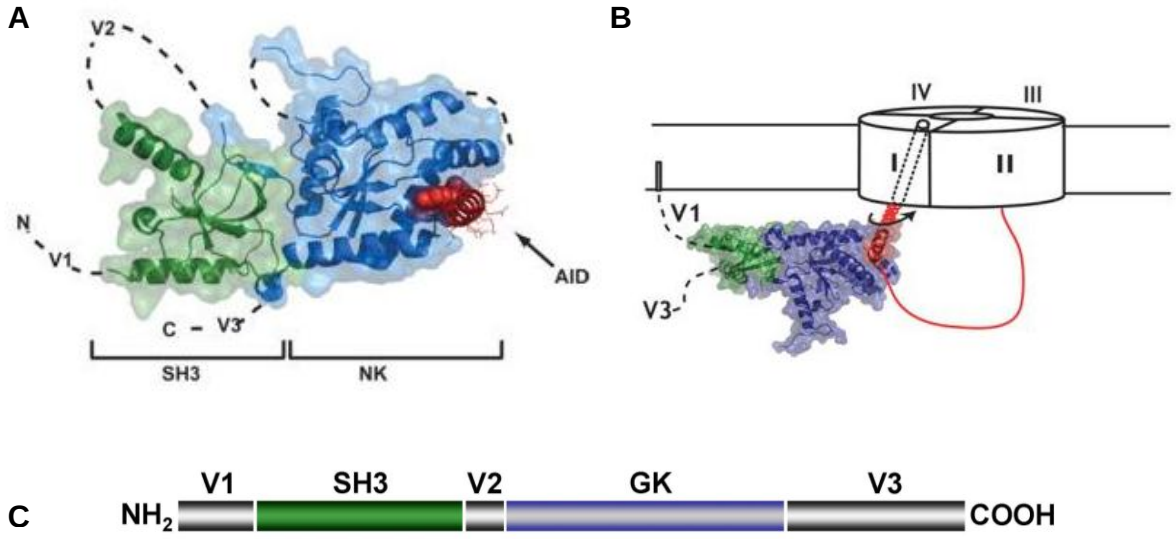


**Figure 1.2:3 (A)The β-AID complex structure adapted from [57]. Shown is the β2a- Cav1.2 AID complex with the SH3 region indicated in green and the NK domain indicated in blue. V1, V2 and V3 show the locations of the 3 variable domains that are absent from the structure. The AID, marked in red, binds to a deep groove in the NK domain – the α binding pocket (ABP). (B) Model of how the β subunit effects the Cav1.2 gating (adapted from [57]). The β subunit influences the movement of IS6. (C) Block diagram of the five domains of the β subunit according to sequence homology among all β subunit isoforms. The SH3 and guanylate kinase (GK) domains are highly conserved whereas regions V1, V2 and V3 are variable.**

Four β subunit isoforms are known, β1 to β4, and each is subject to alternative splicing which leads to further isoforms [41]. The alternative splicing is particularly found in the variable V1 (N-terminus) and V3 (C-terminus) domains and in the so-called HOOK domain (V2). In most cell types, all four gene products are expressed at a small scale, but the proteins show a differentiated subcellular distribution. In skeletal muscle mainly β1a is found [70, 71], β2 is the most abundant isoform in cardiac muscle [72, 73] and β4 is the predominant isoform in the cerebellum [74]; β3 is mostly expressed in brain [71, 75].

The exon structure of the β2 subunit is quite complex. The β2 subunit is encoded by 20 exons, which are alternatively spliced. Depending on the splice variant, it comprises 13 to 14 exons and has a highly variable N-terminus [71, 76].

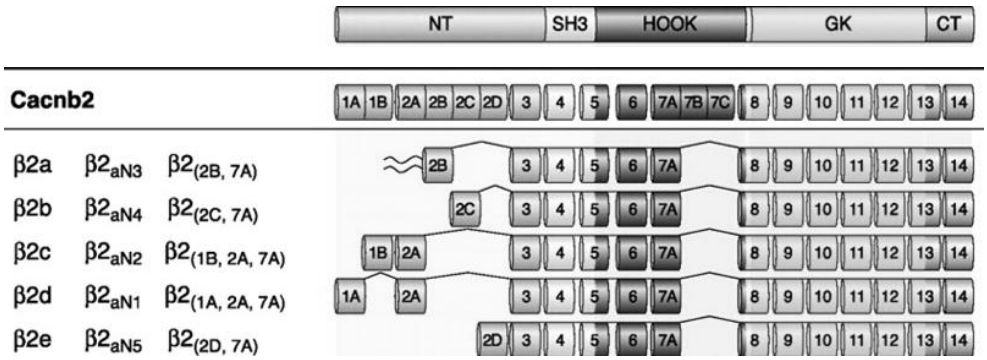


**Figure 1.2:4 Splice variants of the human β2 subunit adapted from [71]. Exons are numbered; the exons indicated by additional letters are alternatively spliced variants. The names of splice variants are, from left to right columns, those used in this study, those proposed by Foell et al. 2004 [76] , and those proposed by Yang and Berggren 2006 [77]. β2a is the only splice variant that can be palmitoylated (indicated by the wave).**

The β subunits can modulate biophysical properties and cell surface expression of the channel. Building a complex with the pore-forming subunit, they lead to increased L-type calcium currents [78, 79], which is also demonstrated by single-channel measurements [79, 80]. Interestingly, all isoforms have different effects on kinetics and voltage-dependence of gating. Therefore, complexes with different β isoforms can lead to altered LTCC function [41, 57, 79, 81].

The variable length of the N-terminus of the β2 splice variants described above has particular effects on open probability, availability and peak current of LTCC. The extent of modulation correlates with the length of the N-terminus and follows a consistent rank order in single-channel measurements of human channel complexes (β2a≈β2b>β2e≈β2c>β2d) [80]. A length-dependent modulation of gating could also be shown for the β1 subunit. Here inactivation rate was diminished by N-terminus truncation of the wildtype β1a subunit in deletion mutants [82].

Furthermore, all four β subunit isoforms increase surface expression of the LTCC complex. One hypothesis postulates that the I-II loop of the Cav1.2 subunit contains an endoplasmic reticulum (ER) retention signal that inhibits the plasma membrane expression of the pore subunit. The β subunit reverses this inhibition by aborting an expression brake contained in β-binding Cav1.2 sequences [83]. Recently, a study purpose a C-terminus dependent rearrangement of intracellular domains of Cav1.2 with binding of the β subunit to the I-II loop and subsequent a shift in balance of power between export signals in the I-II loop and retention signals elsewhere in the Cav1.2 subunit [84]. Another recent study suggests that the increased Cav1.2 membrane expression is due to the prevention of its ubiquitination and

proteasomal degradation by the β subunit [85]. Thus the β subunit may be necessary to protect Cav1.2 against degradation.

### 1.2.3. The α2δ subunit

The α2δ subunit complex is encoded by a single gene and is posttranslationally cleaved. It consists of a large extracellular (α2) and a transmembranic component (δ) and the complex is linked via a disulfide bond (Figure 1.2:5) [86].

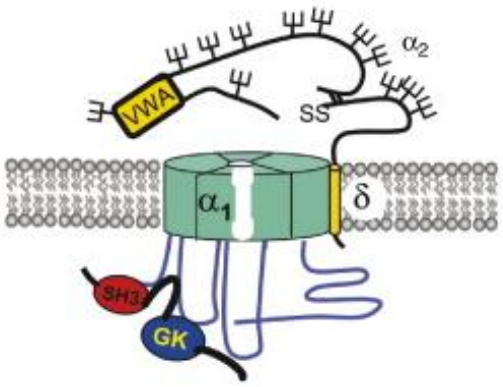


**Figure 1.2:5 Structure of the $\alpha_2\delta$ subunit within the $Ca^{2+}$ channel complex, illustrated as a cartoon adapted from [87]. The $\alpha_2$ protein is located outside of the cell is linked via disulfide bridges to the δ protein. The approximate position of the VWA domain in the $\alpha_2\delta$ subunit is indicated. There are many potential glycosylation sites in $\alpha_2\delta$; the representation of these sites shown here does not accurately reflect the number of sites.**

The α2δ subunit is necessary for proper cell surface expression of the LTCC complex. It promotes trafficking of the Cav subunit to the plasma membrane and increases retention in the membrane [71]. The α2δ subunits can also modify biophysical properties: in heterologous expression system it affects LTCC function by increasing channel density and charge movement [55]. It remains unclear how strong it also affects channel function under physiological conditions.

The α2δ subunit is main target for certain GABA-antagonists such as gabapentin [88], an anti-epileptic and analgesic drug, and the anti-neuropathic pain drug pregabalin [89]. Upregulation of α2δ–1 is associated with neuropathic pain [90].

## 1.3. Aim of the study

Arterial smooth muscle cells undergo multiple phenotypic changes during the development of atherosclerosis. Atherosclerosis is also associated with a reduced expression and function of the L-type calcium channels in VSMCs. In a study from 2006, Tiwari and colleagues discovered an important structural change of the $Ca_V1.2$ subunit in human atherosclerotic lesions, i.e. an exon switch of the alternative exon 21/22 encoding the second transmembrane helix of domain III (Figure 1.3:1 A). In particular, a variety of arterial smooth muscle $Ca_V1.2$ isoforms all containing exon 21 ($Ca_V1.2_{ex\ 21}$) were reported to be replaced by one single isoform containing the alternative exon 22 ($Ca_V1.2_{ex\ 22}$). This postulated splice shift of exon 21/22 is of particular importance since the two splice variants lead to a different sensitivity to DHPs [62, 63]. They characterized and compared the resulting heteromultimeric channel complexes expressed in Xenopus oocytes without detecting major functional consequences in the exon switch [91]. However, they focused on channels coexpressed with β1a subunits, whereas the main β subunits present in smooth muscle cells are considered to be β3 (and maybe β2) subunits [92]. As described above, the different β subunit isoforms are major determents for channel function and expression.

Therefore, our group examined the two human splice variants of $Ca_V1.2$ containing either exon 21 or exon 22 (here named $\alpha_{1c}$ 70 and $\alpha_{1c}$ 77, respectively) in the context of different β subunit isoforms. The data of Tiwari et al. could be confirmed in the context of a β1a subunit in HEK 293 cells. However, strikingly different results were obtained coexpressing these pore subunits with either β2b or β3a subunits (Figure 1.3:1 B).

The splice variant of $Ca_V1.2$ex22 found in atherosclerotic VSMC gave rise to a markedly reduced whole-cell current when coexpressed with β3a subunits. In contrast, coexpressed with a β2b subunit the splice shift had the opposite effect, i.e. higher current density with the exon 22 containing Cav1.2 isoform. Both effects could be partially -but not quantitatively- be explained by the single-channel properties (Figure 1.3:1 C).

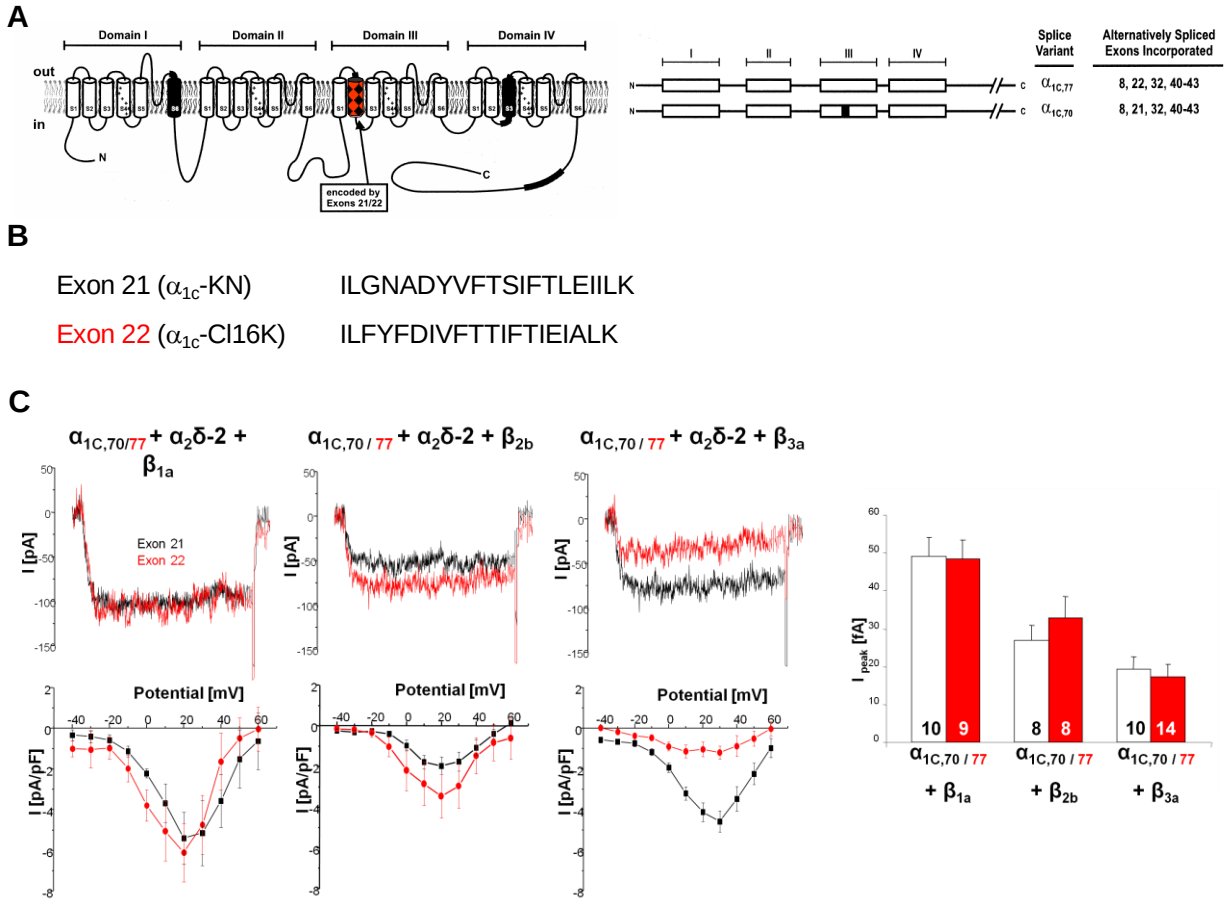


**Figure 1.3:1 Modulation of L-type $Ca^{2+}$-current by β subunits in HEK cells expressing $Cav1.2_{ex21}$ ($\alpha_{1C,70}$) or $Cav1.2_{ex22}$ ($\alpha_{1C,77}$) splice variant. (A) Alternative splicing of exon 21/22 leads to a different III/S2 helix of Cav1.2 in human atherosclerotic smooth muscle cells [91]. (B) Amino acid sequence of exon 21 and exon 22. (C)Whole-cell currents through $\alpha_{1C,70}$ and $\alpha_{1C,77}$ were similar when coexpressed with β1a (-5.6 ± 1.2 pA/pF vs. -6.2 ± 1.2 pA/pF). In contrast, β2b and β3a subunits distinctly modulated currents of $\alpha_{1C}$ isoforms. Currents through $\alpha_{1C,77}$ were significantly lower when coexpressed with β3a ($\alpha_{1C,77}\beta_{3a}$: -1.1 ± 0.3 pA/pF vs. $\alpha_{1C,70}\beta_{3a}$: -4.2 ± 0.5 pA/pF). Conversely, β2b-coexpression led to higher activity with $\alpha_{1C,77}$ ($\alpha_{1C,77}\beta_{2b}$: -4.2 ± 1.3 pA/pF vs. $\alpha_{1C,70}\beta_{2b}$: -1.7 ± 0.6pA/pF). Compared to the respective β1a series, currents were significantly lower with $\alpha_{1C,70}\beta_{2b}$ and $\alpha_{1C,77}\beta_{3a}$. Holding potential: -80mV; pulse duration: 100ms; test potential: -40 to 60 mV. Also shown is the ensemble average single-channel current of $Cav1.2_{ex22}$ and $Cav1.2_{ex21}$ plus indicated β subunit (Rottlaender et al., unpublished).**

The reduced currents in context with the β3 subunit led to the hypothesis that the observed splice shift of Cav1.2 may be the structural mechanism of the calcium current downregulation in diseased arterial smooth muscle cells. Single-channel data could not fully explain the different effects of the two β subunits (Figure 1.3:1 C).

These results illustrated the need to examine the expression pattern of all calcium channel subunits in atherosclerotic human tissue and in relevant mouse models. The aim of this study is to understand the role of differential calcium channel subunit expression in the development of atherosclerotic vessel changes, i.e. smooth muscle cell proliferation and neointima formation. Does the observed splice shift of Cav1.2 in context with a β3 subunit

induce $Ca^{2+}$ current remodeling associated with the dedifferentiation of SMC? And is this splice shift correlated with a differential expression of auxiliary subunits of Cav1.2?

To address these questions, vascular smooth muscle cells from human diseased arteries were isolated by laser capture microdissection. Subsequently, mRNA of calcium channel subunits was quantitatively determined by real-time PCR in unaffected and atherosclerotic samples. The focus was on the β subunit isoforms as they have been shown to effect LTCC function in the context of the two splice variants of Cav1.2.

To complement this approach, Apo E knockout mice (apoE -/-) served as model organism for atherosclerosis [93]. Aorta from these mice and the correspondent wildtype were examined to test the hypothesis that a similar splice shift of Cav1.2 can be detected in murine atherosclerotic lesion. Furthermore, β subunits were quantitatively examined via real-time PCR (qRT-PCR) to test the hypothesis of differential expression of β subunits in the development of atherosclerosis.

Prevailing murine channel complexes were expressed in HEK293 cells followed by electrophysiological assessment to facilitate insight into function of murine LTCC in VSMC in health and disease.

LTCC channel subtypes are targets for drugs for cardiovascular disease and play a role in dedifferentiation of VSMCs in atherosclerosis. The understanding of the molecular composition of the L-type calcium channel complex in health and disease and subsequent functional analysis will provide insights into the development of atherosclerosis and may lead to new ways to modulate LTCC function in pathological states.

# 2. Materials and methods

## 2.1. Messenger RNA (mRNA) analysis of human arterial samples

### 2.1.1. Human sample collection

Samples of human atherosclerotic arteries were obtained from patients undergoing carotid or femoral bypass surgery in the department of vascular surgery of the University Hospital of Cologne. This study was approved by the ethics committee of the University of Cologne (07-203; 11/2007), and participating patients gave written informed consent. Biopsies were taken from femoral or carotid arteries and their side branches during surgery, immersed in 2-methylbutan (Roth, Karlsruhe, Germany) and directly flash frozen in liquid nitrogen. The rare control samples were taken from patients who had a stent surgery or amputations due to non-atherosclerotic reasons (e.g. traumatic rupture of arteries).

**Table 2.1:1 Patient characteristics of arterial samples evaluated in this study. The methods used for investigation included mRNA analysis of whole tissue sample (WTS) and analysis after isolation of vascular smooth muscle cell areas via laser capture microdissection (LCM).**

| patient | sex | age | arterial tissue | method | cardiovascular risk factors |
|---|---|---|---|---|---|
| 3 | f | 78 | carotid | LCM | none |
| 5 | m | 62 | carotid | LCM | none |
| 6 | m | 66 | carotid | LCM | hypertension |
| 8 | f | 82 | femoral | LCM | not known |
| 9 | m | 65 | femoral | LCM | none |
| 10 | m | 59 | carotid | WTS | hypertension |
| 12 | m | 62 | carotid | LCM | cerebralvascular insufficiency (CVI) |
| 17 | m | 75 | femoral | WTS | hypertension, diabetes |

| patient | sex | age | arterial tissue | method | cardiovascular risk factors |
|---|---|---|---|---|---|
| 18 | m | 64 | carotid | LCM | hypertension, hypercholesterolemia |
| 19 | m | 75 | Aorta abdominalis | WTS | hypertension, hypercholesterolemia |
| 20 | m | 70 | branch carotid | WTS | hypertension, diabetes, heart failure, smoking |
| 21 | m | 67 | femoral | WTS | not known |
| 26 | m | 72 | Aorta abdominalis | WTS | hypertension |
| 30 | m | 78 | branch femoral | WTS | hypertension, hypercholesterolemia, smoking, atrial fibrillation |
| 34 | m | 83 | branch femoral control sample | WTS | non-atherosclerotic, smoking, benign hypertension |
| 36 | f | 75 | femoral control sample | WTS | non-atherosclerotic, hypertension, smoking |
| 37 | m | 85 | femoral | LCM | diabetes, hypertension, heart failure, angina pectoris |
| 39 | f | 68 | femoral | LCM | hypertension, alcoholism |
| 40 | m | 63 | branch femoral | WTS | hypercholesterolemia, hypertension |
| 41 | f | 68 | femoral | LCM | hypertension |
| 43 | m | 62 | femoral | WTS | hypercholesterolemia |
| 46 | m | 84 | branch femoral | WTS | coronary heart disease, atrial fibrillation, diabetes, hypertension |

### 2.1.2. Laser capture microdissection (LCM) and Immuno-histochemistry

The arterial biopsies were imbedded in Tissue Tek O.C.T compound (Sakura Finetek Europe, Leiden, Netherlands) and cut in serial cryostat sections (5-7 µm thick) with a cryostat (Leica Microsystems, Nussloch). Every first and third cut was placed on a Superfrost plus slide (Menzel, Braunschweig) for immunohistochemistry; every second and fourth cut on polyethylen membrane slides (Zeiss, Munich) for LCM. Every slide contained 5 to 6 serial cuts.

Serial cuts for the immunohistochemistry were dried overnight and then fixed in an acetone/ methanol mixture (1:1). For immunostaining, two antibodies were used: anti-human smooth muscle actin (SMA; DAKO, Glostrup, Denmark) which marks smooth muscle cells (SMC) and myofibroblasts and anti-Ki67 (DCS, Hamburg, Germany) which marks a nuclear protein that is expressed in proliferative cells. Immunostaining was done automatically by an Autostainer (Medac, Wedel, Germany) following a standard protocol.

After assessment of different fixation methods for subsequent LCM, the following method was picked to be the most effective one for further RNA isolation:

For LCM, serial cryostat sections were fixed in ice-cold ethanol and after short drying period stored at -80°C. To increase the visibility of cell structures, nuclei were stained with hemalum, a complex formed from aluminum ions and oxidized haematoxylin (HE staining; Merck, Darmstadt, Germany) right before LCM. Slides were dried at 50 °C for 10 minutes.

Cuts were characterized with the help of the immunostainings and histology and grouped as atherosclerotic areas and non-affected areas (see chapter 3.1.1).

Laser capture microdissection (PALM Microlaser Technologie, Benried; Zeiss, Munich, Germany) was then used to isolate selected SMC areas. With the corresponding software palmwin® all relevant parameters were regulated, like laser focus and energy. Energy was regulated due to consistence and humidity of the cuts. Circles with a diameter of around 100 µm were cut with the help of a precisely controlled laser. 20 to 30 of these selected areas were then catapulted vertically via laser pulse into an adhesive cap (Zeiss,

Munich; Figure 2.1:1.). After collecting the SMC areas, the cap was deep frozen in liquid nitrogen and stored at -80 °C.

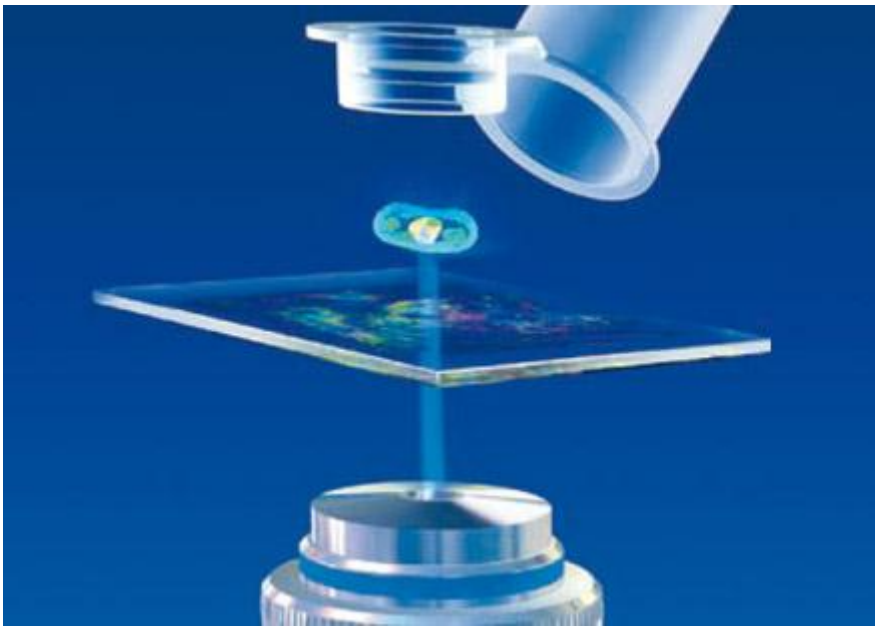

**Figure 2.1:1: Principle of the non-contact laser capture microdissection (www.Zeiss.dk).**

Variation within this method to find optimal conditions included different fixation and HE staining protocols, increased cell amounts and fractional snap freezing with subsequent pooling of microdissected areas of different serial cuts.

## 2.1.3. Isolation of RNA from microdissected samples

The total RNA of the microdissected SMC areas was isolated following the protocol of the NucleoSpin RNA XS kit (Machery-Nagel, Düren, Germany). The microdissected VSMC samples in the cap were centrifuged to transfer the samples into tris-(2-carboxylethyl)-phosphine hydrochlorid (TCEP) containing RA1 buffer. The samples were then homogenized by vortexing for 30 seconds and 20ng of carrier RNA was added to the lysate. DNA was removed with on-column DNAse digestion included in the kit. The RNA was eluted in a volume of 20 µl.

At the end of the isolation protocol, concentration of RNA was determined by measuring the absorbance at 260nm using a Nanodrop 2000 (Thermo Scientific, Wilmington, USA). As a mark of quality, the ratio 260/280 nm had to be between 1.8 and 2.0. As RNA concentrations were very low, quality was exemplary tested with a RNA pico LabChip®

(Agilent RNA 6000 Pico Kit) on an Agilent 2100 bioanalyzer (both from Agilent, Waldbronn, Germany) according to the standard manufacturer's protocol. For measurements, 1 µl of RNA samples were loaded onto the chip. The RNA integrity number (RIN) is a software tool to compare integrity of RNA samples [94] and was taken as a quality marker. The isolated RNA was stored at -80 °C.

As an alternative approach, the RNeasy Micro kit (Qiagen, Hilden, Germany) was used to find optimal isolation efficiency. Controlled by RNA pico LabChip® (s. above) there was no significant difference in RNA isolation efficacy and quality of RNA.

### 2.1.4. Isolation of RNA from whole-tissue samples

Isolation of RNA from whole arterial biopsy samples was carried out with the RNeasy lipid tissue mini kit (Qiagen, Hilden, Germany) following the protocol. Deep-frozen arterial biopsies were homogenized with an Ultra Turrax ® (IKA, Staufen, Germany) in 1 ml of QIAzol lyisis reagent.

The total RNA concentration and 260nm/280nm ratio was measured with a Nano Drop 2000 (Thermo Scientific, Wilmington, USA). As a quality control, the 260nm/280nm had to be between 1.8 and 2.0. A selection of RNA samples were tested with a RNA pico LabChip® as described above. The isolated RNA was stored at -80°C.

### 2.1.5. Reverse transcription into complementary DNA

The isolated RNA was used as a template to synthesize complementary DNA (cDNA) with the QuantiTect Reverse Transcription Kit (Qiagen, Hilden, Germany) following manufacture's protocol. In brief, 12 µl of the RNA from microdissected samples were reverse transcribed to get highest cDNA amounts whereas 400 µg RNA was used from the whole tissues samples in a final volume of 20 µl. Reverse transcriptase master mix contained a mixture of oligo-dT (deoxy-thymine) and random primers for high cDNA yields from all regions of RNA transcript. The following temperature protocol was used: 5 minutes at 42 °C for DNA digestion, 20 minutes at 42 °C for reverse transcription and 3 minutes at 95 °C to inactivate the reverse transcriptase. The resulting cDNA was stored at -20°C.

## 2.1.6. Quantitative real-time PCR

Quantitative real-time PCR (qRT-PCR) was chosen to quantify the gene expression of the subunit isoforms of the L-type calcium channel (LTCC). This method is highly sensitive to low amounts of target and facilitates detection in the early exponential phase of PCR in real time which is seen in figure 2.1.6:1 [95]. Therefore a so-called threshold is set to a value above the background fluorescence and within the log linear phase of the PCR. The detection during the PCR is achieved by using the fluorescent dye SYBR green which binds all double stranded DNA molecules (s. figure 2.1.6:1 A).To avoid false positive detection of genomic DNA, primers were designed intron-spanning or intron-flanking in the case of long flanked introns. Melting curve analysis at the end of each measurement assured exclusion of detecting primer dimers or unspecific amplicons (figure 2.1.6:1 C).

Low concentrations of specific LTCC subunit-containing plasmids were used to confirm that primer pairs are only detecting the specific isoform of subunits. Conventional PCR and agarose gel electrophoresis had to lead to a band of amplified cDNA only with their respective primer pair. In the case of the exon 21- and exon 22-distinguishing primer pairs, qRT-PCR products of whole-tissue samples were sequenced using Eurofins mwg/ operon sequencing services (Ebersberg, Germany).

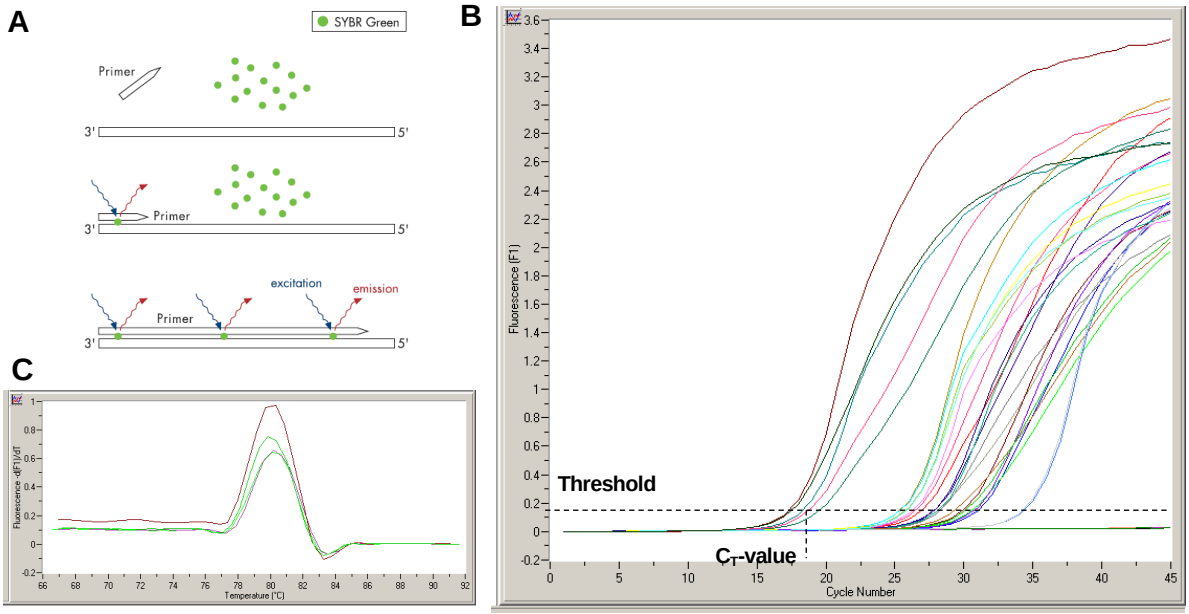


**Figure 2.1:2: Principle of SYBR green detection of double stranded DNA (A; [96]). (B) Example of a qRT-measurement indicating the threshold and the setting of threshold cycle (Ct)-value. (C) Melting curve analysis at the end of each qRT-PCR.**

For qRT-PCR analysis of the human samples, a master mix was prepared containing 2.5 µl cDNA, 10 µl Quanti Tect SYBR Green PCR master mix (Qiagen, Hilden, Germany) and 5.5 µl $H_2O$ per target/ primer pair used for detection (table 2.1.6:1). This master mix was placed into a LightCycler® glass capillary and 1 µl forward and 1 µl reverse primer (10 mM) was added. Besides the primer pairs for the genes of interest 18S RNA was used as reference genes for the amount of analyzed cDNA.

**Table 2.1:2 Specific primer used to detect different isoforms of the LTCC subunits. Primers were designed intron-spanning or intron-flanking to avoid detecting genomic DNA. F stands for forward primer and R for reverse primer.**

| Primer name | Sequence | Gene ID |
|---|---|---|
| β1 common | F 5′ – AAT GTT GGC TAC AAT CCG TCT C –3′ | CACNB1 |
| | R 5′– CCG ATC CAC CAG TCA TTA TTG T–3′ | |
| β2 common | F 5′ – CAA CGT CCA GAT GGT AGC AG-3′ | CACNB2 |
| | R 5′ – CTC CAG ATA GTC GGC AAG GT –3′ | |
| β3 common | F 5′- GTC CTC CCA GTG CCA TCC-3′ | CACNB3 |
| | R 5′– ATC AGA GGG CAT CAA GCT GT –3′ | |

| Primer name | Sequence | Gene ID |
|---|---|---|
| β4 common | F 5′- CAC CAT ATC CCA CAG CAA TTT-3′ | CACNB4 |
| | R 5′- AGT TCT CTG TGG AGT GGT TGC T –3′ | |
| α1c common | F 5′- CAC GAT CTT CAC CAA CCT GA-3′ | CACNA1C |
| | R 5′- CTG AAG GAG GTG TGC TGG A-3′ | |
| Exon 22 | F 5′ -ATC CTA GGC AAT GCA GAC TAT GTC – 3′ | |
| | R 5′-AAA GCC CCA TAA GCA GTC ATC T-3′ | |
| Exon 21 | F 5′ – CAC CAT TGA AAT TGC TCT GAA G –3′ | |
| | R 5′- CAG GTC CAG GAT GTT GAA GTA GT –3′ | |
| 18S RNA | F 5′ - AAA CGG CTA CCA CAT CCA AG –3′ | Rn18S |
| | R 5′- CCT CCA ATG GAT CCT CGT TA –3′ | |

Before analysis, glass capillaries were spin down using a LightCycler® centrifuge. qRT-PCR analysis was performed with a carousel-based LightCycler (Roche Applied Science, Mannheim, Germany) and LightCycler® software 3.5.3 The following temperature protocol was used:

95°C 15 min

95°C 15 sec
60°C 25 sec
72°C 10 sec
) 45 cycles, transition rate 20 °C/ sec

Melting curve analysis

64°C 1 min

Heat up to 94 °C, transition rate 0.1 °C/ sec and continuous acquisition

The threshold cycle (Ct) is the cycle at which the amplification plot crosses the threshold and therefore a significant increase in fluorescence is detected. This value is taken as the characteristic value for each target gene in a sample and a lower Ct value correlates with a higher template amount. Calculation of the difference between the Ct value of the gene

of interest and the Ct value of the reference gene in each sample is used to normalize for the amount of template used:

$\Delta$ Ct = Ct (target gene) – Ct (reference gene)

Relative quantification in qRT-PCR is used to compare differential expression of a gene in different tissues or to compare differential expression in different disease states.

$\Delta\Delta$ Ct = $\Delta$ Ct $_1$ - $\Delta$ Ct $_2$

For statistical analysis student t test of the $\Delta$ ct values was used.

However, the important point of this method is that the expression level of the reference gene must not vary between different tissues or different disease states. Furthermore, the amplification efficiency of the different primer assay must be comparable or must be included in the calculations.

Therefore amplification efficiencies were determined by preparing a dilution series for each gene from whole-tissue samples. Slope of the standard curve (S) was taken to calculate Efficiency (E):

$E = 10^{(-1/S)} - 1$

If the efficiency of two assays is comparable the standard curves of both genes go in parallel. The differences in Ct values of the target and the reference gene will be constant even when amounts of template are varied. In this study the efficiency of primer assays were comparable and hence the $\Delta\Delta$Ct method could be used without further normalization.

For absolute quantification of exon 21 and exon 22, standard curves were prepared using oligonucleotides (sigma-alderich, St.Louis, MO, USA) each representing one exon plus parts of adjacent exons. The standard curve plots Ct values on the y-axes and log amount of standard on the x-axes. Amount of standard was calculated using the following formular:

(X g/µl cDNA / (transcript length in nucleotides x 340)) x 6.022 x10 $^{23}$ = Y molecules/µl

## 2.2. Messenger RNA analysis of murine aortic samples

### 2.2.1. Mouse model

Apo E knockout mice (apoE -/-) served as model organism for atherosclerosis [93]. Knockout mice were backcrossed into a C57/Bl6 background and heterozygous littermates were taken for breeding. Homozygous littermates, not carrying the apoE knockout, were used as wildtype controls (wt). Mice had originally a LysMCre background which has not been used in this work [97]

Mice were grouped into three age-classes to cover different stages of atherosclerosis. Age groups were chosen due to literature: at the age of 12-14 weeks apoE -/- mice develop stage II lesions whereas the older ones evolve stage III and IV lesions [98]. ApoE -/- mice were fed with a western-type diet from the age of 4 to 5 weeks to develop atherosclerotic plaques earlier than with a common diet. Western-type diet consisted of 21 % fat, 0.15 % cholesterol and 19.5 % casein (Altromin, Lage, Germany). To estimate the effect of the diets, also small control groups with apoE -/- mice were fed with normal diet and wt mice fed with western-type diet (Table 2.2:1).

All animal procedures were conducted with respective laws and regulations and conform to the 'Guide for the Care and Use of Laboratory Animals' published by the US National Institutes of Health (NIH Publication No. 85-23, revised 1996).

**Table 2.2:1 Age groups of apoE -/- and wildtype mice fed with either western-type or normal diet used in this study.**

| Genotype | Age | diet | # in group |
|---|---|---|---|
| apoE -/- mice | 12-14 weeks | western-type diet | 14 |
| apoE -/- mice | 16-18 weeks | western-type diet | 8 |
| apoE -/- mice | 22 weeks | western-type diet | 6 |
| apoE -/- mice | 12-14 weeks | normal diet | 4 |
| wildtype mice | 12-14 weeks | normal diet | 10 |
| wildtype mice | 16-18 weeks | normal diet | 7 |
| wildtype mice | 12-14 weeks | western-type diet | 6 |

## 2.2.2. Genotyping

Genomic DNA (gDNA) was isolated from tail clips of 3-4 week old mice using NucleoSpin®96 Tissue Kit and NucleoVac®96 Vacuum Manifold (Macherey-Nagel, Düren, Germany) following manufacturer's protocol. The following specific primers (Metabion, Martinsried, Germany) were used to detect the wt and knockout mice via PCR [97]. Wildtype mice show a band at 155 base pairs (bp) whereas the apoE -/- mice lead to a 245 bp band on a 1% agarose gel.

**Table 2.2:2 Primer pairs used to genotype wt and apoE -/- mice in this work**

| primer name | sequence |
|---|---|
| ApoIMR0180 | 5′-GCC TAG CCG AGG GAG AGC CG-3′ |
| ApoIMR0181 | 5′-TGT GAC TTG GGA GCT CTG CAG C-3′ |
| ApoIMR0182 | 5′-GCC GCC CCG ACT GCA TCT-3′ |

## 2.2.3. Dissection of the aorta

Mice were sacrificed by cervical dislocation and the cardiovascular system was rinsed with phosphate buffered saline (PBS) by perfusion of the right ventricle. The aorta was dissected starting with the descending aorta and including the heart (see figure 2.2.2.:1 A). Aorta was separated from the heart right above the aortic root and dissected from connective tissue (see figure 2.2.2.:1 B). Only the aortic arch was used for further experiments and was flash frozen directly in liquid nitrogen. The hearts were cut in the middle and frozen on top of a metal cap floating in 2-methylbutan in dry ice to achieve an even cutting surface. Heart and aortic arch were stored at -80°C.

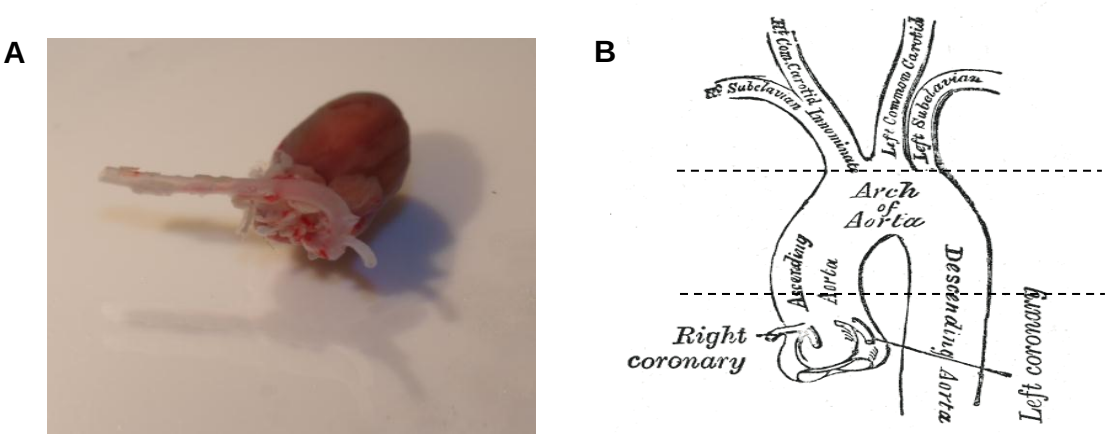


**Figure 2.2:1 (A) Dissected heart of a C57/BL6 wild type mice also showing the aortic arch and descending aorta. (B) The aorta and their branches (Henry Gray's *Anatomy of the Human Body,* 1918). Marked area was taken for later experiments.**

## 2.2.4. Characterization of plaque area

ApoE -/- mice develop increasing stages of atherosclerosis with age. To characterize and quantify the atherosclerotic lesions, frozen mouse hearts were sectioned in a cryostat (Leica microsystems, Wetzlar, Germany) at -20°C. Therefore hearts were embedded in Tissue Freezing Medium® (Leica Microsystems, Nussloch, Germany) and cut in 7 µm thick serial slices. Slices were collected at the level of atrioventricular valves on 24 Superfrost plus slides (Menzel, Braunschweig, Germany) following Figure 2.1:1. Slides were dried overnight in an exicator at room temperature and then stored at -80°C.

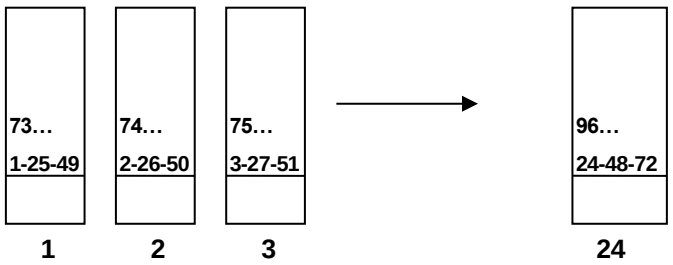


**Figure 2.2:2: Scheme of collecting the heart cuts starting with the first slide down left and ending with the last cut after rounds needed at slide no 24. Hence the interspaces between serial cuts on one slide were originally 168 µm.**

Staining with Toluidin-blue was used for morphometric analysis and atherosclerosis quantification at the level of the aortic valves. For this staining, slides 6, 12, 18 and 24

were fixed in 100 % acetone (Roth, Karlsruhe, Germany) and stained with 0.2 % Toluidin-blue solution (Roth, Karlsruhe,Germany) in PBS. For morphometric analysis, sections were microphotographed with a 4x magnification ocular (Leica microsystems, Wetzlar, Germany). Lesion size was measured on four consecutive sections in 42 mm intervals using Leica Application suite V3.8.0 (Leica microsystems, Wetzlar, Germany). Serial cuts were chosen in the area of the aortic valves where the aortic wall is already clearly distinguishable. Average plaque area was taken from these four serial cuts per mouse heart [99].

### 2.2.5. RNA Isolation

The deep-frozen aortic arches were disrupted and homogenized in Qiazol® (Qiagen, Hilden, Germany) using an Ultra Turrax ® (IKA, Staufen, Germany). Total RNA was isolated with the Qiagen RNeasy lipid tissue mini kit following the manufacturer's protocol. DNA was removed with on column DNase digestion included in the kit. The RNA was eluted in a volume of 60 µl RNase free water. RNA concentration was determined by measuring absorbance at 260nm using a Nanodrop2000 ((Thermo Scientific, Wilmington, USA). The ratio between the absorbance values at 260nm and 280nm was taken as a quality control for RNA purity and should fall between 1.8 and 2.0. The quality of exemplary samples was tested with a RNA pico LabChip® as described above.

### 2.2.6. Reverse transcription into complementary DNA (cDNA)

RNA was reverse transcripted into cDNA using QuantiTect Reverse Transcription kit (Qiagen, Hilden, Germany). Therefore 400 ng total RNA was used and transcription followed manufacturer's protocol as described above in a total volume of 20 µl.

### 2.2.7. Qualitative reverse transcription PCR (RT-PCR)

To detect the presence of the alternative splice variants of the pore-forming Cav1.2 containing either exon 21 or 22, RT-PCR was used followed by an analytic digestion with Avr II (NEB, Frankfurt, Germany). The region spanning exon 18 to exon 27 was amplified with the help of PCR using 200 ng cDNA as a template. PCR was carried out

using DreamTaq™ DNA Polymerase (Fermentas, Burlington, Canada). Cycling program included:

| | | |
|---|---|---|
| 95°C | 3 min | |
| 95°C | 30 sec | 40 cycles |
| 59°C | 30 sec | |
| 72°C | 55 sec | |
| 72°C | 5 min | |

**Table 2.2:3 Primer pairs used to amplify region between exon 18 and exon 27 of $Ca_v1.2$.**

| primer name | sequence |
|---|---|
| Exon18-27 forward | 5′-TTA CAG CCG ATG GAG AAT CC-3′ |
| Exon18-27 reverse | 5′-GTG GAG ACG GTG AAG AGA GC-′3 |

After PCR, samples were purified using a DNA gel extraction kit (Millipore, Billerica, USA) following manufacture's protocol. The purified amplicon was then digested using Avr II in supplied buffer 4 at 37°C for 2 h to differentiate between exon 21- and exon 22-containing Cav1.2.

## 2.2.8. Quantitative real-time PCR (qRT-PCR) of murine aortic samples

As described in section 2.1.6, quantitative real time PCR was chosen to quantify the gene expression of the subunit isoforms of the L-type calcium channel (LTCC). The same protocol was used as described above except small changes which were chosen after optimization of the new assays. All Δct values are given as mean plus standard error of the mean (SEM).

**Reaction mixture**

10 µl SYBR Green Quanti tect mastermix

2 µl template

1.5 µl primer (10 mM) forward (0.75 µM)

1.5 µl primer (10 mM) reverse (0.75 µM)

$H_2O$ ad 20 µl

The annealing temperature of 58 °C was chosen due to experiments finding the best conditions for the cycling protocol of the new primer assays.

**Table 2.2:4 Specific primer pairs used to detect the different isoforms of the LTCC subunits. Primers were designed intron-spanning or intron-flanking to avoid detecting genomic DNA. F stands for forward primer and R for reverse primer.**

| primer name | sequence | gene |
|---|---|---|
| β1 subunit | F 5′- TGG ACA GCC TTC GTC TGC T -3′ | CACNB1 |
| | R 5′- TGG AAC TGG AGT TGT CAC CT -3′ | |
| β2 subunit | F 5′- GGG AGG CAG TAC GTA GAG AAG CT -3′ | CACNB2 |
| | R 5′- TGC AAA TGC AAC AGG TTT TGT C -3′ | |
| β3 subunit | F 5′- TGG AGT CAA CTT TGA GGC CA -3′ | CACNB3 |
| | R 5′- TCC CGA TCC ACC AGT CAT TG -3′ | |
| Cav1.2 subunit | F 5′- TCC GAA CAT TAC AAC CAG CCT -3′ | CACNA1C |
| | R 5′- GCT GTA CAT CTT CAG GAG CA -3′ | |
| Exon 21 | F 5′- CAC CAT TGA AAT TGC TCT AAA G -3′ | Z34810 |
| | R 5′- CAG GTC CAG GAT ATT GAA GTA GT -3′ | |
| Exon 22 | F 5′- ATC CTA GGC AAT GCA GAC TAT GTC -3′ | Z34815 |
| | R 5′- AAA GCC CCG TAA GCA GTC ATC T -3′ | |
| β2a (N3) | F 5′- AGT GCT GCG GGC TGG TAC -3′ | FM872406 |
| | R 5′- AAC CAT AGG ACA CCC GTA CTC -3′ | |
| β2b (N4) | F 5′- ATG CTT GAC AGG CAG TTG GT -3′ | AM259383 |
| | R 5′- CCC CAG GAA TAC TGG ATT -3′ | |
| β2d (N1) | F 5′- ATG GAA GCA CAT CGT CAG ACA CT -3′ | FM872408 |
| | R 5′- CCT GCC GCT CAG CTT CTC TA -3′ | |

| primer name | sequence | gene |
|---|---|---|
| β2e (N5) | F 5′- GAA GGC TGA AGA GTT CGG ACA T -3′ | FM872407 |
| | R 5′- CCT GCC GCT CAG CTT CTC TA -3′ | |
| S29 | F 5′- ATG GGT CAC CAG CAG CTC TA -3′ | Rps29 |
| | R 5′- AGC CTA TGT CCT TCG CGT ACT -3′ | |

Specificity of primer assays for the different isoforms of LTCC subunits was tested using low concentration of plasmid carrying the target sequence. As described in chapter 2.1.6, standard curves of pooled aortic tissue were used for determination of efficiency of primer assays. All efficiencies were comparable and hence no further normalization was necessary.

## 2.3. Electrophysiology

### 2.3.1. Plasmids

The LTCC channel complexes investigated in this work are composed of only murine subunits. The pore-forming $Ca_V1.2$ subunits and β subunits are all kindly provided by Veit Flockerzi (Saarland University, Homburg, Germany). pGFP+ was used as an indicator for successfully transfected cells and was kindly provided by Alexandra Koschak (University of Innsbruck, Austria). All vectors used in this study carry an ampicillin resistance gene.

**Table 2.3:1 Plasmids used in this study to investigate function of murine LTCC in HEK293 cells.**

| Name | Gene | Accession # | vector | publication |
|---|---|---|---|---|
| $Ca_V\alpha 1c$ KN | CACNA1C | FM 872412 | pcAGGS M2 | [100] |
| $Ca_V\alpha 1c$ Cl16K | CACNA1C | s. table 2.3.2:2 | pcAGGS M2 | [100] |
| $Ca_V\beta$ N1 (2d) | CACNB2 | FM 872408 | pcAGGS M1 | [100] |
| $Ca_V\beta$ N4 (2b) | CACNB2 | AM 259383 | pcAGGS M1 | [100] |
| $Ca_V\beta$ 3A | CACNB3 | protein P54285-1 | pcDNA3 | [101] |
| $Ca_V\ \alpha_2\delta$-1 | CACNA2D1 | NM_001110843.1 | pcDSA3 | |
| pGFP+ | | | | [102] |

The pore-forming $Ca_V1.2$ splice variants were both characterized by a short N-terminus which is characteristic for smooth muscle cell Cav1.2 splice variants [60]. The splicing pattern is as follows (only typical alternatively spliced exons are shown):

**Table 2.3:2 Splicing pattern of $Ca_V1.2$ $\alpha_{1c}$ clones (modified after [100])**

| plasmid | 1A/1B | 7/7* | 8A/8B | 9A | 17/17* | 21/22 | 31/32 | 33/33* | bp |
|---|---|---|---|---|---|---|---|---|---|
| $Ca_V\alpha 1c$ KN | 1B | 7 | 8B | 9A | 17 | 21 | 31 | - | 6462 |
| $Ca_V\alpha 1c$ Cl16K | 1B | 7 | 8B | 9A | 17 | 22 | 31 | - | 6462 |

The plasmid encoding the cDNA of $\alpha_2\delta$-1 subunit was originally provided by Norbert Klugbauer (University of Freiburg, Germany) in a pBluescript vector. In order to transfer the cDNA into a mammalian expression vector, the coding cDNA of $\alpha_2\delta$-1 was cloned into a pcDSA3 vector (low copy variant of pcDNA3) as described in chapter 2.3.2.4. Sequence was confirmed by sequencing.

## 2.3.2. DNA cloning and subcloning

### 2.3.2.1. Preparation of Escherichia coli (E.coli) competent cells

**Lysogeny broth (LB) medium** (all components from Roth, Karlsruhe, Germany)

1% (w/v) peptone

0.5% (w/v) yeast extract

1% (w/v) sodium chloride

pH 7.5, autoclaved

**Transformation and storage buffer (TSB)**

10% (w/v) PEG 3000

5% (w/v) DMSO

20 mM $MgCl_2$

LB medium

pH 6.5, filtered sterile

The bacterial strain JM109 is a useful host for cloning. The cell stock-solution (Promega, Madison, WI, USA) was plated on a LB ager and incubated over night at 37°C. Each picked colony was transferred into 10 ml LB medium and was again incubated overnight. 5-10 ml was transferred into a final volume of 250 ml LB broth and let grow to an $OD_{600}$ of 0.3-0.4. The bacteria were harvest by centrifugation at 5000 rpm and 4 °C for 10 min. The pellet was then gently resuspended in 25 ml ice-cold TSB and incubated on ice for 1-2 h. Aliquots were stored at -80°C.

### 2.3.2.2. Transformation of E. coli competent cells

**KCM buffer** (all components from Roth, Karlsruhe, Germany)

500 mM KCl

150 mM CaCl2

250 mM MgCl2

$H_2O$

Aliquots of bacteria were thawed on ice. 100 µl of this bacteria suspension was mixed with 20 µl of 5xKCM buffer and 80 µl $H_2O$. 10 ng of plasmid DNA was added and incubated for 20 min on ice and for 10 min at room temperature. After adding 1 ml of LB medium the mixture was incubated shaking at 37°C for 50 min. It was centrifuged for 30 sec and the pellet was resuspended in 50 ml fresh LB medium and plated on an ampicillin-containing LB agar (50 µg/ml) over night at 37°C.

### 2.3.2.3. Preparation of plasmid DNA

Plasmid DNA mini-preparation was performed according to the following protocol: a single bacterial colony from the LB agar was transferred into 2 ml of LB medium containing 50 µg/µl ampicillin. The tube was incubated over night shaking at 37°C. On the next day 1.5 ml of E. coli culture was transferred in a reaction cup and centrifuged for 30 sec at maximum speed. The pellet was then dispersed in 300 µl resuspension buffer P1 (all buffers from Qiagen, Hilden, Germany). 300 µl lysis buffer P2 was added, mixed and incubated at room temperature for 5 min. Pre-chilled neutralization buffer P3 was added, mixed gently and centrifuged for 15 min at maximal speed. 800 µl of supernatant was transferred into a new reaction cup. DNA was precipitated by adding 750 µl isopropanol (Roth, Karlsruhe, Germany) and contents were mixed well and centrifuged for 15 min at maximum speed. The pellet was then resuspended in 100 µl $H_2O$ and again precipated by adding ethanol (96 %, Roth Karlsruhe, Germany) and centrifugation for 15 min at maximum speed. DNA pellet was air-dried and dissolved in 30 ml TE buffer (pH 8.0).

Endofree® plasmid maxi preparation was performed according to manufacturer's protocol (Endofree® Plasmid Maxi kit; Qiagen, Hilden, Germany) for the electrophysiology experiments.

The concentration of DNA was determined by measuring absorbance at 260nm using a Nanodrop2000 (Thermo Scientific, Wilmington, USA). The ratio between the absorbance values at 260nm and 280nm was taken as a quality control for DNA purity and should fall between 1.8 and 2.0.

### 2.3.2.4. DNA cloning of calcium channel subunit $\alpha_2\delta$ -1

In order to generate a mammalian expression vector, the coding sequence of the murine $\alpha_2\delta$ -1 was subcloned from the pBluescript vector into a pcDSA3 vector. Therefore new restriction sides for Kpn I and Not I were introduced via PCR with a Mfe I restriction side in the middle of the construct.

**Table 2.3:3: Primer used to introduce new restriction sides for subcloning of $\alpha_2\delta$-1 into pcDSA3 vector.**

| primer name | sequence |
|---|---|
| KpnI-$\alpha_2\delta$-fwd | 5′- ATG GTA CCA TGG CTG CTG GCT GCC TGC -3′ |
| $\alpha_2\delta$-NotI-rev | 5′- ATG CGG CCG CTC ACA GTA GGT AGT GTC TGC -3′ |
| $\alpha_2\delta$-MfeI-rev | 5′- TGG GGT TCT TTG GCT GAA GAT TTG G -3′ |
| MfeI-$\alpha_2\delta$-fwd | 5′- TCG TTT TAC ACT CTG TCC CAA TGG C -3′ |

PCR was performed using a master mix containing High fidelity PCR enzyme mix (Fermentas, Burlington, Canada) and corresponding buffer, deoxynucleoside triphosphate (dNTPs; Fermentas, Burlington, Canada) and the respective primer pairs following manufacturer's recommendations. The PCR cycling protocol was including a denaturation step at 95°C for 5 min, a 3-step amplification protocol with 37 cycles of 30 sec at 95°C, 1 min at 60 °C and 1 min at 72°C and a final prolongation step at 72°C for 5 min. The PCR amplification products were purified by exercising the DNA bands from an agarose gel containing 2 µl ethidium bromide stock solution (10 mg/ml; Roth, Karlsruhe, Germany) and the use of a GeneJET® gel extraction kit (Fermentas, Burlington, Canada). Digestion of PCR fragments with restriction endonucleases was

performed in 3 separate reaction mixtures. The pcDSA3 vector was digested with Not I and Kpn I in buffer 2 (10x) and the addition of 0.2 µl BSA at 37°C for 1 h. The two PCR fragments were cut with either Kpn I and Mfe I in buffer 1 or Not I and Mfe I in buffer 4 with the addition of BSA at 37°C for 1 h (all enzymes from NEB, Frankfurt, Germany). Digested DNA fragments were again purified with the help of an agarose gel and GeneJET® gel extraction kit. Purified digested DNA fragment concentrations were determined using a Nanodrop2000 and required amounts of DNA fragments were calculated in regard to basepairs and molecular weight. Determined amounts were used for ligation master mix containing 200 ng of digested vector and 150 ng of each $\alpha_2\delta 1$ fragment. With the help of 2.5 units of T4 DNA ligase (Fermentas, Burlington, Canada) and corresponding buffer, the three fragments were ligated over night at 16°C to result in the insertion of the murine $\alpha_2\delta 1$-coding sequence in a mammalian expression vector pcDSA3. The resulting clones were confirmed by sequencing as described in section 2.3.3. The cloning was successful, but showed one point mutation containing a cytosin instead of a thymin at bp 292. This was corrected by the use of QuikChange II XL site-directed mutagenesis kit® (Stratagene, Santa Clara, CA, USA) according to manufacturer's protocol. Primers were designed using Stratagene's web-based QuikChange® Primer Design Program (B 1.6) according to the kits guidelines. Resulting mutagenesis clone was again sequenced and correctness of the coding sequence of $\alpha_2\delta$ 1 and correct orientation within the vector was confirmed.

### 2.3.3. Sequencing of plasmid DNA

Around 400 ng of plasmid DNA was taken as a template for sequencing. For the PCR master mix 0.25 µl BigDye ® terminator V1.1 (Applied Biosystems, Foster City, CA, USA), 2.25 µl 5x BigDye sequencing buffer and 0.25 µl primer (10 µM) were added. The reaction mixture was diluted to 10 µl. The PCR cycling program included 32 cycles with 10 sec denaturation at 96°C, 5 sec annealing at 55°C and a 4 min elongation step. After amplification the sequencing was done by the Cologne center for Genomics (University of Cologne, Germany) as a service with an Applied Biosystems 3730 DNA analyzer. Sequences were analyzed using FinchTV (Geospiza, Seattle, WA, USA) and MacVector Assembler (Cambridge, UK).

## 2.3.4. Eukaryotic cell culture

Native HEK293 (Human Embryonic Kidney) cells were cultured under normal growth conditions at 37°C and 6% $CO^2$ in 60 mm polystyrene Petri dishes (Falcon, Heidelberg, Germany). All procedures to cultivate or transfect cells were carried out under a sterile laminar flow hood to prevent contamination. Media and PBS were warmed in a water bath at 37°C before use.

**Table 2.3:4: Solutions for cell culture.**

| | |
|---|---|
| Cell culture medium | 500 ml 1xDulbecco's modified Eagle medium (DMEM; Gibco, Grand Island, USA) |
| | 50 ml fetal calf serum (FCS; PAA, Pasching, Austria) |
| | 2.75 ml antibiotics (100x penicillin-streptomycin solution, PAA) |
| PBS | 1x Dulbecco's phosphate-buffered saline (PAA, Pasching Austria) |
| Trypsin | 1x trypsin-ethylenediaminetetraacetate (EDTA: PAA, Pasching, Austria) |

Trypsinization was used to detach the adherent cells from the surface of cell dishes for passaging. Therefore, the culture medium was carefully aspirated from the cell culture dish and cells were gently washed with 4 ml PBS. The cells were incubated with 700 µl Trypsin-EDTA for 2 minutes at 37 °C. Cells were resuspended in 3 ml fresh medium and a fraction of 300-600 µl was transferred into new 60 mm dishes and filled up to 4 ml with cell culture medium. For subculturing cells were routinely passaged twice a week.

## 2.3.5. Transient transfection by non-liposomal reagent

The examined $Ca_V1.2$ channel complexes were expressed in HEK293 cells by using transient transfection of the $Ca_V1.2$ subunits. The pore forming $Ca_V1.2$ subunits $Ca_V1.2_{exon\ 21}$ ($\alpha_{1c}$-KN) or $Ca_V1.2_{exon\ 22}$ ($\alpha_{1c}$-Cl16 K) were coexpressed with one of the β subunits ($\beta_{2b}$, $\beta_{2d}$, $\beta_{3A}$) and the $\alpha_2\delta$-1 subunit. For all experiments an enhanced green fluorescent protein (eGFP) was cotransfected to distinguish the successfully transfected cells. The amounts of $Ca_V1.2$, β subunit, $\alpha_2\delta$–1 and eGFP plasmids were 1 µg, 0.5 µg, 0.75 µg and 0.3 µg,

respectively. The DNA mixture was introduced into the HEK293 cells by Effectene® transfection reagent (Qiagen, Hilden, Germany). In brief, HEK293 cells were seeded onto 60 mm dishes one day before transfection to reach 70-80 % confluency on the day of transfection. The DNA mixture (2.55 µg) was diluted with the DNA-condensation buffer to a total volume of 150 µl and 20 µl enhancer was added, vortexted and incubated at room temperature for 3 minutes. Then, 62.5 µl Effectene® was added and samples were incubated at room temperature for 10 min to allow transfection complex formation. Culture medium was aspirated from seeded cells, cells were washed once with PBS and fresh growth medium was added to the cell. The transfection complexe mixture was diluted in 1 ml growth medium and added drop wise onto the cells. Cells were incubated with transfection complex at 37 °C over night. After incubation, the medium containing the complexes was removed and cells were passaged into 35 mm Petri dishes for electrophysiology.

### 2.3.6. Patch-clamp technique

The patch-clamp technique was developed by Neher and Sakmann in 1976 to measure currents through single acetylcholine-activated channels in cell-attached patches of membrane of frog skeletal muscle [103]. Principle of this method is to electrical isolate a small part of the membrane by attaching the tip of a glass micropipette. A high resistance seal (gigaohm seal, >1GΩ) is achieved by gentle pressing of the tip against the membrane of a cell followed by gentle suction through the pipette.

This gigaohm seal is the requirement for several possible patch-clamp configurations (Figure 2.3.3:1): A) cell-attached recordings where the cell membrane stays intact after gigaseal formation. Small patch size allows current recordings through a single ion channel in the patch. B) inside-out patch made by pulling the membrane patch off the cell into the external solution. C) whole-cell recording is achieved by rupturing the membrane patch using more suction and the cytoplasm is connected to the pipette solution. This configuration is used to investigate the activity of all channels expressed in the patched cell. D) Outside-out patch which can arise out of the whole-cell configuration by pulling away the pipette isolating the piece of membrane patch and building a convex

membrane on the end of the pipette. The configuration under A, B and D can be used for recording of single-channel activity.

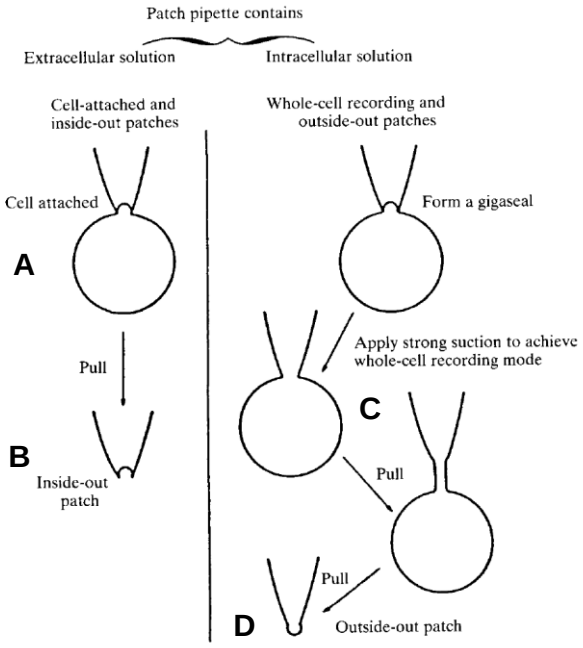


**Figure 2.3:1: Diagram illustrating the different patch-clamp configurations (modified from [104]).**

The patch-clamp technique for whole-cell recordings is based on the voltage-clamp method described by Hodgkin and Huxley in 1952 [105]. It allows to record the transmembrane current and the controlled input is the "clamped" membrane voltage applied to the cell examined [106]. It can be applied to small cells and in vivo measurements.

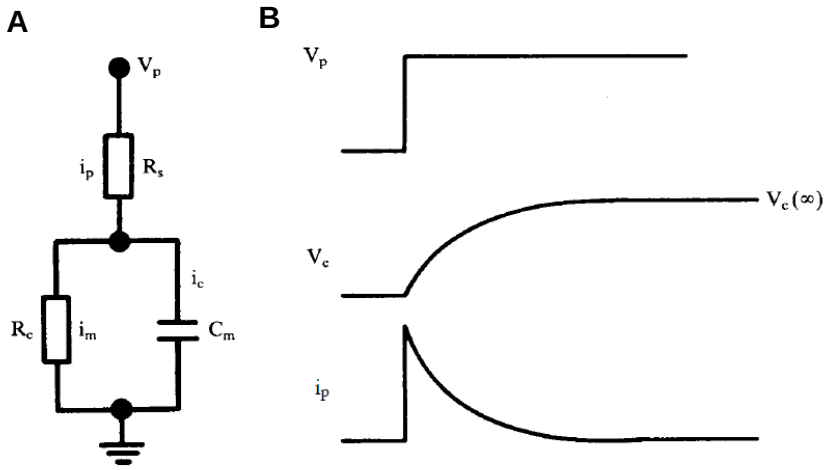


**Figure 2.3:2: (A) Simplified circuit of a whole-cell recording: Current im flows in the cell resistance Rc and ic in the capacitance. Pipette current (ip) equals im +ic and flows in the series resistance Rs between pipette and cell and produces a voltage error Vp –Vc = ipRs. (B) time course of changes of Vc and ip following a step of Vp (adapted from [104]).**

## 2.3.7. Patch-clamp set up

Patch-clamp experiments were performed in a Faraday cage to shield the recording electrode from external alternating current (AC) fields (fig. 2.3.4:1). The apparatus also requires a vibration-cushioned table (Barry controls GmbH, Raunheim, Germany) and an inverted fluorescence microscope (Nikon corporation, Japan). The micropipette, including the recording electrode, is directed by a hydraulic micromanipulator (MHW-103, Narishige International, Tokyo, Japan) towards the cell and a headstage preamplifier (Gain: x1/10, Axon Instruments, CA, USA) is connecting the electrode and the main amplifier (Axopatch 1D, Axon Instruments, CA, USA). Because currents detected in the experiments are at the range of pA to nA, specialized amplifiers are used for high-resolution current recordings. Recording electrode and bath electrode were coated silver wires. For coating, silver wires were cleaned with ethanol and immersed into a 3 M KCL solution. The wire was connected to an anode of a direct current voltage source and a current of 1 mA was applied until the wire was uniformly blackened.


**Figure 2.3:3: Patch-clamp set up: (1) A/D converter (2) patch-clamp amplifier (3) Faraday cage (4) vibration-cushioned table (5) inverted fluorescence microscope (6) headstage with pipette holder (7) hydraulic manipulator**

For preparing the micropipettes, borsilicate glass capillaries (OD/ID: 1.7/1.42 mm, Hilgenberg, Malsfeld, Germany) were cut in 72 mm length and pulled into two symmetrical micropipettes with a P-97 pipette puller (Sutter instruments, CA, USA). Pipettes were prepared on the day of measurement and fire polished using Narishige

Microforge (Tokyo, Japan). Pipette resistance was between 1.8 – 3.0 MΩ for whole cell recordings.

## 2.3.8. Whole-cell recordings

Whole-cell recordings were obtained 48 - 72 hours after transfection. Prior to recordings, cells in 35-mm cultures dishes were washed with freshly prepared external bath solution and maintained at room temperature (19-23 °C). The patch pipettes were filled with filtered pipette solution (0.2 μm injection filter; Braun, Melsungen, Germany) and attached to the pipette holder including the recording electrode. Whole-cell recordings were performed by formation of a gigaohm seal of a fluorescence-positive HEK cell by gentle suction. A stable gigaohm seal is essential before penetrating the membrane for whole-cell channel measurement. The fast capacity transients flanking the 5 mV test pulse (figure 2.3.5:1; A) are mainly associated with pipette capacitance to the bath and are compensated. The potential of the pipette interior is adapted to the estimated membrane potential. Further suction disrupts the small membrane patch building whole-cell configuration (C) and the cell interior is in contact with pipette solution.

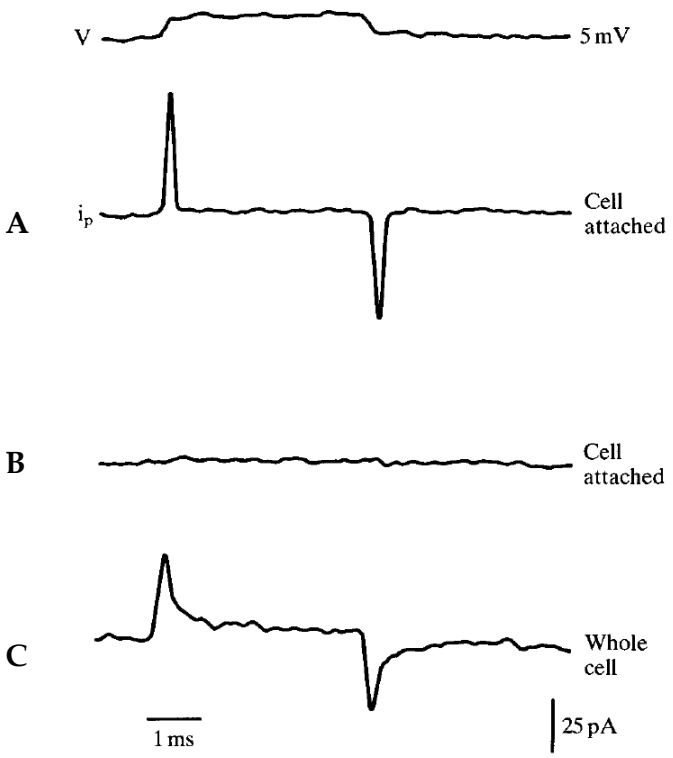


**Figure 2.3:4: The transient currents in a cell-attached record before (A) and after (B) cancellation with $C_{fast}$ and $\tau_{fast}$. These transient currents are due to (pipette) capacitance. (C) A whole-cell recording showing flanking capacity transients due to cell capacitance (modified after [104]).**

For whole-cell recordings, currents were typically elicited from a holding potential of -80 mV to various test protocols using Clampex software pClamp 5.5 and an Axopatch 1D amplifier (Axon Instruments, Foster City, CA, USA). Data were filtered at 2 kHz and digitized at 10 kHz directly onto a personal computer. The experiments were performed with barium as the charge carrier to evaluate the voltage-dependent inactivation in the absence of calcium-dependent inactivation [107]. For data analysis pClamp 5.5, Origin 6.0 and Graph pad prism 4 were applied.

**External bath solution**

| | |
|---|---|
| $BaCl_2$ | 10 mM |
| $MgCl_2$ | 1 mM |
| CsCl | 65 mM |
| TEA-Cl | 65 mM |
| Glucose | 10 mM |
| HEPES | 10 mM |
| pH adjusted to | 7.3 with TEA-OH |

**Internal pipette solution**

| | |
|---|---|
| CsCl | 140 mM |
| $MgCl_2$ | 1 mM |
| Mg-ATP | 4 mM |
| EGTA | 10 mM |
| HEPES | 9 mM |
| pH adjusted to | 7.3 with CsOH |

### 2.3.8.1. Pulse protocols

Current-family protocol was used to obtain current-voltage relationships (I/V) of the recorded cells. Therefore cells were depolarized from a holding potential of -80 mV to the

test pulses (-40 mV to +50 mV) for 150 ms in 10mV steps. Time between single pulses was 5 sec.

To determine the current-voltage relationships, peak current amplitude of each test pulse was calculated by subtraction of the leak current of every trace from the maximal current. The peak current was divided by the respective cell capacitance to obtain the current density-voltage relationships. I/V relationship are presented as mean ± SEM. To determine V 0.5 act and slope factor, I/V curves were fitted by a combined Ohm and Boltzmann relation

$$I_V = G_{max} (V-V_{rev})/(1+\exp[-(V-V_{0.5act})/k])$$

Here $I_V$ is the current density at voltage V, $G_{max}$ is the maximal slope conductance $pF^{-1}$, $V_{0.5act}$ is the half maximal activation voltage, $V_{rev}$ is the reversal potential, and k is the slope factor.

The extent of inactivation at 150 ms (% inactivation) was calculated by the following equation where $I_{150\ ms}$ is a current at the end of the test pulse and I peak the peak amplitude:

$$\%\ \text{inactivation (150 ms)} = 1- (I_{150\ ms}/ I_{peak})$$

The time constant τ was obtained by a mono-exponential fit of the slow inactivation phase of I/V currents.

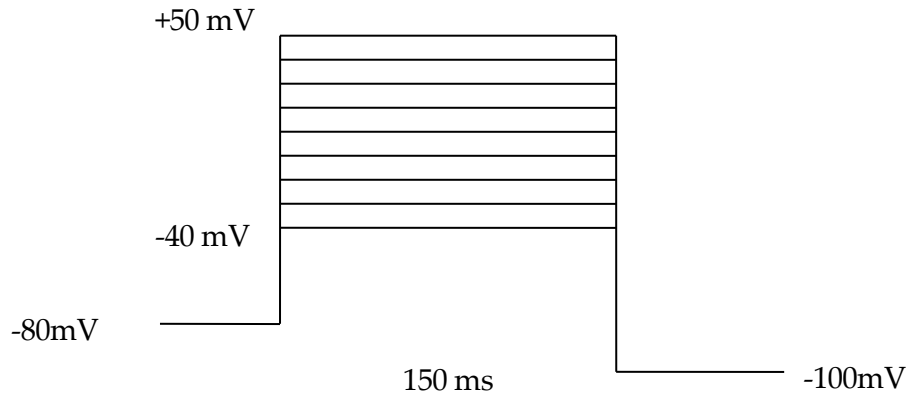


**Figure 2.3:5 Pulse protocol for voltage current family recording**

A two steps tail current protocol was used to determine the current activation of $Ca_V1.2$ channels. Here, Barium tail currents were recorded at -50 mV following different test pulses (between -70mV and +80 mV). The test pulses were repeated every 5 s.

The cell is forced by these pre-pulses to open an amount of channels in relation to the voltage potentials and leading to a voltage-dependent activation. The potential is then stepped back to a standardized potential (-50 mV) to determine the activation – the electromotive force (EMF) is standardized for all episodes and therefore the different currents are caused only by the voltage-dependent activation of the channels. The voltage-dependent activation was calculated by determination of the relative amplitude of the tail currents ($I/I_{max}$) as a function of conditioning potentials. Analysis was performed using the Boltzmann function:

$$I_{max}/(1+\exp[(V_{0.5act}-V)/k_{act}])$$

where $I_{max}$ is the maximum tail current, $V_{0.5act}$ the midpoint of voltage-dependence of activation and $k_{act}$ the slope factor.

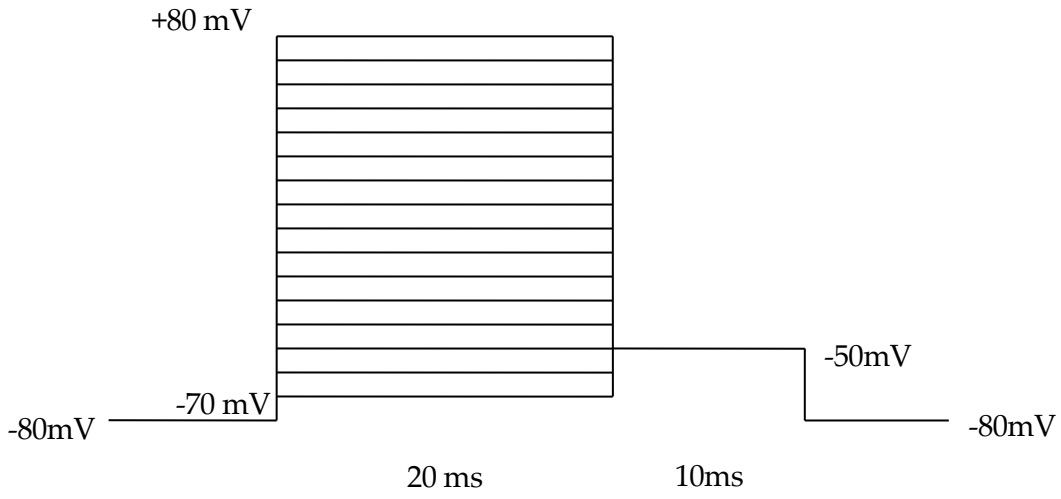


**Figure 2.3:6 Pulse protocol for tail current recordings.**

The voltage dependence of current inactivation of the $Ca_V1.2$ channel was determined using a steady-state inactivation protocol. During the long conditioning prepulse equilibrium (= steady state) is set up between open, closed and inactivation state (figure 2.3.4.1:3). To quantify the part of the channels which are not inactive yet, the cell is

pulsed to + 10 mV forcing all non-inactive channels to open. The voltage-dependence of inactivation was calculated by taking the relative amplitude of the steady-state current ($G/G_{max}$) as a function of the test pulses. Data were fitted with the Boltzmann equation.

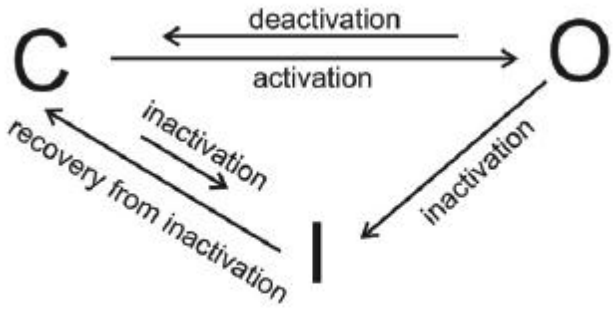


**Figure 2.3:7 Diagram of gating transitions of a voltage-dependent calcium channel (adapted from [106])**

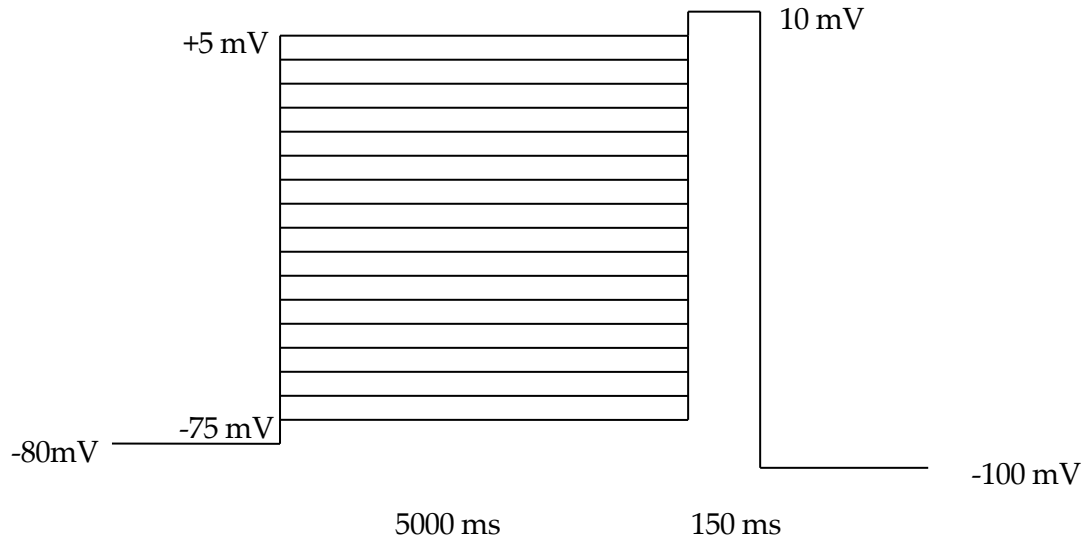


**Figure 2.3:8 Steady-state inactivation protocols. After a 5000ms conditioning pulse a 150 ms test pulse at +10mV was applied. The pre-pulses were ranged between -75mV and +5mV in 5mV steps.**

# 3. Results

## 3.1. Expression-profiling of L-type calcium channel subunits in human arteries

### 3.1.1. Characterization of arterial sections for laser capture microdissection

As a first approach of expression-profiling of L-type calcium channel (LTCC) subunits in human arteries, vascular smooth muscle cell (VSMC) areas were isolated via laser capture microdissection. The subsequent relative quantification via quantitative real time PCR (qRT-PCR) required a definition of atherosclerotic areas with proliferative vascular smooth muscle cells and adjacent control areas. Therefore, immunohistochemical stainings for vascular smooth muscle cells (antibody against smooth muscle actin, SMA) and proliferation (antibody against Ki 67) were used to classify the different areas within one sample. Furthermore, morphology of section accounted for classification.

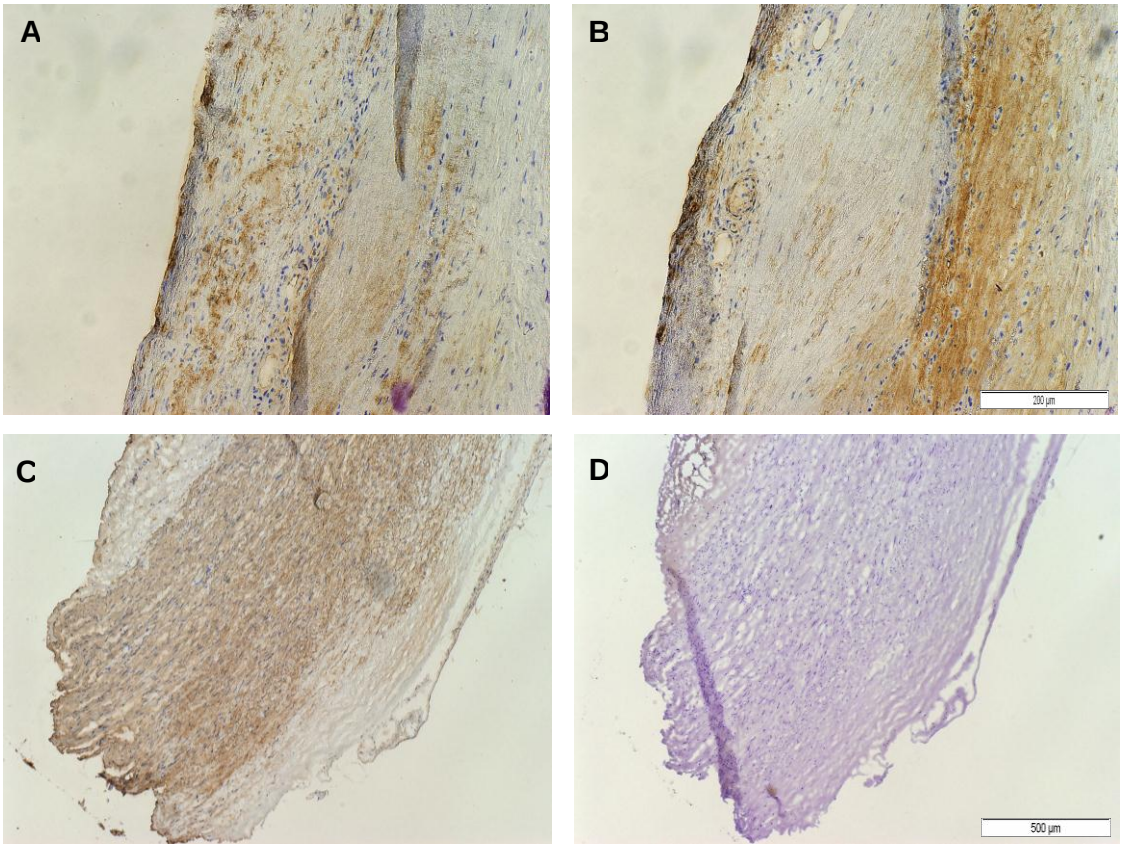


**Figure 3.1:1 Representative immunohistochemical patterns of the arterial preparation used for laser microdissection of VSMC and isolation of RNA from areas of proliferative smooth muscle cells (A,B) and adjacent control areas (C,D) that had no obvious evidence of atherosclerosis. Shown are photo-micrographs after staining of serial sections of femoral arteries with antibodies against smooth muscle actin (SMA, A,C) and and Ki 67 (B,D), a marker of cellular proliferation.**

The implementation of this differentiation within one sample - between atherosclerotic and control areas – revealed difficulties finding both in one sample. The majority of samples showed atherosclerotic changes in cell structure in all serial cuts. Areas with no obvious evidence of atherosclerosis were rarely found and were then reflected throughout the whole sample. Hence the characterization and the following classification were carried out sample wise.

Furthermore the carotid artery samples were showing excessive atherosclerotic changes descend right of out of heavy plaques areas. In contrast the femoral artery samples were represented by more early stage atherosclerotic changes with origin only close the atherosclerotic narrowing due to surgery procedures.

### 3.1.2. Isolation of RNA from microdissected and whole tissue arterial samples

The isolation of sufficient RNA amounts and quality from the microdissected samples proved to be challenging. Variation within the method (chapter 2.1.3) still led to poor RNA amounts. Testing the method with liver biopsy serial cuts led to suitable RNA amounts and quality.

Having a closer look on RNA quality of the whole-tissue artery samples, some RNA samples already show degradation products and low quantity (RIN 5,87, 123 ng/µl; Figure 3.1:2 A) with a validated RNA isolation protocol (as comparison see also Figure 3.2:3). As these tissue biopsies were taken within operation procedures, this low quality could be due to relatively long time duration until flash freezing in liquid nitrogen or great blood amounts containing high amounts of RNases. For further analysis of whole tissue samples, only isolated RNA with high quality was used.

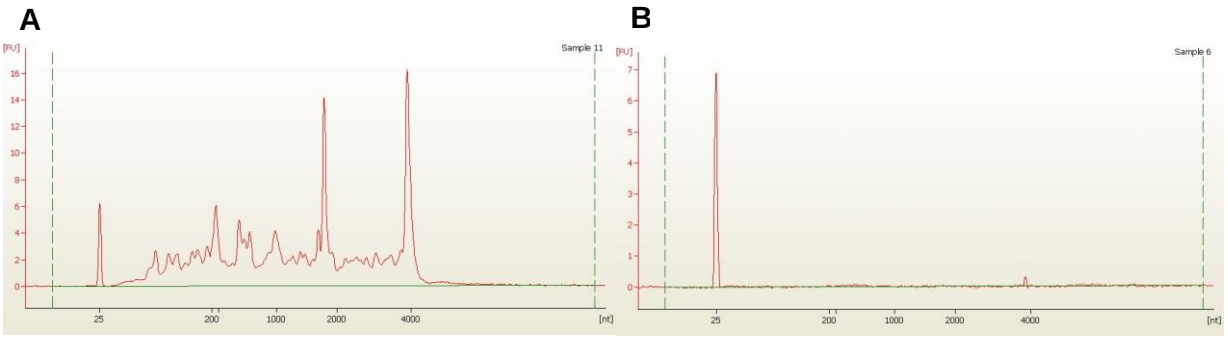


**Figure 3.1:2 Results of a RNA pico LabChip® of (A) isolated RNA from an exemplary human side-branch of the femoral artery (RIN 5, 87, 123 ng/µl) with degradation products and (B) exemplary microdissection sample with no detectable concentration and quality. The detection minimum of a RNA pico LabChip® is going down to 50 pg/µL of total RNA.**

### 3.1.3. Expression-profiling of LTCC subunits in microdissected vascular smooth muscle cells

With the technique of laser capture microdissection, VSMC areas could be isolated from the serial section of arteries. Due to problems isolating sufficient RNA amounts (see chapter 3.1.2) only a few samples could be analyzed with very high Ct values (Ct values around 29-35). With the help of melting curve analysis at the end of each qRT-PCR one can exclude that fluorescence signals arise from contamination or primer dimers and each melting curve could be assigned to the specific amplicon.

**Table 3.1:1 Expression pattern of LTCC subunits in microdissected samples of human arteries. RNA was isolated from microdissected VSMC areas and analyzed by qRT-PCR with 18S RNA as a reference gene. Each column is reflecting one individual sample. The + scale is reflecting the relative mRNA expression levels based upon Δ ct values. No symbol means that expression is not detectable.**

| Human microdissection samples | | | | | | | |
|---|---|---|---|---|---|---|---|
| | Atherosclerotic areas | | | | | control areas | |
| | A. carotis | | A. femoralis | | | A. femoralis | |
| exon 21 | | | | | ++++ | ++++ | |
| exon 22 | | | | ++++ | ++++ | ++ | |
| β1 | | | | | | ++++ | ++++ |
| β2 | ++ | ++++ | ++ | | ++++ | +++ | |
| β3 | | | | | | +++ | |
| β4 | | | | | | +++ | |

| | **Δ ct values** |
|---|---|
| **++++** | up to 11 |
| **+++** | >11 to 13 |
| **++** | >13 to 15 |
| **+** | >15 to 17 |
| + | >17 to 19 |
| + | >19 to 21 |
| | no signal |

The qRT-PCR data reveals that both, exon 21 and exon 22, are expressed on mRNA level – in atherosclerotic as well as in non-atherosclerotic control VSMC areas. The β2 isoform is the only consistently detectable β subunit in the atherosclerotic VSMC areas. In control areas from femoral artery samples all four β subunits are detectable with β1 being predominant.

### 3.1.4. Expression-profiling of L-type calcium channel subunits in whole-tissue samples of human arteries

Since the isolation of sufficient amounts of RNA from the microdissected VSMC was problematic, whole arterial biopsy samples were analyzed as well. The examination of the expression-profile of LTCC subunits in atherosclerotic and non-atherosclerotic whole-tissue samples required a control group for relative quantification using qRT-PCR and the ΔΔct analysis. Samples of patients undergoing stent surgery or amputations due to non-atherosclerotic reasons (e.g. traumatic rupture of arteries) are rare and therefore a problem to serve as control group. In this study, 2 of such samples were collected over the year and taken as a first idea of a control group.

**Table 3.1:2 Expression-pattern of LTCC subunits in whole-tissue samples of human arteries. RNA was isolated from whole tissue samples and analyzed via qRT-PCR. Taking 18S RNA as a reference gene, + scale is reflecting relative mRNA expression levels based upon Δ ct values.**

| Human arteries – whole tissue samples | | | | | | | | | | | |
|---|---|---|---|---|---|---|---|---|---|---|---|
| | Atherosclerotic samples | | | | | | | | | Control | |
| sample | A. carotis | | A. femoralis - branch | | | | A. femoralis | | | A. femoralis | |
| exon 21 | + | + | + | + | ++++ | ++++ | + | + | ++ | ++ | ++ |
| exon 22 | + | + | + | + | ++ | ++ | + | + | + | + | + |
| β1 | + | + | + | ++ | +++ | ++++ | + | + | + | ++ | + |
| β2 | + | + | + | ++ | +++ | ++++ | + | + | + | ++ | + |
| β3 | + | + | + | + | ++ | +++ | + | + | + | + | + |
| β4 | + | | + | ++ | ++ | +++ | + | + | + | + | + |

| | **Δ Ct values** |
|---|---|
| **++++** | up to 11 |
| **+++** | >11 to 13 |
| **++** | >13 to 15 |
| **+** | >15 to 17 |
| + | >17 to 19 |
| + | >19 to 21 |
| | no signal |

The results of the Δct analysis of whole-tissue samples reinforce the finding that exon 21- as well as exon 22-containing Cav1.2 subunit is expressed on mRNA level. The exon 21 containing Cav1.2 seems to be the predominant splice variant. The mRNA of all four β subunits can be found in human arteries, β1 and β2 seem to be more abundant then β3 and β4.

Looking at the expression profile of each sample, inter-individual differences are clearly seen. Also differences between the diverse sources of sample-taking are represented in the variation of data. Due to the variability between the samples of different origin and assumed differences in stage of atherosclerosis, the comparative ΔΔCt analysis was only possible between the atherosclerotic and non-atherosclerotic femoral artery samples.

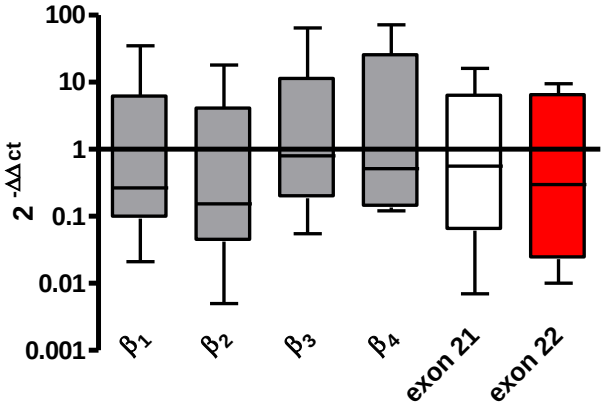


**Figure 3.1:3 Expression-profiling of LTCC subunits in atherosclerotic (n=7) and non-atherosclerotic (n=2) femoral artery whole-tissue samples. Relative expression comparing the two groups is given as $2^{-\Delta\Delta Ct}$ values using S18 rRNA as a reference gene. Data is shown as "box and whisker" plots (median, 1st and 3rd quartile, minimum and maximum). The median of all LTCC subunit mRNA level is decreased in comparison to the atherosclerotic samples. The analysis also displays the high diversity of results.**

The ΔCt analysis supports the findings above, both exon 21 and exon 22 are expressed with exon 21 being predominant spliced exon in the femoral artery samples (data not shown here). All 4 β subunits are expressed looking at the whole tissue samples. The relative expression, comparing atherosclerotic and non-atherosclerotic samples, displays a slight decrease in LTCC subunit expression on mRNA level in atherosclerotic samples.

### 3.1.5. Absolute quantification of exon 21 and exon 22 using oligo standards

Since it was difficult to find non-atherosclerotic control samples or control VSMC areas, an attempt was to establish standards for absolute quantification via qRT-PCR. There were no validated results for absolute quantification using plasmids as calibrator. Calculation of the copy number led to inexact results and the Ct values were ceiling at around a cycle number of 30 due to carryover of plasmids in the low concentration range.

An accurate way of absolute quantification is the use of synthesized oligonucleotides of the specific amplicons plus small overhang. However, they cannot be synthesized easily when size of the amplicon exceed 120 bp due to an increasing error rate. Therefore, the amplicons of primer pairs of exon 21 and exon 22 where chosen to evaluate the standards for absolute quantification.

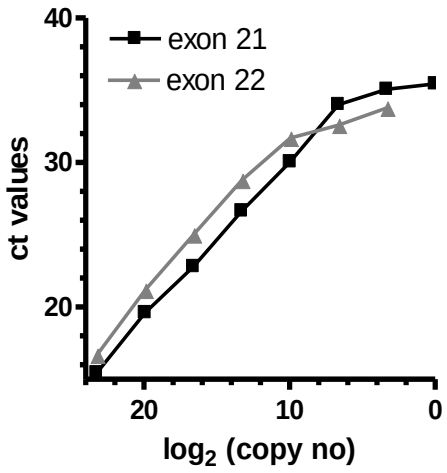


**Figure 3.1:4 Standard curves for determination of concentration of the sample of interest. The Ct values are drawn against the log 2 copy number of oligonucleotide standard. At Ct values around 32 (exon 22) or 34 (exon 21) determined values are showing a ceiling effect.**

The standard curves are also changing their slope factor at around Ct values of 32 (exon 22) and 34 (exon 21). Above these ct values, thus at low copy numbers, the method is not suitable.

# 3.2. Expression-profiling of L-type calcium channel subunits in an atherosclerotic mouse model

## 3.2.1. Development of atherosclerosis in apoE -/- mice

ApoE -/- mice, fed with a western-type diet, develop up to stage V lesions with increasing age [98]. As shown in Figure 3.2:1, the chosen age groups of apoE -/- mice, fed with western-type diet, represent different stages of atherosclerosis. The sections at the height of the aortic sinus show clearly a development of increasing lesion areas with age (74.39 ±13.11 vs. 143.6 ± 6.12 vs. 204.6 ± 14.26 x 1000 $\mu m^2$ given as mean + SEM). The control apoE -/- mice at the age of 12-14 weeks, fed with normal diet, show only small or no atherosclerotic plaques (picture not shown; 5.86 ± 3.4 x 1000 $\mu m^2$). Wildtype C57/Bl6 mice, which were chosen as a healthy control, do not show a development of atherosclerotic plaques. Even those fed with a western-type diet over 8-10 weeks are not showing the development of atherosclerotic lesions (picture not shown).

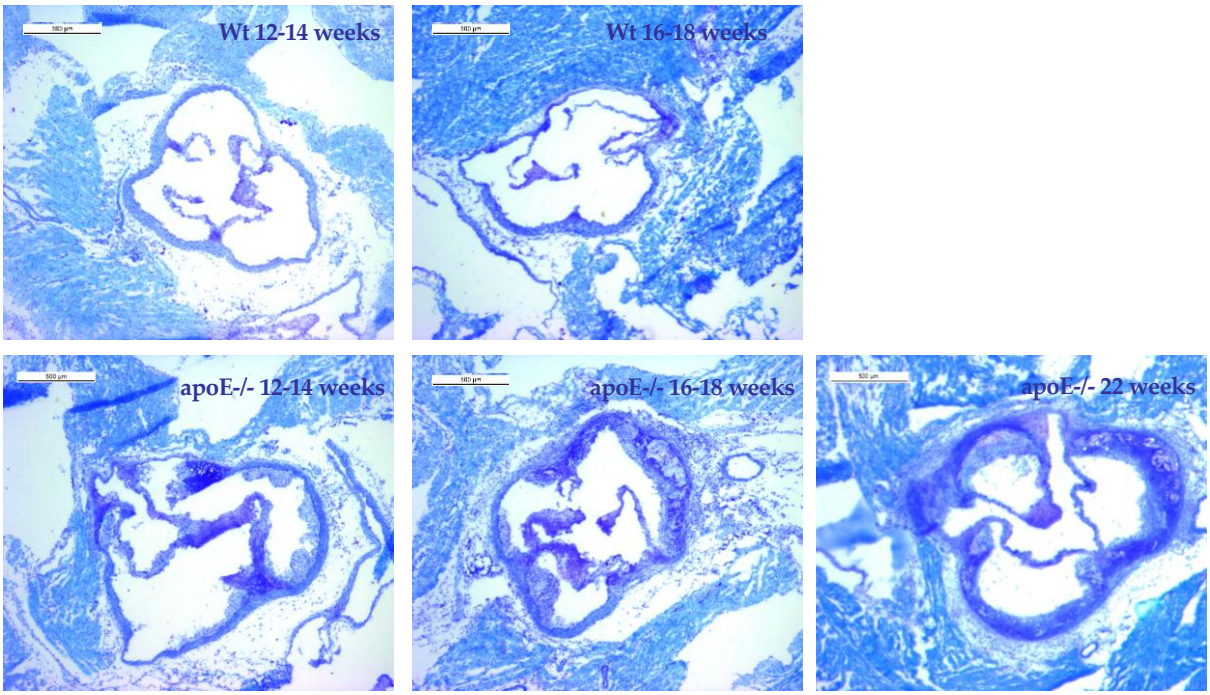


**Figure 3.2:1 Toluidin-blue staining of the aortal cross-sections at the height of the aortic sinus of the animals used in this study. Development of atherosclerosis is seen with increasing age of the apoE -/- mice all fed with western-type diet.**

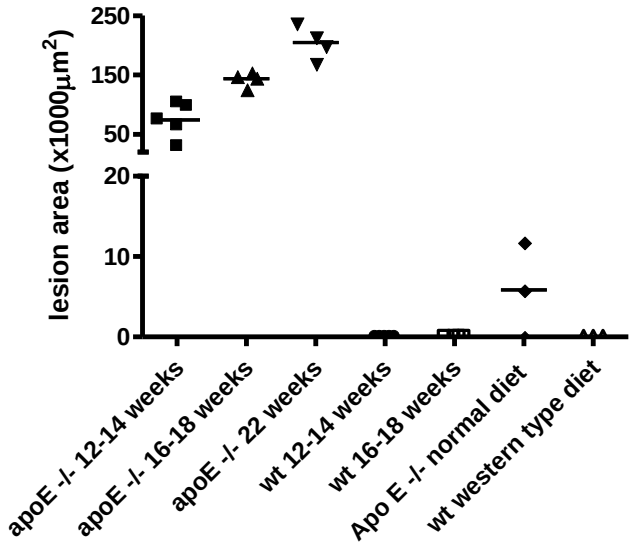


**Figure 3.2:2 Graph is showing quantification of atherosclerotic lesion size at the aortic sinus. The progression of atherosclerosis is seen in the increasing lesion area with increasing age of the apoE -/- mice (74.39 ± 13.11 vs. 143.6 ± 6.12 vs. 204.6 ±14.26 x 1000 µm² given as mean ± SEM ). Control apoE -/- mice fed with a normal diet developed only small lesion areas at the age of 12-14 weeks (5.86 ± 3.4 x 1000 µm²). Values are given as lesion area (x1000 mm2) as a scatter dot-plot with mean.**

In the following mRNA expression studies all apoE -/- mice investigated were fed with a western-type diet from the age of 5 weeks. All wildtype mice were fed with a normal diet.

### 3.2.2. Quality of the isolated RNA

The quality of RNA is essential for quantitative real-time PCR. Poor RNA quality leads to an impairment of data quality [108]. As a quality control with respect to degradation and contamination the results of the RNA pico LabChip® were taken. Results show that the method used to isolate RNA is suitable to result in high quality RNA. All samples showed a RIN value between 8.5 and 9.5 which is a proof for high integrity [109]. The ratios of 28S/18S lay between 1.8 and 2.0.

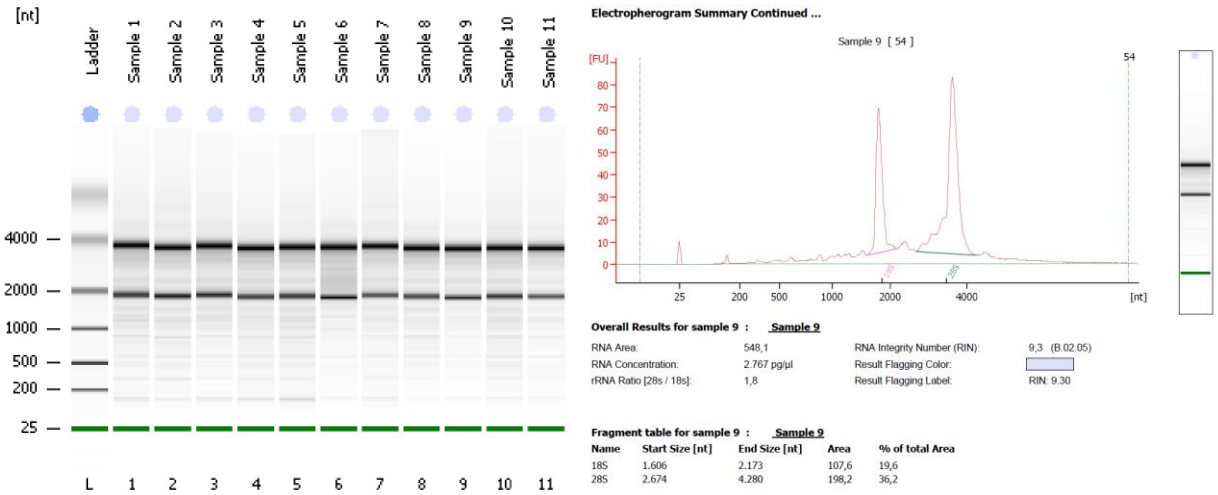


**Figure 3.2:3 Results of a RNA pico LabChip® of murine aortic tissue samples. Result overview showing RNA gel electrophoresis and an exemplary electropherogramm summary including RIN, concentration and rRNA ratio.**

### 3.2.3. Real-time PCR analysis of L-type calcium channel subunits in murine aorta

The mRNA expression level of LTCC subunits was determined in the aortic arch of wildtype and apoE -/- mice using quantitative real-time PCR (qRT-PCR). Different age groups were chosen to represent the progression of atherosclerosis over time.

Transcripts of all three β subunit isoforms investigated were present at different expression levels in all animals. $\beta_2$ and $\beta_3$ are the predominant β subunits in the aorta whereas $\beta_1$ shows only low expression on mRNA level. In apoE-/- mice as well as in wildtype mice both exon 21- and exon 22-containing Cav1.2 subunit mRNA were found. The exon 22-containing splice variant of the pore-forming Cav1.2 is more abundant. In older apoE -/- mice the ratio of exon 21- exon 22 is significantly changing (12-14 weeks old 0.409 ± 0.038 vs. 16-18 weeks

old 0.613 ± 0.107; p=0.0422). The mRNA amount of exon 22 is decreasing whereas exon 21 is staying at the same level (Figure 3.2:4).

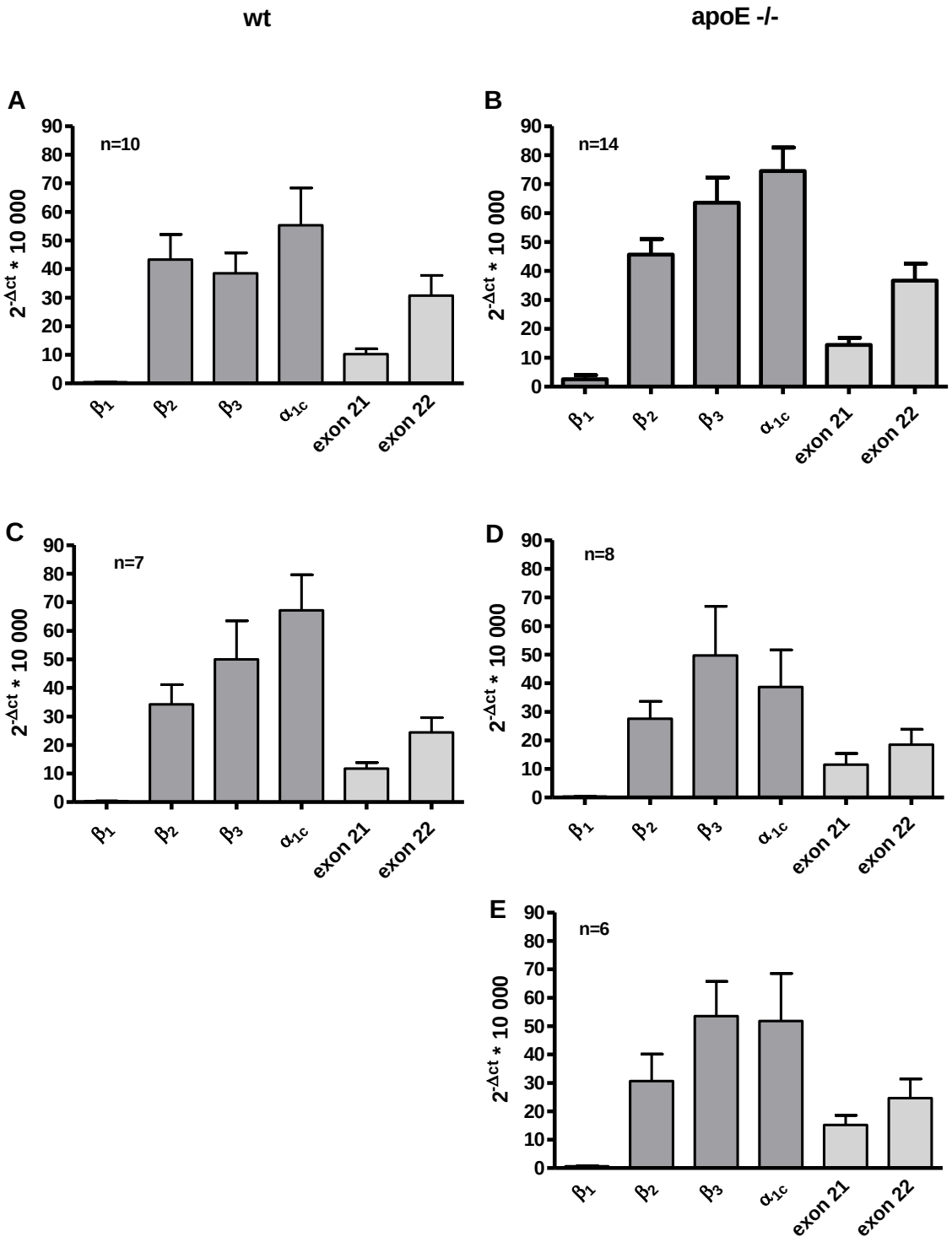


**Figure 3.2:4 Expression-pattern of the LTCC subunits of wt (A,C) and (B) apoE -/- (B,D,E) mice at the different stages of atherosclerosis. The mRNA expression is given as $2^{\Delta ct}$ values using S29 as a reference gene. The top row is showing wt and apoE -/- mice at the age of 12-14 weeks (A,B), the middle row the age group of 16-18 weeks (C,D) and the bottom row is representing apoE -/- mice at the age of 22 weeks (F). $2^{-\Delta ct}$ values are shown as geometrical mean + SEM.**

Relative quantification was used to detect any changes of LTCC isoform expression in between apoE -/- and wildtype or in between further progression of atherosclerosis in older apoE -/- animals. The ΔΔct values show a transient increase of LTCC subunits in apoE -/- mice compared to wt mice at the age of 12-14 weeks. $\beta_1$ and $\beta_3$ are significantly increased (p= 0.0391 and p=0.0217). With increasing age and stage of atherosclerosis LTCC subunits are decreasing (see Figure 3.2:5 B and C) compared to 12-14 week old apoE -/- mice. In contrast, the wt mice do not show a change in mRNA levels with increasing age (Figure 3.2:5 D). At the age of 16-18 weeks $\beta_1$, $\beta_2$ and $\alpha_{1c}$ as well as exon 22 are significantly decreased. In an advanced stage of atherosclerosis at the age of 22 weeks the apoE -/- mice show still a decrease of LTCC subunits on mRNA level compared to 12-14 week old animals but no further decrease compared to 16-18 week old apoE -/-. There is no clear-cut switch of LTCC subunit expression within the development of murine atherosclerosis.

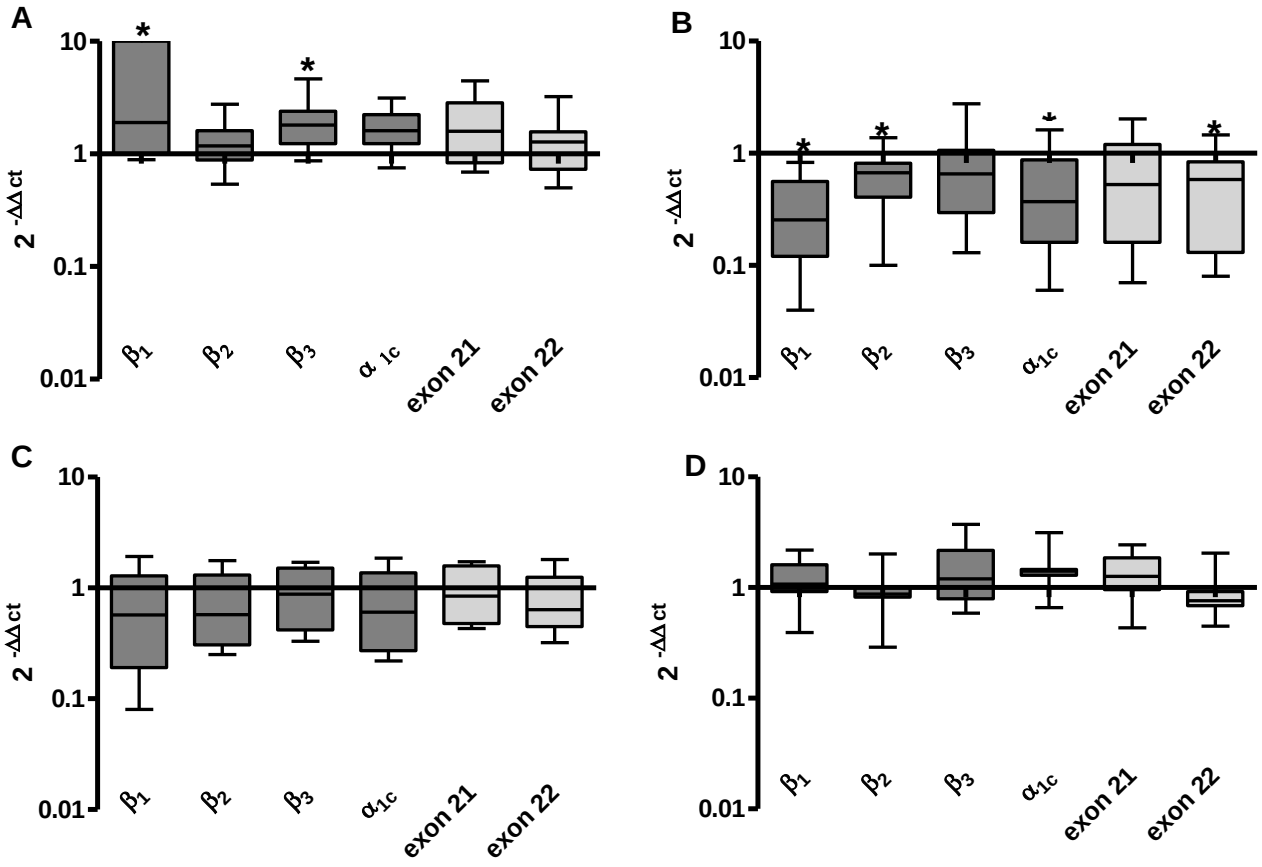


**Figure 3.2:5 Relative expression of LTCC subunits, given as $2^{-\Delta\Delta ct}$ values , of (A) Apo e-/- mice compared to wt mice at the age of 12-14 weeks. (B) is showing 16-18 week old apoE -/- mice compared to 12-14 week old apoE -/- mice and (C) 22 week old ApoE -/- compared to 12-14 week old apoE -/- mice. (D) $2^{-\Delta\Delta ct}$ values of 16-18 week old wt mice compared to 12-14 week old wt mice. Data is shown as "box and whisker" plots**

**(median, 1st and 3rd quartile, minimum and maximum). Significant differences are marked by *$p<0.05$ (Student's t-test of · ct values).**

## 3.2.4. Qualitative detection of exon 21 and exon 22 in the murine aorta

As a confirmation that both alternatively spliced exons 21 and 22 are present, a qualitative PCR method was exercised. Reverse transcriptase-PCR (RT-PCR) with primers spanning exon 18 to 27 of the pore forming Cav1.2 followed by Avr II digestion clearly display that both exons are present in wt and in apo E -/- mice. The single band at the level of 913 bp stands for the undigested exon 21 whereas exon 22 is digested by Avr II and is represented by the two bands at the height of 542 and 371 bp. There is no sign for an exon switch in atherosclerotic aortic tissue.

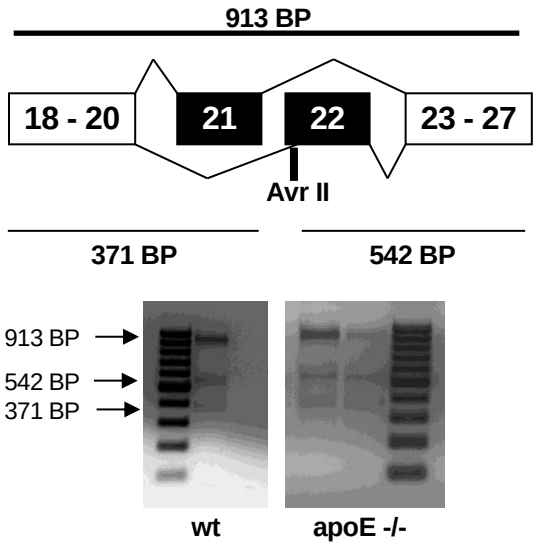


**Figure 3.2:6: Qualitative analysis of the alternative spliced variants of the pore-forming Cav1.2 containing either exon 21 or exon 22. RT-PCR was carried out using primers spanning exon 18 to 27 followed by analytic digestion with Avr II. The band at the height of 913 bp represents undigested exon 21-containing isoforms whereas the bands at 542 bp and 371 bp are products of the digested exon 22.**

## 3.2.5. Expression-profiling of the $\beta_2$ isoforms in murine aorta

The finding of β2 as one of the predominant β subunits in the aortic samples led to further investigation. To get an insight into predominant β2 isoforms expressed in the murine aorta, specific primers for qRT-PCR were designed. To insure that they only detect the demanded β2 isoform, small amounts of plasmids were used as specific templates for qRT PCR. Tests show that the primers used in this study only detect the specific isoform and none of the other $\beta_2$ isoforms.

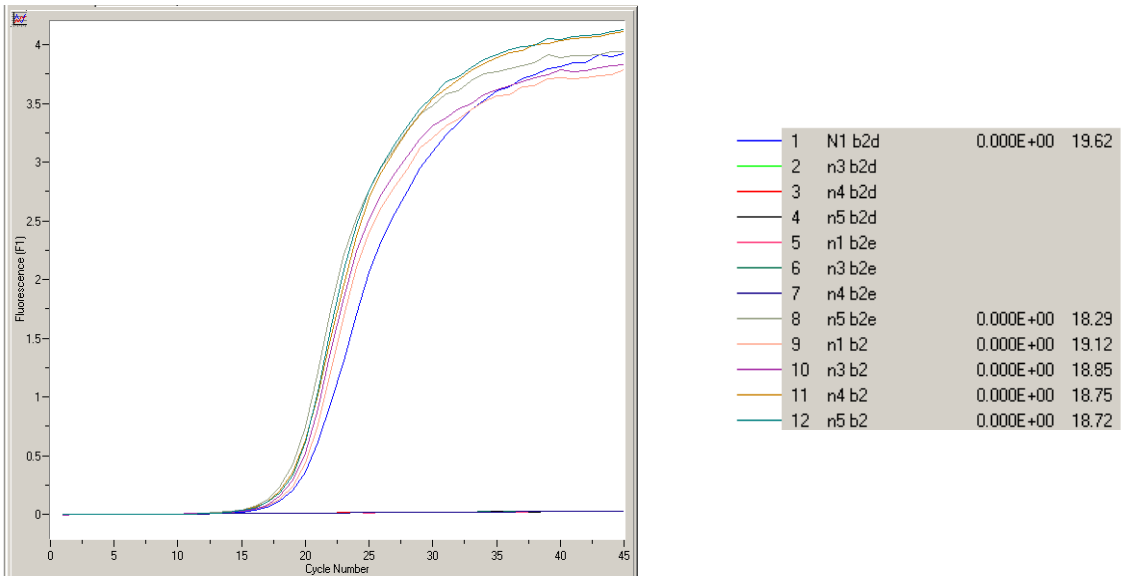


**Figure 3.2:7 qRT PCR testing the specifity of the used primer pairs for the individual β isoform. The $\beta_{2d}$ (b2d) primer assay only detects $\beta_2$ N1 (β2d), whereas the $\beta_{2e}$ primer shows affinity only for the β2 N5 plasmid (nomenclature s. material and methods). Sample 8 to 12 display the comparable efficiencies of the $\beta_2$ common primer for all $\beta_2$ isoforms.**

The analysis via qRT-PCR shows that $\beta_{2d}$ is the main $\beta_2$ isoform expressed on mRNA level in aortic tissue of both apoE -/- and wt mice ($2^{-\Delta ct}$ values: 37.74 ± 12.06 and 25.95 ± 6.95). Only small expression levels of $\beta_{2b}$ and $\beta_{2a}$ subunit isoforms were detected (wt $2^{-\Delta ct}$ values: 7.53 ± 1.96 and 5.14 ± 1.97; apoE -/- $2^{-\Delta ct}$ values: 5.12 ± 3.39 and 2.11 ± 0.85), $\beta_{2e}$ was barely detectable.

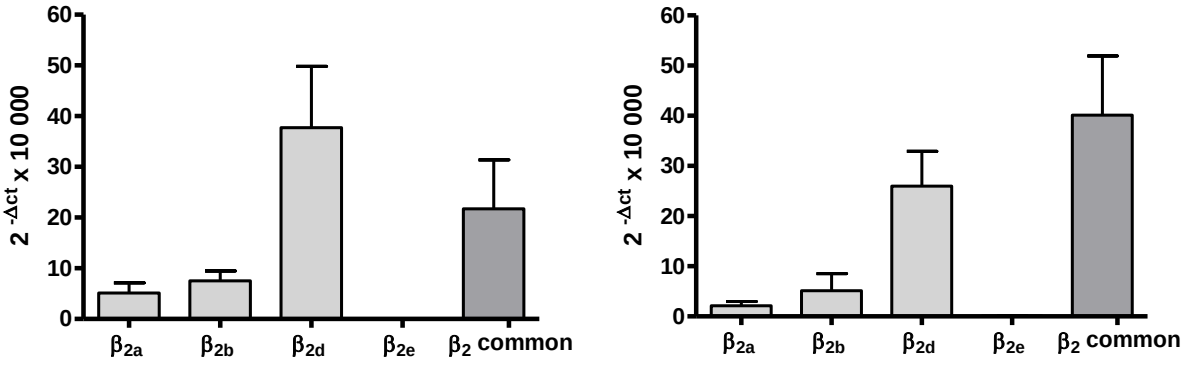


**Figure 3.2:8 Expression pattern of β subunit isoforms on mRNA level. Data is given as $2^{-\Delta ct}$ values with S29 as a reference gene. The graphs are representing the exemplary results of qRT-PCR of 16-18 week old (A) wt and (B) Apo E -/- mice. β2d is the predominant β2 isoform in murine aortic tissue in wt and apoE -/- mice. $2^{-\Delta ct}$ values are shown as geometrical mean + SEM.**

Evaluating the expression level of β2 isoforms in context of the development of atherosclerosis displays also a transient increase of $\beta_{2d}$, $\beta_{2b}$ and $\beta_{2a}$ isoforms at early stages of

atherosclerosis. Comparing 12-14 weeks old apoE -/- mice and wt mice at the same age revealed a significant increase in $\beta_{2d}$ ($p= 0.0087$) as the predominant $\beta_2$ isoform. In later stages of atherosclerosis the $\beta_2$ isoforms also reflect the decrease of LTCC subunits as described above.

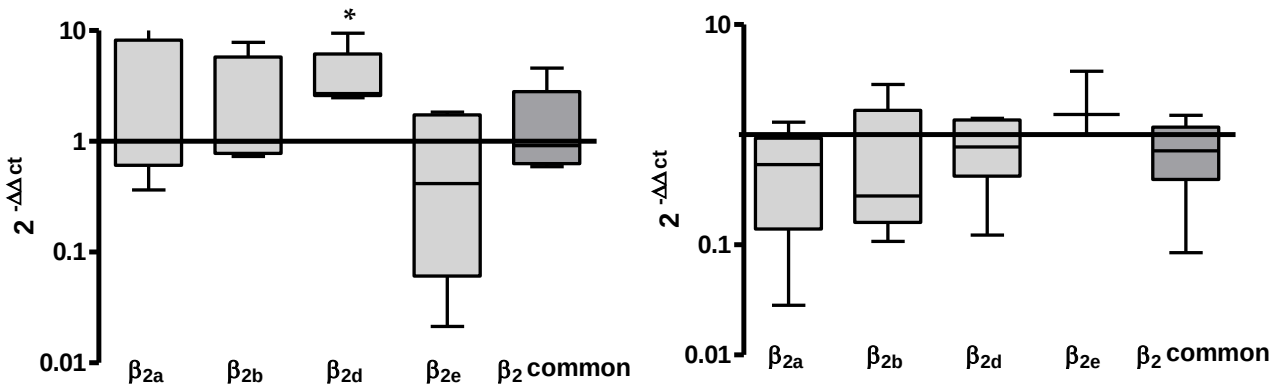


**Figure 3.2:9 Relative expression of β2 subunit isoforms , given as $2^{-\Delta\Delta ct}$ values , of (A) 12-14 week old apoE -/- mice compared to wt mice at the same age. Graph (B) is representing 16-18 week old apoE -/- mice compared to wt mice at the same age. Data is shown as "box and whisker" plots (median, 1st and 3rd quartile, minimum and maximum). Significant differences are marked by *$p$<0.05 (Student's t-test of Δct values).**

# 3.3. Functional studies of murine L-type calcium channels

## 3.3.1. Current density-voltage relationships

To investigate the functional impact of the different β subunit isoforms on the exon 21 (Cav1.2 $_{ex21}$) and exon 22 (Cav1.2 $_{ex22}$) containing splice variants of the Cav1.2 pore-forming subunit, whole-cell currents were measured as described in chapter 2.3.8. The two splice variant of Cav1.2 where coexpressed with $\alpha_2\delta$-1 and either β2b, β2d or β3A in HEK293 cells.

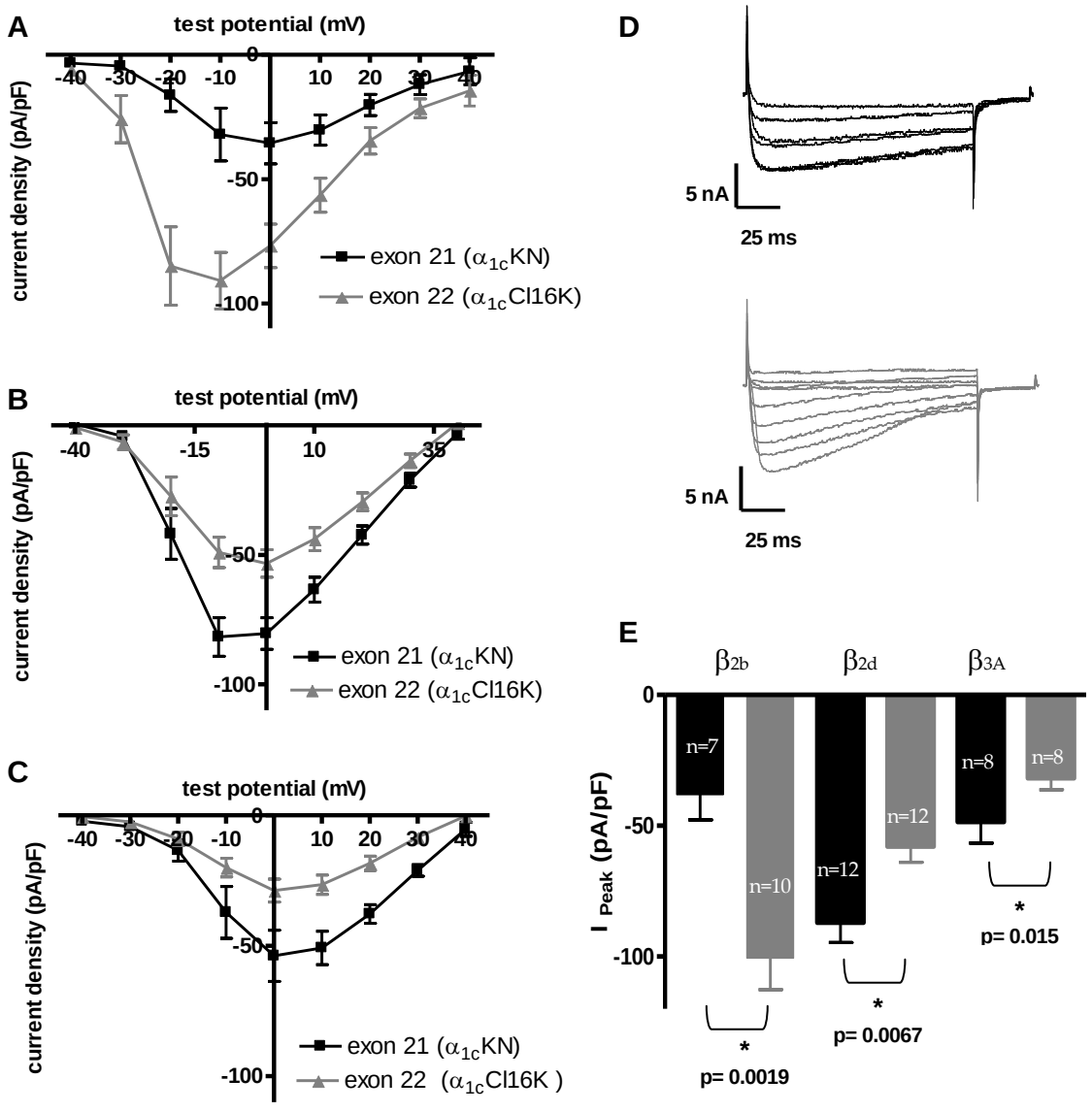


**Figure 3.3:1 (A) Current density-voltage relationships obtained from Cav1.2 channels containing either exon 21 or exon 22 coexpressed with β2b and $\alpha_2\delta$-1 subunits. The maximum current density of the exon 22-containing Cav1.2 subunit is significantly enhanced compared to the exon 21-containing isoform (-94.63 ± 11.90 pA/pF, n=12 vs. -38.05 ± 9.72 pA/pF, n=7) and shifted to the left. (B) I/V relationships of Cav1.2$_{ex\ 21}$ or Cav1.2$_{ex\ 22}$ coexpressed with β2d and an $\alpha_2\delta$-1 subunit. The maximum current density is significantly**

**increased with the Cav1.2$_{ex\ 21}$ isoform compared to channel complex containing Cav1.2$_{ex\ 22}$(-87.03 ± 7.62 pA/pF, n=12 vs. -58.00 ±5.99 pA/pF, n=12). (C) Current density-voltage relationships obtained from either Cav1.2 $_{ex21}$ or Cav1.2 $_{ex22}$ containing channel complexes coexpressed with β3A and $\alpha_2\delta$-1 subunits. The maximum current density is enhanced when the exon 21-containing Cav1.2 is coexpressed (-48.55 ± 8.14 pA/pF, n=8 vs. -31.83 ± 4.41, n=8). (D) Representative whole-cell $Ba^{2+}$-currents of Cav1.2-exon 21 (α1c-KN) or Cav1.2-exon 22 (α1c-Cl16K) with β2b and $\alpha_2\delta$-1 subunit coexpression in HEK293 cells. Exemplary traces were obtained by depolarizing from a holding potential of -80 mV to voltages ranging from -20 mV to +30 mV in 10 mV steps (pulse duration 150 ms). (E) Mean peak current density given as mean + SEM. Significant differences are marked by *$p$<0.05 (Student's t-test of I $_{peak}$).**

The I/V relationships (Figure 3.3:1) uncover the functional relevance of the exon shift of Cav1.2 in combination with different β subunits. Coexpressing Cav1.2$_{ex22}$ with β2b, maximum current densities are significantly enhanced compared to the exon 21-containing isoform of Cav1.2 (-94.63 ± 11.90 pA/pF, n=12 vs. -38.05 ± 9.72 pA/pF, n=7; p=0.0019). In addition, peak current density is shifted to the left to more hyperpolarizing potentials by coexpression of β2b with Cav1.2$_{ex22}$. The β3A subunit is triggering the opposite effect: peak current density is significantly decreased when coexpressed with Cav1.2$_{ex22}$ (-31.83 ± 4.41 pA/pF, n=8 vs. -48.55 ± 8.14 pA/pF, n=8; p=0.015). Interestingly, also the coexpression of β2d leads to a significantly decreased maximum of current density with the exon 22-containing isoform of Cav1.2 (-58.00 ± 5.99 pA/pF, n=12 vs. -87.03 ± 7.62 pA/pF, n=12;p=0.0067).

**Table 3.3:1 Voltage of half-maximum activation ($V_{0.5\ act}$) as determined from I/V relationships of the channel complexes**

| β $_{2b}$ | $V_{0.5\ act}$ | SEM | Slope | SEM | n |
|---|---|---|---|---|---|
| exon 21 ($\alpha_{1C}$ KN) | -9.54 | 2.82 | 6.22 | 0.66 | 5 |
| exon 22 ($\alpha_{1C}$ Cl16K) | -23.03 | 2.07 | 3.63 | 0.45 | 8 |

| β $_{2d}$ | $V_{0.5\ act}$ | SEM | Slope | SEM | n |
|---|---|---|---|---|---|
| exon 21 ($\alpha_{1C}$ KN) | -16.55 | 1.15 | 3.56 | 0.5 | 12 |
| exon 22 ($\alpha_{1C}$ Cl16K) | -14.93 | 2.29 | 4.59 | 0.41 | 11 |

| β $_{3A}$ | $V_{0.5\ act}$ | SEM | Slope | SEM | n |
|---|---|---|---|---|---|
| exon 21 ($\alpha_{1C}$KN) | -7.33 | 1.84 | 6.00 | 0.33 | 8 |
| exon 22 ($\alpha_{1C}$Cl16K) | -8.89 | 1.7 | 6.31 | 0.56 | 7 |

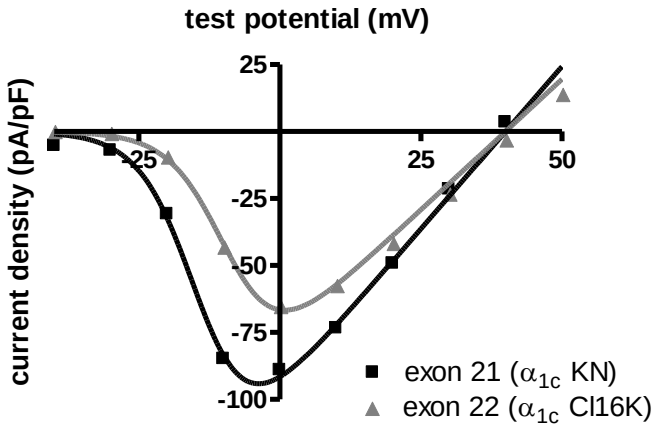


**Figure 3.3:2 Exemplary Boltzmann-Ohm fittings of current density of Cav1.2$_{ex21}$ and Cav1.2 $_{ex22}$ coexpressed with β2d as described in chapter 2.3.8.**

A closer look on activation kinetics reveals also a significantly modulation of voltage-dependence of half-maximum activation ($V_{0.5\ act}$) by Cav1.2$_{ex22}$ when coexpressed with β2b: the $V_{0.5act}$ is shifted to more negative potentials and shows a lower slope factor (Table 3.3:1). The other β subunit isoforms do not lead to significantly changes in activation kinetics of the channel complexes.

## 3.3.2. Time- and voltage-dependent inactivation

To investigate whether inactivation kinetics account for the differences found in the I/V relationships, time- and voltage-dependent inactivation were analyzed. Therefore, the percentage of current that has inactivated after 150 ms of depolarization (% inactivation) and the time constant of inactivation for current decay (τ) were determined [110].

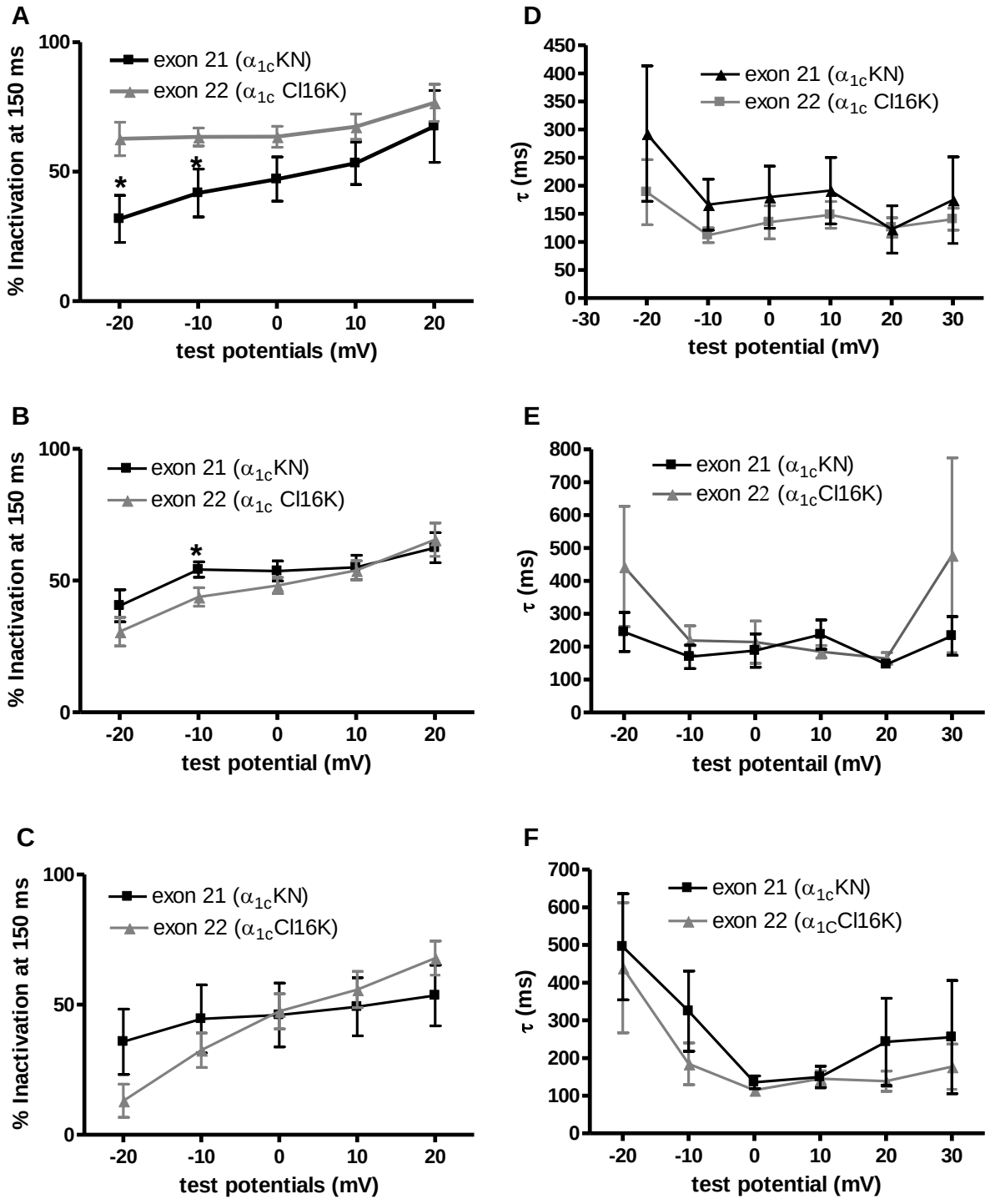


**Figure 3.3:3 Voltage- and time-dependent inactivation: Voltage-dependence of the inactivation rate (determined as the fraction of peak current inactivated after 150 ms of depolarization) of (A) β2b co-expressed with either Cav1.2 $_{ex21}$ (n=7) or Cav1.2 $_{ex22}$ (n=12) (B) β2d coexpressed with either Cav1.2 $_{exon\ 21}$ (n=8) or Cav1.2 $_{ex22}$ and (C) β3A coexpressed with either Cav1.2 $_{ex21}$ (n=8) or Cav1.2 $_{ex22}$ (n=8). (D,E,F) Co-responding inactivation rates indicated by the time constant for inactivation for current decay obtained by mono-exponential fits of the raw data. All data is given as mean ± SEM. Significant differences are marked by *$p$<0.05 (Student's t-test).**

Examining the voltage-dependence of inactivation, channel inactivation was faster and the extent of inactivation was nearly complete with β2b being coexpressed with $Cav1.2_{ex22}$ compared to cotransfection with $Cav1.2_{ex21}$. The other channel complex pairs do not show significant differences. Comparison of characteristics of inactivation time constant (Figure 3.3:3: D,E and F) revealed no major changes between exon 21- and exon 22-containing Cav1.2 coexpressed with the respective β subunit. Hence they are not responsible for the basal current density differences observed in chapter 3.3.1. In addition, steady-state inactivation was not affected by the exon 21 - exon 22 shift in channel complexes containing either β2b or β2d. In the case of β3A, the half-maximum inactivation potential ($V_{0.5inact}$) was shifted to more positive potentials when coexpressed with Cav1.2 exon 22. However, number of experiments that could be analyzed in this respect were only n=4 for $Cav1.2_{ex22}$ and n=2 for $Cav1.2_{ex21}$.

**Table 3.3:2 Steady-state inactivation properties of the characterized Cav1.2 channels following the pulse protocol described in chapter 2.3.8. Data was fitted using the Boltzmann equation, the half-inactivation potentials ($V_{0.5\ inact}$) and slope factors were obtained from these fits.**

| β 2b + | $V_{0.5\ inact}$ | SEM | Slope | SEM | n |
|---|---|---|---|---|---|
| exon 21 ($\alpha_{1c}$-KN) | -37,93 | 2,97 | 7,43 | 0,51 | 5 |
| exon 22 ($\alpha_{1c}$-Cl16K) | -39,14 | 3,29 | 6,43 | 1,55 | 5 |

| β 2d + | $V_{0.5\ inact}$ | SEM | Slope | SEM | n |
|---|---|---|---|---|---|
| exon 21 ($\alpha_{1c}$-KN) | -36,95 | 1,04 | 5,36 | 0,36 | 8 |
| exon 22 ($\alpha_{1c}$-Cl16K) | -34,73 | 1,19 | 5,28 | 0,5 | 9 |

| β 3A + | $V_{0.5\ inact}$ | SEM | Slope | SEM | n |
|---|---|---|---|---|---|
| exon 21 ($\alpha_{1c}$-KN) | -35.14 | 1.48 | 6.08 | 0.26 | 2 |
| exon 22 ($\alpha_{1c}$-Cl16K) | -27.86 | 0.36 | 3.46 | 0.92 | 4 |

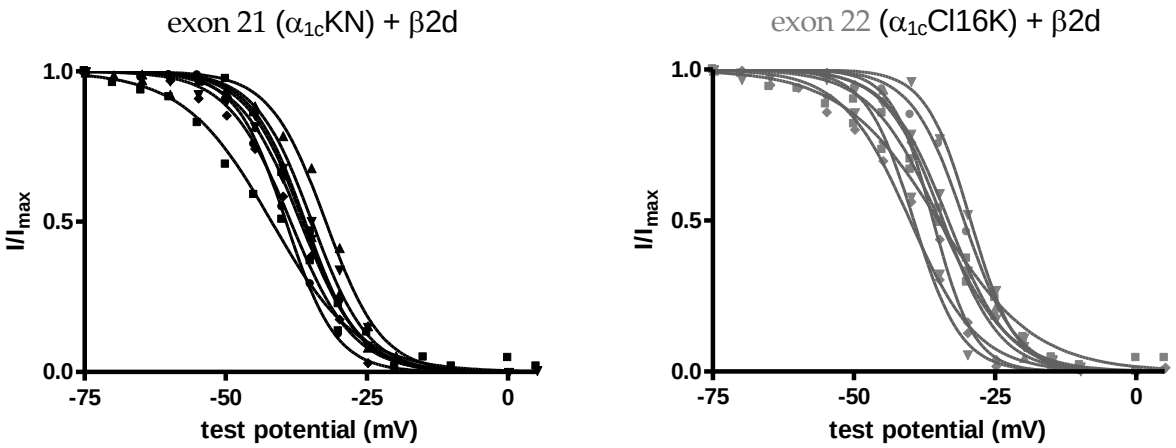


**Figure 3.3:4 Steady -state inactivation curves of β2d fitted with a Boltzmann equation described in chapter 2.3.8. No significant difference is found in the inactivation kinetics coexpressing either Cav1.2 $_{ex\,21}$ or Cav1.2 $_{ex\,22}$.**

# 4. Discussion

## 4.1. Expression profiling of human L-type calcium channel subunits

Voltage-gated calcium channels play an important role in the elasticity and contractility of arterial smooth muscle cells. The contraction of VSMC is triggered by calcium influx through LTCCs [111]. In addition, an increase of cytosolic intracellular calcium is needed for proliferation of VSMC [38]. An exon splice shift in the pore-forming subunit of LTCCs, as described by Tiwari et al. in the development of human atherosclerotic lesions [91], is an important finding as alternative splicing can lead to differential pharmacological and biophysical properties of the channel [60-62, 91, 112]. Earlier functional studies showed that these two splice variants of $Ca_V1.2$ lead to differential electrophysiological properties in the context of different β subunits in HEK293 cells (see chapter 1.3). Therefore, this study intended to examine the expression pattern of auxiliary β subunits in human atherosclerotic and non-effected tissue to link the functional data with characteristically features of VSMC in the development of atherosclerosis. Elucidation of the channel composition can lead to further understanding of mechanism underlying the observed phenotypic changes of VSMC in the development of atherosclerosis.

Reproducing the methods described in the work of Tiwari et al. to insure comparability led to several problems. The theory of finding unaffected as well as atherosclerotic areas in one biopsy turned out to be not practicable. Remodeling of the arterial wall was found in either all or none of the serial cuts of a sample. Therefore no direct comparison of affected and unaffected areas within one sample as published was possible. Hence a direct control group was not available for qRT-PCR analysis and samples from different individuals were compared. This method is implicating a risk to detect not only gene expression differences due to the development of atherosclerosis but also potentially adds a factor of inter-individual differences between patients. This diversity in patient data can include environmental factors and genetics [113].

Furthermore, the isolation of sufficient RNA amounts and quality from the microdissected VSMC areas proved to be very difficult. Hence, analyzable sample number was low and statistical power of the data was small. Taken this as restrictions of the method, the results confirm the predominant β subunit - β2 is consistently found in all analyzed sample, which is conform to earlier findings identifying β3 and β2 as predominant β subunits in VSMC [92]. There is no differential expression pattern of β subunits found in microdissected VSMC areas from healthy and diseased samples. Surprisingly, both exon 21 and exon 22 are detected in atherosclerotic and control areas from femoral arteries. But as described above, small number of samples with sufficient RNA quantity and quality result in low statistical power. Furthermore, RNA amounts were close to detection limit of qRT-PCR, which was determined by standard curves linking copy numbers and ct values.

Due to these problems, mRNA from whole tissue samples was analyzed. With this method also all other cell types in atherosclerotic and non-atherosclerotic arteries are taken into analysis. Hence, detected changes in gene expression level may also reflect the changed composition of the vessel wall during atherosclerosis, implicating also the presence of different cell types [113]. Previous studies, analyzing the expression pattern of LTCC subunits in animal models, also investigated whole-tissue arterial samples, hence leading to a good comparability [92, 114, 115]. No reference gene was found to correlate with the VSMC amount in the analyzed samples. To correct for VSMC number, the marker must be stably expressed in all states of atherosclerotic development. But due to remodeling of SMC, all eligible SMC-marker were demonstrated to exhibit differential expression in atherosclerosis [116, 117]. By comparing the rare control samples with diseased samples from the same area of the femoral artery for relative quantification via qRT-PCR, we could at least reduce the high variability in gene expression resulting from different sample taking sites [113].

The results reinforce the finding that exon 21- and exon 22- containing splice variants of the $Ca_V1.2$ subunit are expressed on mRNA level. Exon 21 is the predominantly expressed exon in human atherosclerotic and non-atherosclerotic arteries. This finding does not confirm the findings from Tiwari et al. in 2006. Looking at β subunit expression, all 4 β subunit isoforms are found on mRNA level. β1 and β2 isoforms are more abundant then β3 and β4. The control samples show the same expression pattern. Published data suggests β2 and β3 as

predominant isoforms but no β1; however these results arise only from aortic tissue from mice [92], rabbit [114] or bovine aortas [115]. In human aortic tissue it was shown that β3 is expressed, but not if this is the predominant β isoform [118]. The detection of β4 is not described in arterial tissue so far, but could be due to the presence of nerve endings containing β4 [71].

Comparing the atherosclerotic and control femoral samples for relative quantification, a slight decrease of all LTCC subunits is shown but no expression shift. Gollasch et al. already observed a similar down-regulation of the Cav1.2 pore forming subunit in cultured dedifferentiated rat aortic A7r5 cells; it was also shown that expression strongly depends on the state of differentiation of VSMCs [44], which is also reflected in this study by the high variation in gene expression of LTCC subunits in the individual human samples.

Taken together, the two approaches used in this study revealed the β2 subunit as the consistently expressed β subunit in both atherosclerotic and non-atherosclerotic arterial tissue. No splice shift could be observed for the alternatively spliced exons 21/22 of the pore forming Cav1.2 subunit. Linking this finding with the functional data derived from electrophysiological studies of the human channel complexes, resulting channels containing the β2 subunit would lead to enhanced current densities with $Ca_V1.2_{ex22}$. This would implicate a decreased expression of LTCC as a mechanism for the observed loss of contractility in VSMC rather than a splice shift of LTCC subunits. Combination of the two expressed Cav1.2 isoform containing either exon 21 or exon 22 with different β subunits could lead to a mechanism for fine-tuning cell function.

## 4.2. The exact stage of atherosclerosis is a critical determinant of pathological LTCC remodeling

The apoE -/- mouse is a well-established model for gaining insights into the pathogenesis of atherosclerosis [98, 113]. This model contributes the controllable and standardized background needed to interpret the findings in human arterial samples [119]. The two different splice variants of Cav1.2 containing either exon 21 or exon 22 are conserved across several species (Figure 4.2:1).

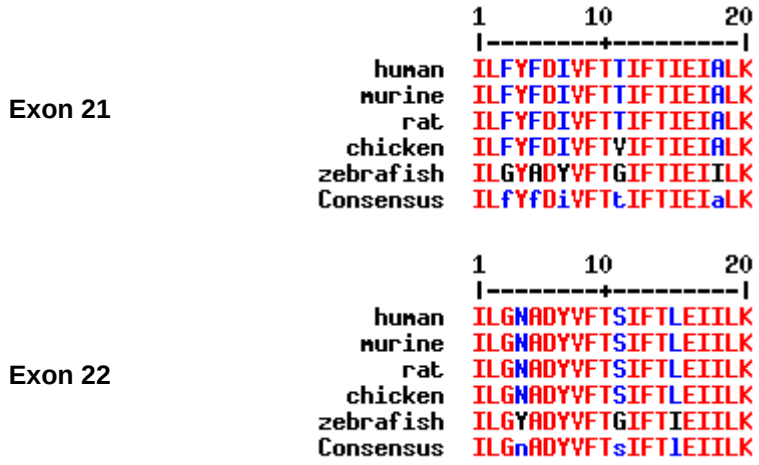


**Figure 4.2:1 Amino acid sequence alignment of alternative spliced exon 21 and exon 22 of Cav1.2 in different species.**

The quantification of the lesion size in the aortic root confirmed that the different age groups of apoE -/- mice investigated represent standardized groups of different stages of atherosclerosis. Environmental factors and inter-individual differences are excluded with this approach.

Here, β3 and β2 are the predominant isoforms of β subunits in atherosclerotic and non-atherosclerotic aortic tissue. Murakami and colleagues already discovered this expression pattern in aortic tissue from wildtype mice. Furthermore, experiments in β3-knockout (β3 -/-) mice revealed a reduced expression of the Cav1.2 subunit in the plasma membrane and a 30 % reduction in $Ca^{2+}$ channel current density [92]. Additional functional expression of the β2 subunit as a predominant β subunit in VSMC would explain why VSMC are still functional in β3 -/- mice. Adding to these findings, this study clarifies that there is no differential expression, i.e. no prominent shift in the predominant β subunit in the development of atherosclerosis.

Since the different splice variants of β2 are known to modulate LTCC in a different manner [80], the expression of the different splice variants was examined. The β2d splice variant proved to be the predominant splice variant of β2 subunits in atherosclerotic and non-atherosclerotic aortic tissue. This is a new finding and important for functional analysis of the channel complexes. Furthermore, in murine aorta both exon 21- and exon 22-containing splice variants of Cav1.2 are expressed. No splice shift in between these exons is observed in atherosclerosis, which confirms the findings in human arterial tissue in this study. The exon 22-containing isoform of Cav1.2 is more abundant in aortic tissue from wildtype and apoE-/-

mice. This finding is surprising since the predominant isoform of Cav1.2 in rat aorta contains exon 21 [120] and also the human data suggest exon 21 as the predominantly expressed exon. This finding should be recognized for transferring data from mouse models to the human level. The alternatively spliced exons lead to voltage-dependent conformational changes of the channel, which affect DHP binding. The exon 21-containing Cav1.2 isoform reveals a reduced sensitivity to DHPs [112]; a splice shift could therefore influence therapy with DHPs. Hence the knowledge about the predominant splice variant could be beneficial in future individualized therapy of atherosclerosis. DHPs are potent antihypertensive drugs and additionally nifedipin as a representative was shown to reduce proliferation in VSMCs [40, 121, 122].

By quantifying the lesion area in the aortic root, this study clearly shows that the chosen age groups represent different stages of atherosclerosis and can represent the progression of the disease. Therefore, comparing the different age groups of apoE -/- is providing insights into molecular changes of LTCC in the progression of atherosclerosis. As described above, no splice shift was observed in β subunits or the alternative spliced exon 21/22. Nevertheless, the expression level of LTCC subunits changed in the different stages of atherosclerosis. An initial increase of all LTCC subunits on mRNA level at the age of 12-14 weeks is followed by a significant decrease at the age of 16-18 weeks. This indicates that the exact stage of atherosclerosis is a critical determinant of pathological LTCC remodeling. The age group of 22 weeks is also showing a decrease of all channel subunits, but not at a significant level which could be due to low animal number at this group. The expression levels in more advanced stages of atherosclerosis correlates with those in the human atherosclerotic samples; the stage of atherosclerosis in the aortic arch of the older apoE -/- mice closely reflects the human state of atherosclerosis found in the bypass biopsies [1]. The temporary up-regulation of the LTCC subunits at earlier stages of atherosclerosis (12-14 week old apoE -/-) on mRNA level could be reflecting a compensation mechanism for decreasing functionality of atherosclerotic VSMC. The strong dependence of expression levels of LTCC on the exact stage of atherosclerosis explains why examined human expression level show high variability. The serial aortic cuts reveal high variation in the stage of atherosclerosis in the different biopsies of patient undergoing stent surgery. Therefore, the human sample collection represents different stages of atherosclerosis as well as differential environmental

factors. A classification of the human samples into different stages of atherosclerosis would help to unravel this issue but would also require a huge number of human samples and clear definitions of stages.

## 4.3. Modulation of murine L-type $Ca^{2+}$-channel currents by the exon 21/exon 22 splice shift of $Ca_V1.2$

The function of voltage-gated calcium channels has major impact on the contractility of VSMC. The influx of external calcium ($Ca^{2+}$) regulates intracellular free $Ca^{2+}$ - thereby arterial tone - and is important for additional biological processes inside the cell. An increase of cytosolic intracellular $Ca^{2+}$ is for example needed for proliferation of VSMC [38].

Our group could show several times that β subunit isoforms and their splice variants have unique influence on channel-gating and expression of the channel complex in the membrane [80-82]. Recently, an effect on whole-cell currents could be shown for the human channel complexes containing either the $Ca_V1.2_{ex\ 21}$ or $Ca_V1.2_{ex\ 22}$ subunit (see chapter 1.3). In the context of different β subunits (β2b and β3a), strikingly different effects were observed on whole-cell currents of LTCC.

In the investigated murine channel complexes, the combination with different β subunit isoforms reinforces the functional relevance of the exon 21/exon 22 splice shift. The effect of the β2b and β3a subunits on the two splice variants of $Ca_V1.2$ is comparable to the evaluated human channel complexes in whole-cell measurements. The channel complexes containing β3A lead to a significantly reduced current density together with the exon 22-containing $Ca_V1.2$. In contrast, channel complexes containing β2b lead to an increased current density together with a shift of peak current density towards more hyperpolarizing potentials with the exon 22-containing $Ca_V1.2$. This leftward shift is also represented in the activation kinetics. The investigation of the time-dependent inactivation – determined as time constant τ – did not reveal significant differences in between the $Ca_V1.2_{ex21}$ and $Ca_V1.2_{ex22}$ in combination with the different β subunits. Hence, they do not explain the differential effects of β subunits found in the I/V relationships.

The group around Tiwari already published preliminary data coexpressing $Ca_V1.2_{ex21}$ and $Ca_V1.2_{ex22}$ with a β2a subunit in Xenopus oocytes. These channel complexes feature a faster

recovery from inactivation with CaV1.2$_{ex22}$ and a shift of the channel activation curve to more negative potentials, already indicating a β subunit dependent effect on the exon21/exon22 splice shift [91]. In previous studies, it has also been shown that different β subunit isoforms reveal diverse effects on L-type Ca2+ channel currents [57, 123, 124]. In a study from 2002, Colecraft and colleagues found distinctive effects of β subunit isoforms on channel inactivation kinetics and on the degree of enhancement of whole-cell current density. GFP-fused β subunits were overexpressed in cultured adult rat heart cells and led to an enhancement of current density with a rank order of β2≈β4>β1b>β3. Furthermore β subunits uniquely altered the rate of current inactivation. β2a and β4 markedly reduced rates of inactivation compared with control whereas inactivation was not significantly altered with β1b and β3 [79].

Surprisingly, in this study β2d showed qualitatively the same effect on current density as β3A. Maximum peak current densities are significantly enhanced with the exon 21-containing Cav1.2. This is in contrast with the expectation of a similar effect on the Cav1.2 splice variants by β2b since these splice variants of β2 share more structure homology. However, they differ by the length of their N-terminus: β2b has a shorter N-terminus compared to β2d which was shown to lead to increased open probability, availability, and peak current in single channel measurements [80]. On whole-cell level in recombinant human channel complexes, β2b and β2d exhibit comparable fast inactivation kinetics, in contrast to β2a and β2e which showed slower channel inactivation kinetics and a smaller fraction of channels recovering from inactivation with fast kinetics [125]. In recombinant murine channel complexes containing a heart specific isoform of Cav1.2 with a short N-terminus, β2d had a significant effect on steady state activation compared to the other β2 splice variants - the midpoint of activation of normalized I/V curves was shifted to more depolarizing potentials. Furthermore, β2d and β2b accelerated inactivation kinetics which also led to slower activation compared to β2a and β2e [100].

Taken together, single-channel measurements could reveal further insides into gating parameters of the investigated channel complexes. Previous studies could also show effects of the different β subunit isoforms on single channel gating, namely open probability [79] and single-channel activity [126].

Linking this functional analysis to the expression profiling of LTCC subunits, a possible mechanism for fine-tuning would arise for VSMCs to modulate channel function by complex formation of different β subunits and Cav1.2 splice variants.

During atherosclerosis, VSMCs switch from a contractile phenotype to a synthetic, i.e. non-contractile and proliferative phenotype. L-type calcium channel play a major role in $Ca^{2+}$ homeostasis and are important effectors in VSMC excitation-contraction coupling as well as for excitation-transcription coupling. Studies could show that $Ca^{2+}$ entry through LTCC are associated with activation of the smooth muscle differentiation marker genes SMα-actin and SM-myosin heavy chain (SM-MHC) [44, 127]. Functional remodeling of VSMCs during dedifferentiation implicates down-regulation of functional L-type calcium channels - a decreased $I_{Ca2+}$ as well as a decreased expression of Cav1.2 was shown in cultured dedifferentiated rat aortic A7r5 cells [44]. This was additionally shown in primary, proliferative VSMCs from the neointima of rat aorta [128]. In human cultured cells from saphenous vein, a re-differentiation of VSMCs - indicated by an increase of α-actin - was linked to increased intracellular $Ca^{2+}$ and chemotaxis mediated by Cav1.2 [45]. Taking this as a background, our functional data reveal that the combination of the predominant β subunits, β2d and β3a, with the exon 22-containing Cav1.2 would mirror a non-contractile and proliferative VSMC phenotyp with reduced function of LTCCs. Furthermore, the observed secondary decrease of LTCC subunit expression on mRNA level is consistent with observed down-regulation of LTCC expression in primary and cultured rat aortic cells.

The differential effect of the β subunit splice variants on the two splice variants of Cav1.2 only differing by exon 21/22 cannot be explained by known structure-function relationships. The alternative-spliced exon 21/22 encodes for the second transmembrane helix of domain III and the linker between IIIS1 and IIIS2 of Cav1.2. No subunit interaction-site is described for this region of the pore-forming subunit. Furthermore, this region is not known to be an important area for specific channel functions up to date [55]. On the other hand, the mutually exclusive exons 21 and 22 are known to modify sensitivity to DHP as revealed by inhibition of whole-cell currents - although detected binding sites for DHP are located in the IS6, IIIS5, IIIS6 and IVS6 transmembrane regions of Cav1.2 [62, 63, 65, 129, 130]. Our data may hint to additional unknown functions of the transmembrane helix of domain III and

the linker between IIIS1 and IIIS2 which seem to account for the mutual dependence of pore splice variants and β-subunit isoforms.

Taken together, β subunits modulate L-type calcium currents in an isoform- and splice variant-specific manner. This study could show that in addition to the differential splicing of Cav1.2, specific regulation of β subunits represents another important determinant of Cav1.2 remodeling in VSMC. This is suggesting a new possible regulatory mechanism for VSMC in health and disease.

## 4.4. Conclusion and outlook

Taken together, the data described in this study demonstrates the functional relevance of the splice shift of Cav1.2 exon 21/22 in the context of the different β subunit isoforms (β1, β2, β3) in recombinant human and murine channels. The β2 isoform in human arterial tissue and additionally β3 in murine aortic tissue are the predominant β isoforms expressed on mRNA level. Exon 21 as well as exon 22 is found in human and murine arterial tissue. There is no qualitative switch in human atherosclerotic tissue of LTCC subunits observed in this study. Additionally, no switch of LTCC subunits is observed in murine atherosclerosis. However, atherosclerosis is linked to a differential expression level of Cav1.2 and β subunit isoforms. This indicates complex stage-dependent changes in atherosclerosis which likely explain variability found in human samples and possibly causes functional remodeling. The ability of Cav1.2, containing either exon 21 or exon 22, to couple with either β2 or β3 could provide a mechanism for fine-tuning VSMC function.

This work was not designed to elucidate why there are different effects on current density of the channel complexes containing $Ca_V1.2_{ex21}$ or $Ca_V1.2_{ex22}$ in combination with different β subunits. Single-channel analysis would be necessary to gain further insights into single channel gating of the prevailing murine channel complexes. Possible occurrence of discrepancies between whole-cell and single-channel currents may suggest additional effects of β-subunits on membrane targeting. Therefore channel subunits can be examined by confocal fluorescence microscopy. Imaging of the surface expression of, e.g., hemagglutinin (HA)-tagged Cav1.2 splice variants could reveal potential variations in the membrane localization in combination with different β subunits. Immunoluminescence could be compared between permeabilized and non-permeabilized cells which would allow

to quantify the relative proportion of Cav1.2 channels that are inserted into the plasma membrane [85]. Additionally immunohistochemistry with specific antibodies against the Cav1.2 pore forming subunit and against specific markers for inner cell structure, like the endoplasmatic reticulum or the golgi apparatus, can display distinct localization of the Cav1.2 coexpressed with the different β subunits and α2δ-1.

The differential effect of β subunits on the two splice variants of Cav1.2 only differing by exon 21/22 cannot be explained by structure-function relationships so fare. Further analysis of this region within the pore-forming subunit including structure-function analysis with the help of deletion-mutants investigated via patch clamp electrophysiology could reveal further details for the understanding of structure-function relationships.

# 5. Summary

Cardiovascular voltage-gated L-type calcium channels (LTCCs) are heteromeric protein complexes consisting of a pore-forming $Ca_V1.2$ subunit, an intracellular β subunit and a $\alpha_2\delta$ subunit complex. The function of voltage-gated calcium channels has major impact on the function and contractility of vascular smooth muscle cells (VSMCs). The influx of external calcium ($Ca^{2+}$) regulates intracellular free $Ca^{2+}$ - thereby arterial tone - and is important for additional biological processes inside the cell. An increase of cytosolic intracellular $Ca^{2+}$ is for example needed for proliferation of VSMCs.

It has been reported that in human atherosclerosis, vascular smooth muscle $Ca_V1.2$ isoforms containing exon 21 are replaced by one single isoform containing the alternative exon 22. Previous functional studies in our group reveal that this splice shift has major effects on LTCC function, depending on the β subunit co-expressed: a $\beta_3$ subunit together with $Ca_V1.2_{exon\ 21}$ led to markedly reduced current density compared to $Ca_V1.2_{exon\ 22}$. Coexpression of a $\beta_2$ subunit with either $Ca_V1.2_{exon\ 21}$ or $Ca_V1.2_{exon\ 22}$ had the opposite effect.

The present work examined the LTCC subunit expression pattern in both human and murine atherosclerotic arterial tissues. Samples of human atherosclerotic arteries were obtained from patients undergoing carotid or femoral arterial bypass surgery. Human vascular smooth muscle tissue was isolated by laser microdissection or the whole arterial sample was examined. Mouse aorta was isolated from healthy wildtype and atherosclerotic apoE-knockout (-/-) animals. LTCC subunit mRNA expression was quantified by qRT-PCR. Furthermore, the electrophysiology of the most abundant murine $Ca_V1.2$ channel complexes was characterized at whole-cell level.

In human arterial samples, mRNA of all 4 β subunits, $\beta_{1\text{-}4}$, is expressed along with $Ca_V1.2$. The $\beta_2$ subunit mRNA seemed to be most consistently and predominantly expressed. Both exon 21- and exon 22-containing $Ca_V1.2$ subunit mRNA isoforms were found in atherosclerotic and non-affected tissue. Atherosclerosis was associates with a slight decrease of LTCC channel subunits in femoral arterial tissue.

In murine aortic tissue, both exon 21- and exon 22 containing $Ca_V1.2$ subunit mRNA was detected in healthy and diseased tissue. The $\beta_{2d}$ and $\beta_3$ subunits are the predominant β isoforms in arterial tissue. Furthermore, atherosclerosis is associated with a transient increase of $Ca_V1.2$ channel subunits ($\beta_{2d}$, $\beta_3$, $Ca_V1.2$) followed by a strong decrease in later stages of atherosclerosis.

In recombinant murine channels the combination with different β subunit isoforms uncovers the functional relevance of the exon 21-exon 22 structural diversity. The channel complexes containing $\beta_{2d}$ and $\beta_3$ lead to a significantly reduced current density together with the exon 22 containing $Ca_V1.2$. In contrast channel complexes containing $\beta_{2b}$ cause an increased current density together with a shift of peak current density towards more hyperpolarizing potentials.

Taken together, the data described in this study demonstrate the functional relevance of the splice shift of Cav1.2 exon 21/22 in the context of the different β subunit isoforms (β1, β2, β3) in recombinant human and murine channels. The β2 isoform in human arterial tissue and additionally β3 in murine aortic tissue are the predominant β isoforms expressed on mRNA level. In murine aorta, β2d is the predominant β2 splice variant. Exon 21 as well as exon 22 are found in human and murine arterial tissue. This study do not hint at a clear cut "atherosclerotic" change of expression pattern, but indicates that the exact stage of atherosclerosis is a critical determinant of pathological LTCC remodelling.

# 6. Literature


1. Libby P, Ridker PM, Hansson GK. (2011) Progress and challenges in translating the biology of atherosclerosis. Nature, 473, 317-25.
2. Meens MJ, Pfenniger A, Kwak BR. (2012) Risky communication in atherosclerosis and thrombus formation. Swiss Med Wkly, 142, w13553.
3. Libby P. (2003) Vascular biology of atherosclerosis: overview and state of the art. Am J Cardiol, 91, 3A-6A.
4. Libby P, Ridker PM, Hansson GK. (2009) Inflammation in atherosclerosis: from pathophysiology to practice. J Am Coll Cardiol, 54, 2129-38.
5. Rocha VZ, Libby P. (2009) Obesity, inflammation, and atherosclerosis. Nat Rev Cardiol, 6, 399-409.
6. Manduteanu I, Simionescu M. (2012) Inflammation in atherosclerosis: a cause or a result of vascular disorders? J Cell Mol Med.
7. Imes CC, Austin MA. (2012) Low-Density Lipoprotein Cholesterol, Apolipoprotein B, and Risk of Coronary Heart Disease: From Familial Hyperlipidemia to Genomics. Biol Res Nurs.
8. Roger VL, Go AS, Lloyd-Jones DM, Adams RJ, Berry JD, Brown TM, Carnethon MR, Dai S, de Simone G, Ford ES, Fox CS, Fullerton HJ, Gillespie C, Greenlund KJ, Hailpern SM, Heit JA, Ho PM, Howard VJ, Kissela BM, Kittner SJ, Lackland DT, Lichtman JH, Lisabeth LD, Makuc DM, Marcus GM, Marelli A, Matchar DB, McDermott MM, Meigs JB, Moy CS, Mozaffarian D, Mussolino ME, Nichol G, Paynter NP, Rosamond WD, Sorlie PD, Stafford RS, Turan TN, Turner MB, Wong ND, Wylie-Rosett J. (2011) Heart disease and stroke statistics--2011 update: a report from the American Heart Association. Circulation, 123, e18-e209.
9. Roger VL, Go AS, Lloyd-Jones DM, Benjamin EJ, Berry JD, Borden WB, Bravata DM, Dai S, Ford ES, Fox CS, Fullerton HJ, Gillespie C, Hailpern SM, Heit JA, Howard VJ, Kissela BM, Kittner SJ, Lackland DT, Lichtman JH, Lisabeth LD, Makuc DM, Marcus GM, Marelli A, Matchar DB, Moy CS, Mozaffarian D, Mussolino ME, Nichol G, Paynter NP, Soliman EZ, Sorlie PD, Sotoodehnia N, Turan TN, Virani SS, Wong ND, Woo D, Turner MB. (2012) Heart disease and stroke statistics--2012 update: a report from the American Heart Association. Circulation, 125, e2-e220.
10. Stary HC, Chandler AB, Dinsmore RE, Fuster V, Glagov S, Insull W, Jr., Rosenfeld ME, Schwartz CJ, Wagner WD, Wissler RW. (1995) A definition of advanced types of atherosclerotic lesions and a histological classification of atherosclerosis. A report from the Committee on Vascular Lesions of the Council on Arteriosclerosis, American Heart Association. Arterioscler Thromb Vasc Biol, 15, 1512-31.
11. Smith SC, Jr., Milani RV, Arnett DK, Crouse JR, 3rd, McDermott MM, Ridker PM, Rosenson RS, Taubert KA, Wilson PW. (2004) Atherosclerotic Vascular Disease Conference: Writing Group II: risk factors. Circulation, 109, 2613-6.
12. Faxon DP, Fuster V, Libby P, Beckman JA, Hiatt WR, Thompson RW, Topper JN, Annex BH, Rundback JH, Fabunmi RP, Robertson RM, Loscalzo J. (2004) Atherosclerotic Vascular Disease Conference: Writing Group III: pathophysiology. Circulation, 109, 2617-25.

13. Fowkes FG, Housley E, Riemersma RA, Macintyre CC, Cawood EH, Prescott RJ, Ruckley CV. (1992) Smoking, lipids, glucose intolerance, and blood pressure as risk factors for peripheral atherosclerosis compared with ischemic heart disease in the Edinburgh Artery Study. Am J Epidemiol, 135, 331-40.
14. Hiatt WR, Hoag S, Hamman RF. (1995) Effect of diagnostic criteria on the prevalence of peripheral arterial disease. The San Luis Valley Diabetes Study. Circulation, 91, 1472-9.
15. Meijer WT, Hoes AW, Rutgers D, Bots ML, Hofman A, Grobbee DE. (1998) Peripheral arterial disease in the elderly: The Rotterdam Study. Arterioscler Thromb Vasc Biol, 18, 185-92.
16. Corrado E, Rizzo M, Aluigi L, Patti AM, Coppola G, Muratori I, Caccamo G, Balasus F, Novo S. (2012) Prediction of vascular events in subjects with subclinical atherosclerosis and the metabolic syndrome: the role of markers of inflammation. Int Angiol, 31, 219-26.
17. Goldstein JL, Brown MS. (2009) The LDL receptor. Arterioscler Thromb Vasc Biol, 29, 431-8.
18. Davignon J, Lussier-Cacan S, Ortin-George M, Lelievre M, Bertagna C, Gattereau A, Fontaine A. (1977) Plasma lipids and lipoprotein patterns in angiographically graded atherosclerosis of the legs and in coronary heart disease. Can Med Assoc J, 116, 1245-50.
19. Creager MA, Jones DW, Easton JD, Halperin JL, Hirsch AT, Matsumoto AH, O'Gara PT, Safian RD, Schwartz GL, Spittell JA. (2004) Atherosclerotic Vascular Disease Conference: Writing Group V: medical decision making and therapy. Circulation, 109, 2634-42.
20. Collins R, Armitage J, Parish S, Sleight P, Peto R, Collaborati HPS. (2002) MRC/BHF Heart Protection Study of cholesterol lowering with simvastatin in 20536 high-risk individuals: a randomised placebo-controlled trial. Lancet, 360, 7-22.
21. Pedersen TR, Kjekshus J, Berg K, Haghfelt T, Faergeman O, Thorgeirsson G, Pyorala K, Miettinen T, Wilhelmsen L, Olsson AG, Wedel H, Kristianson K, Thomsen H, Nordero E, Thomsen B, Lyngborg K, Andersen GS, Nielsen F, Talleruphuus U, Mcnair A, Egstrup K, Simonsen EH, Simonsen I, Vejbychristensen H, Sommer L, Eidner PO, Klarholt E, Henriksen A, Mellemgaard K, Launbjerg J, Freuergaard P, Nielsen L, Madsen EB, Ibsen H, Andersen U, Enemark H, Haarbo J, Martinsen B, Dahlstrom CG, Thyrring L, Thomassen K, Jensen G, Rasmussen SL, Skov N, Hansen KN, Larsen ML, Haastrup B, Hjaere I, Thuroe A, Leth A, Munch M, Worck R, Nielsen B, Thorn AG, Pedersenbjergaard O, Fournaise B, Sigurd B, Enk B, Nielsen H, Jacobsen L, Svendsen TL, Hoegholm A, Munter H, Kaufmann P, Haunso S, Grande P, Eriksen C, Nielsen HH, Jurlander B, Pinborg T, Pindborg J, Tost H, Christiansen BD, Oppenhagen M, Egede F, Hvidt S, Kjaerby T, Lemming L, Klausen I, Miettinen TA, Vanhanen H, Strandberg TE, Holtta K, Luomanmaki H, Pekuri T, Vuorinen A, Pasternack A, Oksa H, Siitonen L, Rimpi R, Kesaniemi YA, Lilja M, Korhonen T, Rantala A, Rantala M, Savolainen M, Ukkola O, Laine L, Virkkala L, Lehto S, et al. (1994) Randomized Trial of Cholesterol-Lowering in 4444 Patients with Coronary-Heart-Disease - the Scandinavian Simvastatin Survival Study (4s). Lancet, 344, 1383-1389.
22. Tonkin A, Aylward P, Colquhoun D, Glasziou P, Harris P, MacMahon S, Magnus P, Newel D, Nestel P, Sharpe N, Hunt D, Shaw J, Simes RJ, Thompson P, Thomson A, West M, White H, Simes S, Hague W, Caleo S, Hall J, Martin A, Mulray S, Barter P, Beilin L, Collins R, McNeil J, Meier P, Willimott H, Smithers D, Wallace P, Sullivan D, Keech A, Ischaemic L-TIP. (1998) Prevention of cardiovascular events and death with pravastatin in patients with coronary heart disease and a broad range of initial cholesterol levels. New England Journal of Medicine, 339, 1349-1357.

23. Sacks FM, Pfeffer MA, Moye LA, Rouleau JL, Rutherford JD, Cole TG, Brown L, Warnica JW, Arnold JMO, Wun CC, Davis BR, Braunwald E. (1996) The effect of pravastatin on coronary events after myocardial infarction in patients with average cholesterol levels. New England Journal of Medicine, 335, 1001-1009.
24. Ridker PM, Cannon CP, Morrow D, Rifai N, Rose LM, McCabe CH, Pfeffer MA, Braunwald E. (2005) C-reactive protein levels and outcomes after statin therapy. N Engl J Med, 352, 20-8.
25. Ridker PM, Danielson E, Fonseca FA, Genest J, Gotto AM, Jr., Kastelein JJ, Koenig W, Libby P, Lorenzatti AJ, Macfadyen JG, Nordestgaard BG, Shepherd J, Willerson JT, Glynn RJ. (2009) Reduction in C-reactive protein and LDL cholesterol and cardiovascular event rates after initiation of rosuvastatin: a prospective study of the JUPITER trial. Lancet, 373, 1175-82.
26. Cannon CP, Braunwald E, McCabe CH, Rader DJ, Rouleau JL, Belder R, Joyal SV, Hill KA, Pfeffer MA, Skene AM, Evaluatio PA. (2004) Intensive versus moderate lipid lowering with statins after acute coronary syndromes. New England Journal of Medicine, 350, 1495-1504.
27. Nissen SE, Tuzcu EM, Schoenhagen P, Brown BG, Ganz P, Vogel RA, Crowe T, Howard G, Cooper CJ, Brodie B, Grines CL, DeMaria AN, Investigators R. (2004) Effect of intensive compared with moderate lipid-lowering therapy on progression of coronary atherosclerosis - A randomized controlled trial. Jama-Journal of the American Medical Association, 291, 1071-1080.
28. Psaty BM, Smith NL, Siscovick DS, Koepsell TD, Weiss NS, Heckbert SR, Lemaitre RN, Wagner EH, Furberg CD. (1997) Health outcomes associated with antihypertensive therapies used as first-line agents. A systematic review and meta-analysis. JAMA, 277, 739-45.
29. Zamani P, Ganz P, Libby P, Sutradhar SC, Rifai N, Nicholls SJ, Nissen SE, Kinlay S. Relationship of antihypertensive treatment to plasma markers of vascular inflammation and remodeling in the Comparison of Amlodipine versus Enalapril to Limit Occurrences of Thrombosis study. Am Heart J, 163, 735-40.
30. Stylianou IM, Bauer RC, Reilly MP, Rader DJ. (2012) Genetic basis of atherosclerosis: insights from mice and humans. Circ Res, 110, 337-55.
31. Tabas I. (2009) Macrophage death and defective inflammation resolution in atherosclerosis. Nat Rev Immunol, 10, 36-46.
32. Matturri L, Ottaviani G, Lavezzi AM. (2005) Natural history of perinatal coronary atherosclerosis. Progress in Coronary Artery Disease, 67-70.
33. Matturri L, Ottaviani G, Lavezzi AM. (2005) Early atherosclerotic lesions in infancy: role of parental cigarette smoking. Virchows Arch, 447, 74-80.
34. Owens GK, Kumar MS, Wamhoff BR. (2004) Molecular regulation of vascular smooth muscle cell differentiation in development and disease. Physiol Rev, 84, 767-801.
35. Kocher O, Gabbiani G. (1986) Cytoskeletal features of normal and atheromatous human arterial smooth muscle cells. Hum Pathol, 17, 875-80.
36. Aikawa M, Sakomura Y, Ueda M, Kimura K, Manabe I, Ishiwata S, Komiyama N, Yamaguchi H, Yazaki Y, Nagai R. (1997) Redifferentiation of smooth muscle cells after coronary angioplasty determined via myosin heavy chain expression. Circulation, 96, 82-90.
37. Kocher O, Gabbiani F, Gabbiani G, Reidy MA, Cokay MS, Peters H, Huttner I. (1991) Phenotypic features of smooth muscle cells during the evolution of experimental carotid artery intimal thickening. Biochemical and morphologic studies. Lab Invest, 65, 459-70.

38. Magnier-Gaubil C, Herbert JM, Quarck R, Papp B, Corvazier E, Wuytack F, Levy-Toledano S, Enouf J. (1996) Smooth muscle cell cycle and proliferation. Relationship between calcium influx and sarco-endoplasmic reticulum Ca2+ATPase regulation. J Biol Chem, 271, 27788-94.
39. Kanzaki M, Shibata H, Mogami H, Kojima I. (1995) Expression of calcium-permeable cation channel CD20 accelerates progression through the G1 phase in Balb/c 3T3 cells. J Biol Chem, 270, 13099-104.
40. Sunagawa M. (2010) Involvement of Ca(2+) channel activity in proliferation of vascular smooth muscle cells. Pathophysiology, 17, 101-8.
41. Catterall WA. (2000) Structure and regulation of voltage-gated Ca2+ channels. Annu Rev Cell Dev Biol, 16, 521-55.
42. Wamhoff BR, Dixon JL, Sturek M. (2002) Atorvastatin treatment prevents alterations in coronary smooth muscle nuclear Ca2+ signaling in diabetic dyslipidemia. J Vasc Res, 39, 208-20.
43. Dixon JL, Stoops JD, Parker JL, Laughlin MH, Weisman GA, Sturek M. (1999) Dyslipidemia and vascular dysfunction in diabetic pigs fed an atherogenic diet. Arterioscler Thromb Vasc Biol, 19, 2981-92.
44. Gollasch M, Haase H, Ried C, Lindschau C, Morano I, Luft FC, Haller H. (1998) L-type calcium channel expression depends on the differentiated state of vascular smooth muscle cells. FASEB J, 12, 593-601.
45. Patel MK, Clunn GF, Lymn JS, Austin O, Hughes AD. (2005) Effect of serum withdrawal on the contribution of L-type calcium channels (CaV1.2) to intracellular Ca2+ responses and chemotaxis in cultured human vascular smooth muscle cells. Br J Pharmacol, 145, 811-7.
46. Barg S, Ma X, Eliasson L, Galvanovskis J, Gopel SO, Obermuller S, Platzer J, Renstrom E, Trus M, Atlas D, Striessnig J, Rorsman P. (2001) Fast exocytosis with few Ca(2+) channels in insulin-secreting mouse pancreatic B cells. Biophys J, 81, 3308-23.
47. Bers DM. (2002) Cardiac excitation-contraction coupling. Nature, 415, 198-205.
48. Orrenius S, Zhivotovsky B, Nicotera P. (2003) Regulation of cell death: the calcium-apoptosis link. Nat Rev Mol Cell Biol, 4, 552-65.
49. Catterall WA, Striessnig J, Snutch TP, Perez-Reyes E. (2003) International Union of Pharmacology. XL. Compendium of voltage-gated ion channels: calcium channels. Pharmacol Rev, 55, 579-81.
50. Zuccotti A, Clementi S, Reinbothe T, Torrente A, Vandael DH, Pirone A. (2011) Structural and functional differences between L-type calcium channels: crucial issues for future selective targeting. Trends in Pharmacological Sciences, 32, 366-375.
51. Lacinova L. (2005) Voltage-dependent calcium channels. Gen Physiol Biophys, 24 Suppl 1, 1-78.
52. Liao P, Soong TW. (2010) CaV1.2 channelopathies: from arrhythmias to autism, bipolar disorder, and immunodeficiency. Pflugers Arch, 460, 353-9.
53. Splawski I, Timothy KW, Sharpe LM, Decher N, Kumar P, Bloise R, Napolitano C, Schwartz PJ, Joseph RM, Condouris K, Tager-Flusberg H, Priori SG, Sanguinetti MC, Keating MT. (2004) Ca(V)1.2 calcium channel dysfunction causes a multisystem disorder including arrhythmia and autism. Cell, 119, 19-31.
54. Birnbaumer L, Campbell KP, Catterall WA, Harpold MM, Hofmann F, Horne WA, Mori Y, Schwartz A, Snutch TP, Tanabe T, et al. (1994) The naming of voltage-gated calcium channels. Neuron, 13, 505-6.

55. Bodi I, Mikala G, Koch SE, Akhter SA, Schwartz A. (2005) The L-type calcium channel in the heart: the beat goes on. J Clin Invest, 115, 3306-17.
56. Ertel EA, Campbell KP, Harpold MM, Hofmann F, Mori Y, Perez-Reyes E, Schwartz A, Snutch TP, Tanabe T, Birnbaumer L, Tsien RW, Catterall WA. (2000) Nomenclature of voltage-gated calcium channels. Neuron, 25, 533-5.
57. Van Petegem F, Minor DL, Jr. (2006) The structural biology of voltage-gated calcium channel function and regulation. Biochem Soc Trans, 34, 887-93.
58. Black DJ, Halling DB, Mandich DV, Pedersen SE, Altschuld RA, Hamilton SL. (2005) Calmodulin interactions with IQ peptides from voltage-dependent calcium channels. Am J Physiol Cell Physiol, 288, C669-76.
59. Blaich A, Welling A, Fischer S, Wegener JW, Kostner K, Hofmann F, Moosmang S. (2010) Facilitation of murine cardiac L-type Ca(v)1.2 channel is modulated by calmodulin kinase II-dependent phosphorylation of S1512 and S1570. Proc Natl Acad Sci U S A, 107, 10285-9.
60. Liao P, Yu D, Li G, Yong TF, Soon JL, Chua YL, Soong TW. (2007) A smooth muscle Cav1.2 calcium channel splice variant underlies hyperpolarized window current and enhanced state-dependent inhibition by nifedipine. J Biol Chem, 282, 35133-42.
61. Cheng X, Pachuau J, Blaskova E, Asuncion-Chin M, Liu J, Dopico AM, Jaggar JH. (2009) Alternative splicing of Cav1.2 channel exons in smooth muscle cells of resistance-size arteries generates currents with unique electrophysiological properties. Am J Physiol Heart Circ Physiol, 297, H680-8.
62. Soldatov NM, Bouron A, Reuter H. (1995) Different Voltage-Dependent Inhibition by Dihydropyridines of Human Ca2+ Channel Splice Variants. Journal of Biological Chemistry, 270, 10540-10543.
63. Zuhlke RD, Bouron A, Soldatov NM, Reuter H. (1998) Ca2+ channel sensitivity towards the blocker isradipine is affected by alternative splicing of the human alpha(1C) subunit gene. Febs Letters, 427, 220-224.
64. Morel N, Buryi V, Feron O, Gomez JP, Christen MO, Godfraind T. (1998) The action of calcium channel blockers on recombinant L-type calcium channel alpha1-subunits. Br J Pharmacol, 125, 1005-12.
65. Welling A, Ludwig A, Zimmer S, Klugbauer N, Flockerzi V, Hofmann F. (1997) Alternatively spliced IS6 segments of the alpha 1C gene determine the tissue-specific dihydropyridine sensitivity of cardiac and vascular smooth muscle L-type Ca2+ channels. Circ Res, 81, 526-32.
66. Liao P, Yong TF, Liang MC, Yue DT, Soong TW. (2005) Splicing for alternative structures of Cav1.2 Ca2+ channels in cardiac and smooth muscles. Cardiovasc Res, 68, 197-203.
67. Wang J, Thio SS, Yang SS, Yu D, Yu CY, Wong YP, Liao P, Li S, Soong TW. (2011) Splice variant specific modulation of CaV1.2 calcium channel by galectin-1 regulates arterial constriction. Circ Res, 109, 1250-8.
68. Yang Y, Chen X, Margulies K, Jeevanandam V, Pollack P, Bailey BA, Houser SR. (2000) L-type Ca2+ channel alpha 1c subunit isoform switching in failing human ventricular myocardium. J Mol Cell Cardiol, 32, 973-84.
69. Van Petegem F, Clark KA, Chatelain FC, Minor DL, Jr. (2004) Structure of a complex between a voltage-gated calcium channel beta-subunit and an alpha-subunit domain. Nature, 429, 671-5.
70. Gregg RG, Messing A, Strube C, Beurg M, Moss R, Behan M, Sukhareva M, Haynes S, Powell JA, Coronado R, Powers PA. (1996) Absence of the beta subunit (cchb1) of the

skeletal muscle dihydropyridine receptor alters expression of the alpha 1 subunit and eliminates excitation-contraction coupling. Proc Natl Acad Sci U S A, 93, 13961-6.

71. Buraei Z, Yang J. (2010) The β subunit of voltage-gated Ca2+ channels. Physiol Rev, 90, 1461-506.
72. Hullin R, Matthes J, von Vietinghoff S, Bodi I, Rubio M, D'Souza K, Friedrich Khan I, Rottlander D, Hoppe UC, Mohacsi P, Schmitteckert E, Gilsbach R, Bunemann M, Hein L, Schwartz A, Herzig S. (2007) Increased expression of the auxiliary beta(2)-subunit of ventricular L-type Ca(2)+ channels leads to single-channel activity characteristic of heart failure. PLoS One, 2, e292.
73. Chu PJ, Larsen JK, Chen CC, Best PM. (2004) Distribution and relative expression levels of calcium channel beta subunits within the chambers of the rat heart. J Mol Cell Cardiol, 36, 423-34.
74. Vance CL, Begg CM, Lee WL, Haase H, Copeland TD, McEnery MW. (1998) Differential expression and association of calcium channel alpha1B and beta subunits during rat brain ontogeny. J Biol Chem, 273, 14495-502.
75. Ludwig A, Flockerzi V, Hofmann F. (1997) Regional expression and cellular localization of the alpha1 and beta subunit of high voltage-activated calcium channels in rat brain. J Neurosci, 17, 1339-49.
76. Foell JD, Balijepalli RC, Delisle BP, Yunker AM, Robia SL, Walker JW, McEnery MW, January CT, Kamp TJ. (2004) Molecular heterogeneity of calcium channel beta-subunits in canine and human heart: evidence for differential subcellular localization. Physiol Genomics, 17, 183-200.
77. Yang SN, Berggren PO. (2006) The role of voltage-gated calcium channels in pancreatic beta-cell physiology and pathophysiology. Endocr Rev, 27, 621-76.
78. Cens T, Mangoni ME, Nargeot J, Charnet P. (1996) Modulation of the alpha 1A Ca2+ channel by beta subunits at physiological Ca2+ concentration. FEBS Lett, 391, 232-7.
79. Colecraft HM, Alseikhan B, Takahashi SX, Chaudhuri D, Mittman S, Yegnasubramanian V, Alvania RS, Johns DC, Marban E, Yue DT. (2002) Novel functional properties of Ca(2+) channel beta subunits revealed by their expression in adult rat heart cells. J Physiol, 541, 435-52.
80. Herzig S, Khan IF, Grundemann D, Matthes J, Ludwig A, Michels G, Hoppe UC, Chaudhuri D, Schwartz A, Yue DT, Hullin R. (2007) Mechanism of Ca(v)1.2 channel modulation by the amino terminus of cardiac beta2-subunits. FASEB J, 21, 1527-38.
81. Jangsangthong W, Kuzmenkina E, Bohnke AK, Herzig S. (2011) Single-channel monitoring of reversible L-type Ca(2+) channel Ca(V)alpha(1)-Ca(V)beta subunit interaction. Biophys J, 101, 2661-70.
82. Jangsangthong W, Kuzmenkina E, Khan IF, Matthes J, Hullin R, Herzig S. Inactivation of L-type calcium channels is determined by the length of the N terminus of mutant beta(1) subunits. Pflugers Arch, 459, 399-411.
83. Bichet D, Cornet V, Geib S, Carlier E, Volsen S, Hoshi T, Mori Y, De Waard M. (2000) The I-II loop of the Ca2+ channel alpha1 subunit contains an endoplasmic reticulum retention signal antagonized by the beta subunit. Neuron, 25, 177-90.
84. Fang K, Colecraft HM. (2011) Mechanism of auxiliary beta-subunit-mediated membrane targeting of L-type (Ca(V)1.2) channels. Journal of Physiology-London, 589, 4437-4455.
85. Altier C, Garcia-Caballero A, Simms B, You HT, Chen LN, Walcher J, Tedford HW, Hermosilla T, Zamponi GW. (2011) The Cav beta subunit prevents RFP2-mediated ubiquitination and proteasomal degradation of L-type channels. Nature Neuroscience, 14, 173-U252.

86. Klugbauer N, Marais E, Hofmann F. (2003) Calcium channel alpha2delta subunits: differential expression, function, and drug binding. J Bioenerg Biomembr, 35, 639-47.
87. Davies A, Kadurin I, Alvarez-Laviada A, Douglas L, Nieto-Rostro M, Bauer CS, Pratt WS, Dolphin AC. (2010) The alpha(2)delta subunits of voltage-gated calcium channels form GPI-anchored proteins, a posttranslational modification essential for function. Proceedings of the National Academy of Sciences of the United States of America, 107, 1654-1659.
88. Fuller-Bicer GA, Varadi G, Koch SE, Ishii M, Bodi I, Kadeer N, Muth JN, Mikala G, Petrashevskaya NN, Jordan MA, Zhang SP, Qin N, Flores CM, Isaacsohn I, Varadi M, Mori Y, Jones WK, Schwartz A. (2009) Targeted disruption of the voltage-dependent calcium channel alpha(2)/delta-1-subunit. American Journal of Physiology-Heart and Circulatory Physiology, 297, H117-H124.
89. Field MJ, Cox PJ, Stott E, Melrose H, Offord J, Su TZ, Bramwell S, Corradini L, England S, Winks J, Kinloch RA, Hendrich J, Dolphin AC, Webb T, Williams D. (2006) Identification of the alpha2-delta-1 subunit of voltage-dependent calcium channels as a molecular target for pain mediating the analgesic actions of pregabalin. Proc Natl Acad Sci U S A, 103, 17537-42.
90. Li CY, Song YH, Higuera ES, Luo ZD. (2004) Spinal dorsal horn calcium channel alpha(2)delta-1 subunit upregulation contributes to peripheral nerve injury-induced tactile allodynia. Journal of Neuroscience, 24, 8494-8499.
91. Tiwari S, Zhang Y, Heller J, Abernethy DR, Soldatov NM. (2006) Atherosclerosis-related molecular alteration of the human CaV1.2 calcium channel alpha1C subunit. Proc Natl Acad Sci U S A, 103, 17024-9.
92. Murakami M, Yamamura H, Suzuki T, Kang MG, Ohya S, Murakami A, Miyoshi I, Sasano H, Muraki K, Hano T, Kasai N, Nakayama S, Campbell KP, Flockerzi V, Imaizumi Y, Yanagisawa T, Iijima T. (2003) Modified cardiovascular L-type channels in mice lacking the voltage-dependent Ca2+ channel beta3 subunit. J Biol Chem, 278, 43261-7.
93. Zhang SH, Reddick RL, Piedrahita JA, Maeda N. (1992) Spontaneous hypercholesterolemia and arterial lesions in mice lacking apolipoprotein E. Science, 258, 468-71.
94. Schroeder A, Mueller O, Stocker S, Salowsky R, Leiber M, Gassmann M, Lightfoot S, Menzel W, Granzow M, Ragg T. (2006) The RIN: an RNA integrity number for assigning integrity values to RNA measurements. BMC Mol Biol, 7, 3.
95. Wong M, Medrano J. (2005) Real-time PCR for mRNA quantitation. BioTechniques 39 1-11.
96. Qiagen. (2009) Critcal factors for successful Real-Time PCR. In: Sample and Assay technologies. Qiagen.
97. Kardakaris R, Gareus R, Xanthoulea S, Pasparakis M. (2011) Endothelial and macrophage-specific deficiency of P38alpha MAPK does not affect the pathogenesis of atherosclerosis in ApoE-/- mice. PLoS One, 6, e21055.
98. Whitman SC. (2004) A practical approach to using mice in atherosclerosis research. Clin Biochem Rev, 25, 81-93.
99. Gareus R, Kotsaki E, Xanthoulea S, van der Made I, Gijbels MJ, Kardakaris R, Polykratis A, Kollias G, de Winther MP, Pasparakis M. (2008) Endothelial cell-specific NF-kappaB inhibition protects mice from atherosclerosis. Cell Metab, 8, 372-83.

100. Link S, Meissner M, Held B, Beck A, Weissgerber P, Freichel M, Flockerzi V. (2009) Diversity and developmental expression of L-type calcium channel beta2 proteins and their influence on calcium current in murine heart. J Biol Chem, 284, 30129-37.
101. Murakami M, Wissenbach U, Flockerzi V. (1996) Gene structure of the murine calcium channel beta3 subunit, cDNA and characterization of alternative splicing and transcription products. Eur J Biochem, 236, 138-43.
102. Grabner M, Dirksen RT, Suda N, Beam KG. (1999) The II-III loop of the skeletal muscle dihydropyridine receptor is responsible for the Bi-directional coupling with the ryanodine receptor. J Biol Chem, 274, 21913-9.
103. Neher E, Sakmann B, Steinbach JH. (1978) The extracellular patch clamp: a method for resolving currents through individual open channels in biological membranes. Pflugers Arch, 375, 219-28.
104. Ogden D, Stanfield PR. (1987) Patch clamp techniques for single channel and whole-cell recording. In: Microelectrode techniques: the Plymouth workshop handbook. Vol. 2nd edition. The Company of Biologists, Cambridge.
105. Hodgkin AL, Huxley AF. (1952) A quantitative description of membrane current and its application to conduction and excitation in nerve. J Physiol, 117, 500-44.
106. Karmazinova M, Lacinova L. (2010) Measurement of Cellular Excitability by Whole Cell Patch Clamp Technique. Physiological Research, 59, S1-S7.
107. Lee KS, Marban E, Tsien RW. (1985) Inactivation of calcium channels in mammalian heart cells: joint dependence on membrane potential and intracellular calcium. J Physiol, 364, 395-411.
108. Salowsky R, Henger A. (2002) High sensitivity quality control of RNA samples using the RNA 6000 Pico LabChip kit. In: Application. Vol. 5988-8554EN. Agilent Technologies.
109. Mueller O, Lightfoot S, Schroeder A. (2004) RNA Integrity Number (RIN) – Standardization of RNA Quality Control. Agilent Application Note, 5989-1165EN.
110. Spaetgens RL, Zamponi GW. (1999) Multiple structural domains contribute to voltage-dependent inactivation of rat brain alpha(1E) calcium channels. J Biol Chem, 274, 22428-36.
111. Webb RC. (2003) Smooth muscle contraction and relaxation. Adv Physiol Educ, 27, 201-6.
112. Soldatov NM, Bouron A, Reuter H. (1995) Different voltage-dependent inhibition by dihydropyridines of human Ca2+ channel splice variants. J Biol Chem, 270, 10540-3.
113. Bijnens AP, Lutgens E, Ayoubi T, Kuiper J, Horrevoets AJ, Daemen MJ. (2006) Genome-wide expression studies of atherosclerosis: critical issues in methodology, analysis, interpretation of transcriptomics data. Arterioscler Thromb Vasc Biol, 26, 1226-35.
114. Hullin R, Singerlahat D, Freichel M, Biel M, Dascal N, Hofmann F, Flockerzi V. (1992) Calcium-Channel Beta-Subunit Heterogeneity - Functional Expression of Cloned Cdna from Heart, Aorta and Brain. Embo Journal, 11, 885-890.
115. Reimer D, Huber IG, Garcia ML, Haase H, Striessnig J. (2000) beta Subunit heterogeneity of L-type Ca2+ channels in smooth muscle tissues. Febs Letters, 467, 65-69.
116. Zhang QJ, Goddard M, Shanahan C, Shapiro L, Bennett M. (2002) Differential gene expression in vascular smooth muscle cells in primary atherosclerosis and in stent stenosis in humans. Arteriosclerosis Thrombosis and Vascular Biology, 22, 2030-2036.

117. Doroudi R, Andersson M, Svensson PA, Ekman M, Jern S, Karlsson L. (2005) Methodological studies of multiple reference genes as endogenous controls in vascular gene expression studies. Endothelium-Journal of Endothelial Cell Research, 12, 215-223.
118. Collin T, Lory P, Taviaux S, Courtieu C, Guilbault P, Berta P, Nargeot J. (1994) Cloning, Chromosomal Location and Functional Expression of the Human Voltage-Dependent Calcium-Channel Beta-3 Subunit. European Journal of Biochemistry, 220, 257-262.
119. Allayee H, Ghazalpour A, Lusis AJ. (2003) Using mice to dissect genetic factors in atherosclerosis. Arteriosclerosis Thrombosis and Vascular Biology, 23, 1501-1509.
120. Tang ZZ, Hong X, Wang J, Soong TW. (2007) Signature combinatorial splicing profiles of rat cardiac- and smooth-muscle Cav1.2 channels with distinct biophysical properties. Cell Calcium, 41, 417-28.
121. Nilsson J, Sjolund M, Palmberg L, Von Euler AM, Jonzon B, Thyberg J. (1985) The calcium antagonist nifedipine inhibits arterial smooth muscle cell proliferation. Atherosclerosis, 58, 109-22.
122. Jackson CL, Bush RC, Bowyer DE. (1988) Inhibitory effect of calcium antagonists on balloon catheter-induced arterial smooth muscle cell proliferation and lesion size. Atherosclerosis, 69, 115-22.
123. Olcese R, Qin N, Schneider T, Neely A, Wei X, Stefani E, Birnbaumer L. (1994) The amino terminus of a calcium channel beta subunit sets rates of channel inactivation independently of the subunit's effect on activation. Neuron, 13, 1433-8.
124. Wei SK, Colecraft HM, DeMaria CD, Peterson BZ, Zhang R, Kohout TA, Rogers TB, Yue DT. (2000) Ca(2+) channel modulation by recombinant auxiliary beta subunits expressed in young adult heart cells. Circ Res, 86, 175-84.
125. Takahashi SX, Mittman S, Colecraft HM. (2003) Distinctive modulatory effects of five human auxiliary beta2 subunit splice variants on L-type calcium channel gating. Biophys J, 84, 3007-21.
126. Hullin R, Khan IF, Wirtz S, Mohacsi P, Varadi G, Schwartz A, Herzig S. (2003) Cardiac L-type calcium channel beta-subunits expressed in human heart have differential effects on single channel characteristics. J Biol Chem, 278, 21623-30.
127. Wamhoff BR, Bowles DK, Owens GK. (2006) Excitation-transcription coupling in arterial smooth muscle. Circ Res, 98, 868-78.
128. Quignard JF, Harricane MC, Menard C, Lory P, Nargeot J, Capron L, Mornet D, Richard S. (2001) Transient down-regulation of L-type Ca(2+) channel and dystrophin expression after balloon injury in rat aortic cells. Cardiovasc Res, 49, 177-88.
129. Striessnig J. (1999) Pharmacology, structure and function of cardiac L-type Ca(2+) channels. Cell Physiol Biochem, 9, 242-69.
130. Tikhonov DB, Zhorov BS. (2009) Structural model for dihydropyridine binding to L-type calcium channels. J Biol Chem, 284, 19006-17.

# 7. Eigene Veröffentlichungen

Auszüge dieser Arbeit wurden bereits an anderer Stelle veröffentlicht.

## Kongressbeiträge (Posterpräsentation)

Böhnke AK, Odenthal M, Gawenda M, Matthes J, Hein P, Herzig S

Structural remodelling of L-type calcium channel subunits in human and murine atherosclerosis.

European Calcium Channel Conference (2012), Innsbruck, Österreich

Böhnke AK, Odenthal M, Polykratis A, Gawenda M, Matthes J, Hein P, Herzig S

Structural remodeling of L-type calcium channel subunits in human and murine atherosclerosis.

35th Meeting of the European Working Group on Cardiac Cellular Electrophysiology (2011), Oslo, Norwegen

Böhnke AK, Odenthal M, Polykratis A, Gawenda M, Matthes J, Hein P, Herzig S

Structural remodeling of L-type calcium channel subunits in human and murine atherosclerosis. Naunyn-Schmiedeberg's Arch Pharmacol (2011); **38 3 (Suppl 1)**; 42:P147

77. Jahrestagung der Deutschen Gesellschaft für experimentelle und klinische Pharmakologie und Toxikologie e.V. (DGPT 2011), Frankfurt

Böhnke AK, Odenthal M, Gawenda M, Matthes J, Hein P, Herzig S

Expression pattern of L-type calcium channel subunits in human and murine atherosclerosis. Biophys. J. (2011); **100 (3)** pp.568a

Biophysical Society 55th Annual Meeting (2011), Baltimore, Maryland, USA

# 8. Erklärung

Hiermit versichere ich, Ann Kristin Böhnke, dass ich die hier vorliegende Arbeit selbstständig angefertigt und keine anderen, als die angegebenen Hilfsmittel und Quellen benutzt habe. Ferner erkläre ich, die vorgelegte Arbeit an keiner anderen Hochschule als Dissertation eingereicht zu haben.

Köln, 18.7.2012

Ann Kristin Böhnke